

UNIVERSITÀ DEGLI STUDI DI PADOVA

LEOPOLD-FRANZENS UNIVERSITÄT INNSBRUCK

ALBERT-LUDWIGS UNIVERSITÄT FREIBURG

HOME INSTITUTION: UNIVERSITÀ DEGLI STUDI DI PADOVA,
DIPARTIMENTO DI FARMACOLOGIA ED ANESTESIOLOGIA

HOST INSTITUTION: LEOPOLD-FRANZENS UNIVERSITÄT INNSBRUCK,
INSTITUT FÜR BIOCHEMISCHE PHARMAKOLOGIE

HOST INSTITUTION: ALBERT-LUDWIGS UNIVERSITÄT FREIBURG,
INSTITUT FÜR EXPERIMENTELLE UND KLINISCHE PHARMAKOLOGIE UND TOXIKOLOGIE

DOCTORAL DISSERTATION IN

"MOLECULAR AND CELLULAR PHARMACOLOGY"
"FARMACOLOGIA MOLECOLARE E CELLULARE"

DOCTORAL PROGRAMME
XXI CICLE

Molecular and functional analysis of the Drosophila Dynamin-like GTPase atlastin

COORDINATOR: *Prof. Sisto Luciani*
Department of Pharmacology and Anesthesiology, University of Padova

SUPERVISOR: *Prof. Gabriella Cargnelli*
Department of Pharmacology and Anesthesiology, University of Padova

EXTERNAL SUPERVISOR: *Dott. Andrea Daga*
Dulbecco Telethon Institute at the E. Medea Scientific Institute, Conegliano

DOCTORAL CANDIDATE: *Jessica Tosetto*

31 December 2008

INDEX

ABBREVIATIONS

A Alanine

Ala Alanine

CD Circular dichroism

Datl Datlastin

DPC Dodecil-Phosphate-Coline

ER Endoplasmic reticulum

F Phenylalanine

IHC Immunohystochemestry

ICC Immunocystochemestry

K Lysine

L Leucine

Leu leucine

Met Mehionine

P Proline

Phe Phenylalanine

PDI Protein Disulfide Isomerise

PBS Phoshate Buffered Saline

TFE Trifluoroethanol

F Phenylalanine

Val Valine

Abstract

Mutations in the gene encoding the large oligomeric GTPase Atlastin-1 are responsible for SPG3a, a common autosomal dominant Hereditary Spastic Paraplegia.

Recent studies carried out in our laboratory have shown that the *Drosophila* ortholog of human Atlastin-1 (Datlastin) is required for homotypic fusion of ER membranes. Homotypic fusion activity is critical for the both the biogenesis and maintenance of the ER and a proper ER architecture is essential for ER functionality. Datlastin specifically localizes to ER membranes and alteration of its expression levels *in vivo* in *Drosophila* has revealed that Datlastin depletion causes ER fragmentation, while its overexpression results in the formation of expanded ER elements consistent with excessive fusion of ER membranes.

Using different experimental approaches, we demonstrate that Datlastin has the ability to homo-oligomerize and that Datlastin molecules localized on distinct ER membranes can form trans-oligomeric complexes. In contrast, GTPase-deficient Datlastin is inactive and unable to form trans-oligomeric complexes due to its failure to self-associate. These results suggest that Datlastin undergoes GTPase-dependent homo-oligomerization thereby mediating the tethering of adjacent ER membranes that precedes homotypic fusion. We further show that Datlastin contains a coiled-coil region responsible for mediating oligomerization. Mutations disrupting the structure of the coiled-coil inactivate Datlastin by preventing tethering and the subsequent fusion of ER membranes. The close membrane localization of the coiled-coil Datlastin domain provides a mechanism for the very close apposition between ER membranes that must occur during Datlastin mediated fusion.

These results provide an explanation of the mechanisms underlying Datlastin mediated membrane fusion and lay the foundations for understanding the mechanics of ER biogenesis and maintenance that are presently unknown.

Riassunto

Mutazioni a carico del gene *spg3a* codificante per Atlastina-1 sono responsabili di una forma autosomica dominante di paraplegia spastica ereditaria.

Ricerche condotte nel laboratorio in cui ho svolto il dottorato dimostrano che Datlastina, l'ortologo in *Drosophila* di Atlastina-1, promuove la fusione omotipica delle membrane del reticolo endoplasmico (ER).

La fusione omotipica è un processo essenziale per il corretto funzionamento del ER poiché regola la biogenesi e il mantenimento della sua complessa struttura.

Datlastina è una proteina integrale delle membrane del ER. In *Drosophila*, in seguito alla deplezione di Datlastina il ER risulta frammentato, mentre la sua sovraespressione induce la comparsa di cisterne di ER dilatate riconducibili ad una attività di iperfusione.

Questa tesi ha come oggetto lo studio del meccanismo con cui atlastina media la fusione omotipica delle membrane del ER. La fusione tra membrane si divide in tre fasi: l'avvicinamento, l'"ancoraggio" e la fusione finale dei due strati fosfolipidici.

Attraverso un approccio biochimico, questo lavoro dimostra che Datlastina è capace di oligomerizzare e che molecole di Datlastina presenti su distinte membrane del reticolo endoplasmico sono in grado di associarsi a formare dei complessi in trans. Al contrario, forme mutate di Datlastina prive di attività GTPasica sono inattive ed incapaci sia di associarsi, sia di formare complessi in trans. Questi risultati suggeriscono che Datlastina, attraverso una oligomerizzazione dipendente dall'attività GTPasica, è in grado di avvicinare membrane adiacenti di reticolo endoplasmico per la loro successiva fusione.

Analisi di modelling molecolare ed esperimenti di dicroismo circolare hanno permesso di identificare un dominio coiled-coil responsabile dell'oligomerizzazione di Datlastina. Mutazioni che distruggono la struttura del dominio coiled-coil inattivano Datlastina che risulta incapace sia di avvicinare sia di fondere le membrane del reticolo endoplasmico.

La stretta vicinanza richiesta durante la fusione tra due membrane è soddisfatta, nel processo mediato da Datlastina, dalla prossimità dei domini coiled-coil ai domini transmembrana.

Questi risultati forniscono una spiegazione del meccanismo con cui Datlastina opera nella fusione delle membrane del reticolo endoplasmico e consentono una maggiore comprensione dei processi biofisici coinvolti nella fusione delle membrane.

1 Introduction

1.1 Drosophila in the study of neurodegenerative diseases

A growing number of neurodegenerative diseases, as well as other human diseases, are being modelled in *Drosophila*.

Drosophila is used as a platform to identify and validate cellular pathways that contribute to neurodegeneration and to identify promising therapeutic targets by using a variety of approaches from screens to target validation. The unique properties and tools available in the *Drosophila* system, coupled with the fact that testing *in vivo* has proven highly productive, have accelerated the progress of testing therapeutic strategies in mice and, ultimately, humans.

1.1.1 How fly models can complement other systems

In studying human neurodegenerative diseases, one typically employs multiple systems, including cell-based models in which one can generate stably expressing lines and phenocopy cellular aspects of disease. However, in many cases, the response of the intact organism is not fully recapitulated in cell lines. *In vitro*, intersecting physiological pathways and responses (e.g., neurotransmitter circuitry and interactions with support cells, etc.) are eliminated, nonautonomous cellular influences are removed, and new parameters such as those used to immortalize cells, are often introduced, thus reducing the ability of cultured cells to mirror *in vivo* pathology. It can also be very difficult to obtain a functional measure of the impact of pathogenic proteins in *in vitro* systems.

In contrast, although mice and other mammalian model systems offer *in vivo* opportunities and extensive similarity to the human brain, the length of time and cost required to perform experiments comparable to those possible in flies can be prohibitive. Flies, on the other hand, are a minuscule system model with a rapid generation time, inexpensive culture requirements, large progeny numbers produced in a single cross and a small highly annotated genome devoid of genetic redundancy. Flies allow excellent genetic manipulation and the pathways are considered generally highly conserved with vertebrates.

A comparative genome analysis reveals that approximately 75% of all human disease genes have a *Drosophila* ortholog (Fortini, Skupski et al. 2000; Reiter, Potocki et al. 2001).

Drosophila has homologues of genes that, when disrupted, cause a broad spectrum of human diseases such as neurological disorders, cancer, developmental disorders, metabolic and storage disorders and cardiovascular disease, as well as homologues of genes required for the visual, auditory and immune systems. This and other bioinformatic analyses indicate that *Drosophila* can serve as a complex multicellular assay system for analysing the function of a wide array of gene functions involved in human diseases (Table 1).

Disease	Human gene symbol	Fly gene symbol	Gene product
Dysmorphology			
Synpolydactyly	*HOXD13*‡	*Abd-B*§	Transcription factor
Single bone in zeugopod	*HOXD3–HOXD13* (heterozygous deletion)	*Abd-B*§	Transcription factor
Hand-foot-genital syndrome	*HOXA13* or heterozygous *HOXA11–13* deletion	*Abd-B*§	Transcription factor
Aniridia	*PAX6*	*ey*§, *toy*§	Transcription factor
Townes-Brocks syndrome	*SALL1*	*salm*§, *sal*§	Transcription factor
Saethre-Chotzen syndrome	*TWIST1*	*twi*§	Transcription factor
Pfieffer syndrome	*FGFR1*, *FGFR2*	*htl*§	RTK
Apert syndrome	*FGFR2*	*htl*§	RTK
Crouzon syndrome	*FGFR3*	*htl*§	RTK
Saethre-Chotzen syndrome-like	*FGFR3*, gain-of-function?	*htl*§	RTK
Alagille syndrome	*JAG1*	*Ser*§, *Dl*§	Notch ligand
Spondylocostal dysostosis	*DLL3*	*Dl*§	Notch ligand
Primary congenital glaucoma	*CYP1B1*	*Cyp18a1*§	Cytochrome P450
Cardiac disease			
Congenital heart disease	*NKX2-5* *GATA4*	*tin*§ *pnr*§	Transcription factor Transcription factor
Holt–Oram syndrome	*TBX5*	*Doc1–Doc3*§	Transcription factor
DiGeorge syndrome	*TBX1*	*org-1*§, *bi*§	Transcription factor
Venous malformations	*TEK*	*htl*§	RTK
Neurological			
Spinocerabellar ataxia	*SCA1* (also known as *ATXN1*) *SCA2* (also known as *ATXN2*) *SCA6* (also known as *CACNA1A*) *SCA14* (also known as *PRKCG*) *SCA17* (also known as *TBP*)	*CG4547* *CG5166* *cac*§, *Ca-α1D*§ *inaC*§, *Pkc53E* *Tbp*§	Transcription cofactor? Unknown Ca^{2+} ion channel Ca^{2+}-dependent PKC TATA binding protein
Huntington disease	*HD*	*huntingtin*§	Axonal transport?
Spinal and bulbar muscular atrophy 3	*AR*	*ERR*, *svp*§	Androgen receptor
Parkinson disease	*PARK2* *PARK5* (also known as *UCHL1*) *PARK7* *NR4A2* *MAPT* *PINK1* *SNCA*	*park*§ *Uch* *dj-1β*, *CG6646* *Hr38*§ *tau*§ *CG4523*§ None known	E3-ubiquitin ligase Ubiquitin pathway Androgen-R regulator? Nuclear hormone receptor Microtubule binding PTEN-induced kinase Dopamine transmission?
Alzheimer disease	*PSEN1*, *PSEN2* *APP*	*Psn*§ *Appl*§	γ-Secretase Signalling, axonal transport?
Fragile X syndrome	*FMR1*	*Fmr1*§	Translational regulator
Angelman syndrome	*UBE3A*	*dube3A*§	E3-ubiquitin ligase
Cancer			
Tuberous sclerosis	*TSC1*, *TSC2*	*tsc1*§, *tsc2*§	GAP for RHEB in TOR pathway
Endometrial carcinoma	*PTEN*	*Pten*§	Negative regulator PI3K
No known disease mutations in homologue	*LATS1*	*wts*§ (also known as *lats*)	Cyclin regulation?
Renal cancer lines	*SAV1*	*sav*§	Cyclin regulation?
No known disease mutations in homologue	*MST1*, *MST2* (also known as *STK3*)	*hpo*§	Cyclin regulation?
Bladder and colorectal cancer	RAS family genes	*Ras85D*§	RTK signalling
No known disease mutations in homologues	*SCRIB*, *LLGL1*, *DLG1*	*scrib*§, *l(2)gl*§, *dlg1*§	Cell polarity, metastasis in the presence of RAS-V12
B-cell leukaemia	*CCND1*	*CycD*§	Cell cycle
Melanoma	*CDK4*	*Cdk4*§	Cell cycle
Retinoblastoma	*RB1*	*Rbf*§, *Rbf2*	Cell cycle
Hepatocellular carcinoma	*TP53*	*hth*§ ($e<10^{-10}$)	Cell cycle
Ectodermal dysplasia	*TP73L*	*hth*§ ($e<10^{-7}$)	Cell cycle

Table 1 Categories of human disease genes well suited to analysis in *Drosophila melanogaste*r (Bier 2005)

Neurological disorders have been particularly amenable to analysis in *Drosophila*. Actually, *Drosophila* has a complex nervous system and the fly brain, similarly to

mammals, is organised into area with separated specialized functions such as learning, memory, olfaction and vision.

The anatomy and development of *Drosophila* nervous system has been extensively characterized and many tools are available to identify specific neuronal subtypes. Neuronal functions (i.e. synaptic transmission) and survival can been measured in flies, as can learning and memory.

Drosophila has been used to model neurodegenerative diseases ranging from tauopathy, Alzheimer's disease (AD), and Parkinson's disease (PD) to fragile X syndrome as well as several polyglutamine–repeat diseases such as Spinocerabellar ataxia and Huntington's disease (Muqit and Feany 2002; Marsh and Thompson 2004).

1.2 Diseases can be modeled in flies

There are three main approaches to modelling human diseases, including neurodegenerative disorders, in *Drosophila*.

Traditionally, forward-genetic approaches have been used. Mutations are selected on the basis of a neurodegenerative phenotype, and human homologues of the identified *Drosophila* gene products are plausible candidates for involvement in neurodegenerative diseases. Alternatively, 'reverse genetics' can be used. In this case, the *Drosophila* homologue of a specific gene that is implicated in a human disease is targeted, and phenotypes that result from altered expression of the gene are studied. Useful phenotypes can emerge by reducing or eliminating (knocking out) gene expression, or by overexpressing the gene product.

An even more direct path from human disease to invertebrate model is possible with certain human disorders: those caused by a toxic dominant gain-of-function mechanism. If disease is produced in humans by the action of a toxic protein, it might not be necessary, or even desirable, to manipulate the invertebrate homologue of the human disease-related gene. Instead, simple expression of the toxic human protein in the model organism might accurately model the disease. Toxic dominant mechanisms almost certainly operate in neurodegenerative disorders such as Huntington's disease and amyotrophic lateral sclerosis (ALS).

Nearly all of the current fly models of neurodegenerative diseases have been made using the GAL4/UAS (upstream activating sequence) system which allows the ectopic expression of a transgene in a specific tissue or cell type (Brand and Perrimon 1993).

In this system, a human disease-related transgene is placed under the control of the yeast transcriptional activator GAL4. In the absence of GAL4, the transgene is inactive. When flies that carry the human disease-related transgene are crossed to flies that express GAL4 in a specific tissue or cell type, the transgenic protein is made only in the tissues that have GAL4 (Figure 1).

Many cell-type and developmentally regulated GAL4 ('driver') lines exist at present, and are readily available from public stock centres. So, the effect of expressing a human disease-related transgene in many different tissues and at various developmental times can be assayed without creating many independent transgenic fly strains. This system provides a particular advantage for studying neurodegenerative disease, because the issue of cell-type specificity can be readily addressed.

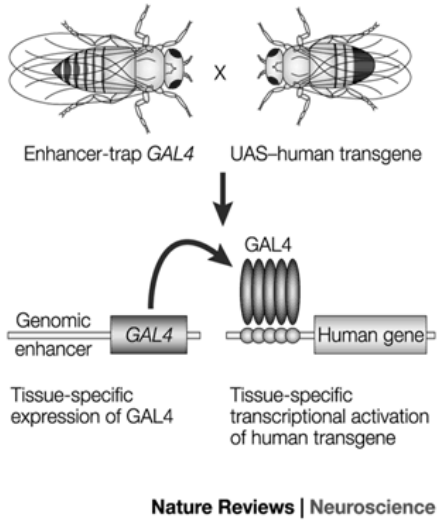

Figure 1 GAL4/UAS (upstream activating sequence) system allows the ectopic expression of a human transgene in a specific tissue or cell type[1]

[1] Two transgenic fly lines are created. In the first (UAS–human-transgene fly), the human disease-related transgene is placed downstream of a UAS activation domain that consists of GAL4-binding sites. GAL4 is a yeast transcriptional activator; in the absence of ectopically expressed GAL4, the transgene is inactive in these transgenic flies. The transgene is activated by crossing these flies to transgenic flies that express GAL4 (enhancer-trap GAL4 fly), also known as the 'drivers'. A wide array of 'driver' flies have been

Once relevant *Drosophila* models of neurodegenerative disease have been created, the genetic potential of the system can be exploited. Second-site modifier analysis identifies unlinked mutations that either suppress or enhance neurodegeneration. Such modifier genes encode proteins that are involved in the pathogenesis of the neurodegenerative process in flies, and potentially in the human disease as well. One strength of genetic analysis in *Drosophila* is that the whole cellular cascade that mediates neurodegeneration, including both specific interactors and downstream elements, can be defined. In practical terms, the phenotype that is used to select genetic modifiers should be externally visible, easily scored and involve structures that are not essential for viability. Abnormalities of the *Drosophila* eye have therefore been the phenotypes of choice in modifier screens.

Modifier identification can follow both biased and non-biased strategies. In the biased 'candidate' approach, mutations are selected on the basis of pre-existing hypotheses, and these mutations are tested for their ability to suppress or enhance neurodegeneration. Candidate testing can rapidly confirm the role of suspected mediators, but is limited by preformed hypotheses. The second approach is to do an unbiased forward-genetic screen. A forward-genetic screen interrogates the genome for mutations that modify a neurodegenerative phenotype, without bias as to possible function. Random mutations are produced by chemical or insertional mutagenesis, and the ability of these mutations to suppress or enhance the phenotype of interest is tested. The unbiased approach has the potential to identify new proteins, or to implicate previously defined cellular pathways that were not suspected to be important in neurodegenerative disease (Muqit and Feany 2002).

---

made and characterized. The GAL4 gene is placed downstream of a cell- or tissue-specific promoter. Examples include the pan-neural promoter elav (embryonic lethal, abnormal vision) or the eye-specific promoter GMR (Glass Multimer Response). So, the transgene will be activated in the progeny of this cross in a specific cell or tissur type, depending on the ‘driver’. This is especially important in studying neurodegenerative diseases, as questions regarding cell-type specific death can be investigated. Muqit, M. M. and M. B. Feany (2002). "Modelling neurodegenerative diseases in Drosophila: a fruitful approach?" Nat Rev Neurosci **3**(3): 237-43.

1.3 Hereditary Spastic Paraplegia

Hereditary spastic paraplegia (or "hereditary spastic paraparesis") (HSP) was first described by Strümpell in 1880 as a neurodegenerative disorder.

At present, HSP is used to describe a group of genetically and clinically heterogeneous neurodegenerative disorders in which the predominant feature is the progressive spasticity associated with mild weakness of the lower limbs, which may be accompanied by urinary urgency and subtle vibratory sense impairment (McDermott, White et al. 2000).

Neuropathological analysis of tissues from patients with HSP has revealed axonal degeneration of the distal portions of the corticospinal tracts and the spinocerebellar tracts, which together constitute the longest motor and sensory axons of the central nervous system (CNS) (Schwarz and Liu 1956; Behan and Maia 1974; Reid 1997).

Clinically these disorders are conventionally subdivided into "pure" (or "uncomplicated") forms, when the above features occur in isolation, and "complicated" forms in the presence of additional neurologic or systemic impairments such as mental retardation, cerebellar ataxia, dementia, optic atrophy, retinopathy, extrapyramidal disturbance, epilepsy and motor neuropathy (Harding 1993; Reid 1997). Age of symptom onset, rate of progression, and degree of disability are often variable between different genetic types of HSP, as well as within individual families in which all subjects have precisely the same HSP gene mutation.

HSPs may have autosomal dominant, recessive and X-linked inheritance (Table 2, Table 3, Table 4). To date 38 loci have been mapped on different chromosomes. Fifteen loci segregate with autosomal dominant (AD) forms, twenty follow an autosomal recessive pattern of inheritance and three *loci* lie on the X chromosome (Depienne, Stevanin et al. 2007).

Locus	Chromosome region	Gene or protein	Discriminating features	Reference
Pure forms				
SPG3A	14q12–q21	Atlastin	Predominantly early onset	MIM182600 [2,3•,4••,5]
SPG4	2p22	Spastin		MIM182601 [4••,5–8,9•,10•, 11,12•,13–16,17••]
SPG6	15q11.2–q12	NIPA1	Predominantly adult onset	MIM600363
SPG8	8q24	KIAA0196	Predominantly adult onset	MIM603563 [18•]
SPG10	12q13	KIF5A	Predominantly early onset	MIM604187 [19]
SPG12	19q13	Unknown	Predominantly early onset	MIM604805
SPG13	2q24–q34	HSP60	Predominantly adult onset	MIM605280
SPG19	9q33–q34	Unknown	Predominantly adult onset	MIM607152
SPG31	2p12	REEP1		MIM610250 [20•]
SPG33	10q24.2	ZFYVE27		MIM610244 [21•]
SPG37	8p21.1–q13.3	Unknown		[22•]
Complex forms				
SAX1	12p13	Unknown	Spastic ataxia	MIM108600 [23]
SPG9	10q23.3–q24.2	Unknown	Cataract, motor neuropathy, short stature, skeletal abnormalities, gastro-oesophageal reflux	MIM601162
SPG17	11q12–q14	BSCL2/Seipin	Silver syndrome – severe distal wasting	MIM270685 [24]
SPG29	1p31–p21		Sensorineural hearing impairment, pes cavus, neonatal hyperbilirubinemia without kernicterus, hiatal hernia	MIM609727

MIM, Mendelian Inheritance in Man at http://www.ncbi.nlm.nih.gov/sites/entrez?db=OMIM.

Table 2 Autosomal dominant forms of hereditary spastic paraplegias (Depienne, Stevanin et al. 2007)

Gene	Protein	Locus	Age at onset (years)	Associated signs	Number of families	Reference
SPG1	L1CAM	Xq28	Infancy	Corpus callosum hypoplasia, retardation, adducted thumbs, spastic paraplegia, hydrocephalus	>100 but few with the spastic paraplegia phenotype	MIM303350
SPG2	PLP	Xq21	1–18	Quadriparesis, congenital nystagmus, mental retardation, seizures	>75 but few with the spastic paraplegia phenotype	MIM312920
SPG16	Unknown	Xq11.2	Infancy	Pure (severe)	1	MIM300206

Table 3 X-linked forms of hereditary spastic paraplegias (Depienne, Stevanin et al. 2007)

Gene	Protein	Locus	Age at onset (years)	Associated signs	Origin and number of families	Reference
Pure forms						
SPG5	Unknown	8p	1–40		>12 families	MIM270800 [31]
SPG24	Unknown	13q	1		Saudi-Arabia ($n=1$)	MIM607584 [28]
SPG28	Unknown	14q	6–15		Morocco ($n=1$)	MIM609340 [29]
SPG30	Unknown	2q	12–21		Algeria ($n=1$)	MIM610357 [30]
Complex forms						
SPG7	Paraplegin	16q	11–42	Cerebellar signs, PNP, pes cavus, optic atrophy	Many	MIM602783 [26,27,32–34]
SPG14	Unknown	3q	~30	Distal motor neuropathy, mental retardation, pes cavus, visual agnosia	Italy ($n=1$)	MIM605229
SPG27	Unknown	10q	2–45	Cerebellar ataxia, PNP, mental retardation, microcephaly, facial and skeletal dysmorphia, blepharophimosis	French Canadian and Tunisia ($n=2$)	MIM609041
SPG11 (AR-HSP-TCC)	Spatacsin	15q	1–23	Mental retardation or cognitive impairment, PNP, TCC	Mediterranean basin, Japan ($n>30$)	MIM610844 [35–37,38••]
SPG15 (Kjellin syndrome)	Unknown	14q	13–23	Pigmented maculopathy, wasting, dysarthria, cerebellar signs, mental retardation	Ireland, Arabian families ($n=5$)	MIM270700 [39]
SPG20 (Troyer syndrome)	Spartin	13q	Early childhood	Mental retardation, cerebellar signs, developmental delay and short stature	Amish founder	MIM275900
SPG21 (Mast syndrome)	Maspardin	15q	20–40	Extrapyramidal syndrome, premature aging, cognitive decline, dysarthria, TCC, periventricular white matter hyperintensities, cataract, dystonia, cerebellar signs, PNP, chorea, distal wasting	Amish founder	MIM248900
SPG23 (Lison syndrome)	Unknown	1q	Early childhood	Abnormalities of skin and hair pigmentation, facial and skeletal dysmorphia, postural tremor, cognitive impairment, premature aging	Arab-Israelian ($n=1$)	MIM270750
SPG25	Unknown	6q	30–46	Prolapsed intervertebral disks, multiple disc herniation, bilateral cataract, congenital glaucoma	Italy ($n=1$)	MIM608220
SPG26	Unknown	12cen	22–42	Intellectual impairment, distal muscle wasting, dysarthria, PNP	Kuwait and Spain ($n=2$)	MIM609105
SPG32	Unknown	14q	6–7	Pontine dysraphia, mental retardation, TCC	Portugal ($n=1$)	MIM611251 [40]
TCC + epilepsy	Unknown	8q	1–7	Mental deterioration, epilepsy, TCC	Saudi-Arabia ($n=2$)	[41]
SPOAN	Unknown	11q	Infancy	Optic atrophy, PNP	Brazil ($n=1$)	MIM609541
ARSACS	Sacsin	13q	Early childhood	Ataxia, dysarthria, distal wasting, nystagmus, retinal striation, PNP	Quebec, Japan, Mediterranean basin	MIM270550 [42–47]
ARSAL	Unknown	2q	Variable	Spastic ataxia with leucodystrophy	Quebec ($n=17$)	[48]
SAX2	Unknown	17p	Variable	Cerebellar ataxia, dysarthria	Morocco, Algeria, France ($n=4$)	[49]

MIM, Mendelian Inheritance in Man at http://www.ncbi.nlm.nih.gov/sites/entrez?db=OMIM; PNP, polyneuropathy; AR, autosomal recessive; TCC, thin corpus callosum; SPOAN, spastic paraplegia, optic atrophy, and neuropathy; ARSACS, autosomal recessive spastic ataxia of Charlevoix Saguenay; ARSAL, autosomal recessive spastic ataxia with frequent leucoencephalopathy; SAX2, spastic ataxia 2.

Table 4 Autosomal recessive forms of hereditary spastic paraplegias (Depienne, Stevanin et al. 2007)

Differential diagnosis is now becoming easier because of the availability of more precise and sophisticated neuroradiological investigation techniques, biochemical tests and genetic analysis.

The very recent discovery of many HSP genes is rapidly shaping new concepts of the pathophysiologic mechanisms of HSP. Whereas the uniform clinical appearance of uncomplicated HSPs initially suggested that a common biochemical disturbance underlies most types of HSP, this appears to not be the case. Rather, it appears that very long central nervous system axons (i.e., corticospinal tracts and dorsal column fibers)

are particularly vulnerable to a number of distinct biochemical disturbances and that the highly similar clinical features of genetically diverse types of uncomplicated HSP reflect the limited repertoire of symptoms from corticospinal tracts and, to a lesser extent, dorsal column fiber disturbance.

At this stage, five different molecular processes appear to be involved in different genetic types of HSP.

1) Myelin composition affecting long, central nervous system axons. X-linked SPG2 HSP is due to proteolipid protein gene mutation, an intrinsic myelin protein (Dube, Mlodzienski et al. 1997).

2) Embryonic development of corticospinal tracts. X-linked SPG1 is due to mutations in L1 cell adhesion molecule which plays a critical role in the embryonic differentiation of corticospinal tracts guidance of neurite outgrowth during development, neuronal cell migration, and neuronal cell survival (Kenwrick, Watkins et al. 2000).

3) Oxidative phosphorylation deficit. Two HSP genes (SPG7/paraplegin and SPG13/chaperonin 60) encode mitochondrial proteins (Hansen, Durr et al. 2002). Abnormal appearing mitochondria (ragged red fibers) and cytochrome C oxidase deficient fibers are noted in muscle biopsies of some (but not all) subjects with SPG7/parapegin mutation.

4) Axonal transport. SPG10 autosomal dominant HSP is due to mutations in kinesin heavy chain (KIF5A) a molecular motor that participates in the intracellular movement of organelles and macromolecules along microtubules in both anterograde and retrograde directions (Reid, Kloos et al. 2002).

5) Cytoskeletal disturbance. Spastin (SPG4) is a microtubule severing protein whose mutations are pathogenic through a disturbance in the axonal cytoskeleton (Errico, Ballabio et al. 2002).

There is currently no “cure” for HSP. Physical therapy accompanying with a regular exercise and stretching program play an important role in treating HSP symptoms (Fink 2003). While exercise or physical therapy do not prevent or reverse the damage to the nerve fibers, it will help HSP patients in maintaining mobility, retaining or improving muscle strenght, minimizing atrophy of the muscles due to disuse, increasing endurance (and reducing fatigue), preventing spasms and cramps, maintaining or improving range of motion, and providing cardiovascular conditioning.

1.4 Atlastin

1.4.1 The SPG3A gene

Among 11 loci for ADHSP, two most common genes have been identified: SPG4 on chromosome 2p22, which accounts for approximately 40% of all pure ADHSP, and SPG3A on chromosome 14q11-q21, which is responsible for 10% of cases (Zhao, Alvarado et al. 2001). All of the SPG3A mutations described so far have occurred in autosomal dominant pure HSP families showing childhood onset (i.e. before 10 years of age). Twenty different missense mutations and one insertion have been reported in the SPG3A gene (Namekawa, Ribai et al. 2006): the predominance of missense mutations suggests that pathogenesis may be due to either a toxic gain of function, or a dominant negative effect, but haploinsufficiency cannot be excluded.

The SPG3A gene consists of 14 exons spread over 69 kb of genomic DNA, from which a 2,2 kb cDNA is transcribed.

1.4.2 Human atlastin-1

1.4.2.1 Structure

The SPG3A gene encodes a 558 amino-acid protein atlastin-1 (Zhao, Alvarado et al. 2001; Zhu, Patterson et al. 2003). Member of the dynamin superfamily of large GTPases, atlastin-1 presents a N-terminal GTPase domain that contains the four canonical GTP binding motifs of large GTPases (Praefcke and McMahon 2004), a mid-portion, two transmembrane domains and a short C-terminal region. Atlastin-1 is an integral membrane protein with both the N-terminal GTP-binding and the C-terminal domains exposed to the cytoplasm (Zhu, Patterson et al. 2003) (Figure 2).

Like many members of the dynamin/Mx/GBP superfamily (Shin, Takatsu et al. 1999; Prakash, Praefcke et al. 2000; Zhang and Hinshaw 2001; Haller and Kochs 2002), atlastin-1 forms homo-oligomers, but it is unclear if it forms dimeric or tetrameric structures (Zhu, Patterson et al. 2003).

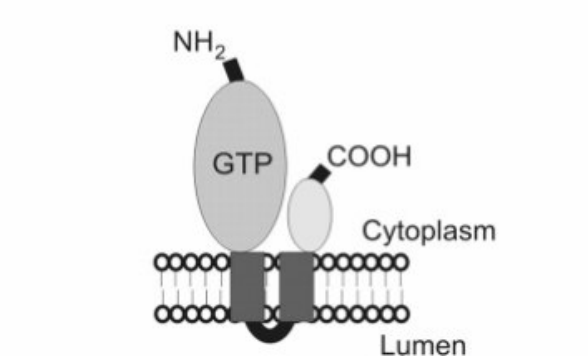

Figure 2 Schematic structure of the proposed atlastin-1 membrane topology (Zhu, Patterson et al. 2003)

1.4.2.2 Localization

The atlastin-1 protein is most abundant in brain, although it is also present at much lower levels in other tissues, including lung, smooth muscle, adrenal gland, kidney, and testis. Within the brain, atlastin-1 is prominently enriched in the lamina V pyramidal neurons in the cerebral cortex, a subpopulation of which exhibits a distal axonopathy in patients with SPG3A HSP.

At the subcellular level, atlastin-1 has been localized to Golgi cisternae and to Endoplasmic reticulum membranes (Zhu, Patterson et al. 2003; Evans, Keller et al. 2006; Namekawa, Ribai et al. 2006; Sanderson, Connell et al. 2006).

1.4.2.3 Previous studies

Atlastin-1 has been proposed to be required for Endoplasmic reticulum and Golgi apparatus morphology.

The expression, in cell cultures, of atlastin-1 mutants lacking GTPase activity, but not the expression of the wild type form, results in alterations of ER morphology which displays a more tubular phenotype. These ER structure changes are due to loss of interconnections between three-way junctions which are points of homotypic fusion events (Rismanchi, Soderblom et al. 2008).

Moreover, overexpression of both wild type and GTPase deficient atlastin-1 mutants results in fragmentation of the Golgi structure into “mini stacks” (Rismanchi, Soderblom et al. 2008).

Atlastin-1 has also been supposed to be implicated in vesicle trafficking at the ER/Golgi interface and in the maturation of the Golgi complex. Expression, in cell cultures, of atlastin-1 GTPase deficient mutants appears to prevent vesicle formation from the ER (Namekawa, Muriel et al. 2007).

Perturbation of ER and Golgi morphology and/or alteration in vesicle trafficking may result in a defective transport along axon expecially in the corticospinal neurons which present the longest axons in humans.

Experiments carried out in rat motor neurons primary cultures showed the presence of atlastin-1 in the axonal growth cones, but not at the synapses. Knock-down of atlastin-1 in these cortical neurons results in the inhibition of axon formation and elongation suggesting a possible role of atlastin-1 in neurite outgrowth during neuronal development (Zhu, Soderblom et al. 2006). Thus, the "long axonopathy" in early-onset SPG3a may results from an abnormal development of axons because of atlastin-1 loss.

1.4.2.4 Atlastin subfamily

In addition to atlastin-1 humans have two other atlastin family members: atlastin-2 and atlastin-3.

These three forms are present in a variety of rodents and higher mammals, but some species such as *Drosophila* and *C. elegans* possess only one atlastin, indicating that the three atlastins in higher species may have at least partially overlapping functions.

Atlastin -2 and atlastin-3 are highly similar structurally to atlastin-1: they are transmembrane proteins with N- and C- terminals facing the cytoplasm and they are capable of oligomerization.

While atlastin-1 is largely localized to brain, atlastin-2 and atlastin-3 are expressed at higher levels in peripheral tissues and much less so in the brain (Zhu, Patterson et al. 2003; Rismanchi, Soderblom et al. 2008). At the subcellular level, atlastin-2 and atlastin-3 show prominent localization to the Endoplasmic reticulum. Knock down of atlastin-2 and atlastin-3 in HeLa cells causes abnormalities in Golgi morphology, most commonly fragmentation; and the expression of mutant forms of atlastin-2 or -3 that lack GTPase activity results in changes of Endoplasmic reticulum morphology with loss of typical reticularization. These data suggest a possible role of atlastin-2and atlastin-3 in both Golgi and Endoplasmic reticulum morphogenesis, but they do not appear to be required for ER-to-Golgi trafficking (Rismanchi, Soderblom et al. 2008).

1.4.3 *Drosophila* atlastin (Datlastin)

The *Drosophila* genome contains a single highly conserved atlastin-1 ortholog: Datlastin (Datlastin maps to the 96A13 band of the third chromosome). As shown in Figure 3, the *Drosophila* protein reveals an extensive homology, with 56% of identity and 77% of similarity, with human atlastin-1.

```
humanatlastin   MAKNRRDRNSWGGFSEKTYEWSSEEEEPVKKAGPVQVLIVKDDHSFELDETALNRILLSE 60
datlastin       ----------------------------MGGSAVQVINASEEHTFVLNEDALSEVLMRD 31

humanatlastin   AVRDKEVVAVSVAGAFRKGKSFLMDFMLRYMYN----QESVDWVGDYNEPLTGFSWRGGS 116
datlastin       EVKDRFVCVVSVAGAFRKGKSFLLDFFLRYMYSKYVHHDATDWLGGESDPLEGFSWRGGS 91

humanatlastin   ERETTGIQIWSEIFLINKPDGKKVAVLLMDTQGTFDSQSTLRDSATVFALSTMISSIQVY 176
datlastin       ERDTTGILMWSDIFLHDYPNGDKIAIILLDTQGAFDSQSTVRDCATVFALSTMLSSVQIY 151

humanatlastin   NLSQNVQEDDLQHLQLFTEYGRLAMEETFLKPFQSLIFLVRDWSFPYEFSYGADGGAKFL 236
datlastin       NLSQNIQEDDLQHLQLFTEYGRLALADTGKKPFQRLQFLVRDWSFPYEAEYGALGGDKIL 211

humanatlastin   EKRLKVSGNQHEELQNVRKHIHSCFTNISCFLLPHPGLKVATNPNFDGKLKEIDDEFIKN 296
datlastin       KRRLEVSDKQHPELQSLRRHISSCFTEVACFLMPHPGLNVATNPKFDGRLQDITPEFKSS 271

humanatlastin   LKILIPWLLSPESLDIKEINGNKITCRGLVEYFKAYIKIYQGEELPHPKSMLQATAEANN 356
datlastin       LRSLVPMLLAPDNLVYKEISGQRVRARDLIQYFQSYMNIYKGNELPEPKSMLVATAEANH 331

humanatlastin   LAAVATAKDTYNKKMEEICGGDKPFLAPNDLQTKHLQLKEESVKLFRGVKKMGGEEFSRR 416
datlastin       LTAVAAAKELYGQLMEEVCGGTRPYLSTAHLQTEHLRVKDKALFQFAAKRKMGGEEFTEK 391

humanatlastin   YLQQLESEIDELYIQYIKHNDSKNIFHAARTPATLFVVIFITYVIAGVTGFIGLDIIASL 476
datlastin       FRKQLEDDLEEVFTNYQAHNESKNIFKAARTPAVYFACAVIMYILSGIFGLVGLYTFANF 451

humanatlastin   CNMIMGLTLITLCTWAYIRYSGEYRELGAVIDQVAAALWD-------QGSTNEALYKLYS 529
datlastin       CNLVMGVALLTLALWAYIRYSGELSDFGGKLDDFATLLWEKFMRPIYHGCMEKGIHHVAT 511

humanatlastin   AAATHRHLYHQAFPTPKSESTEQSEKKKM- 558
datlastin       HATEMAVGGGAASYRSQTSVNASNGKVKRS 541
```

Figure 3 Alignment of *H. sapiens* and *D. melanogaster* atlastin amino acids sequences. Identical residues are highlighted in red.

A *Drosophila* line containing a null mutation in Datlastin gene has been isolated (Lee, Paik et al. 2006).

Datlastin null flies (atl1) are smaller in body size and have a shorter life span than wild-type ones. Loss of Datlastin was shown to give rise to motor dysfunctions: as atl1 flies age loose general mobility. This phenotype is associated with an age-dependent degeneration of dopaminergic neurons. These data suggest that Datlastin function in dopaminergic neurons is one of the important factors in preventing paralysis and retaing mobility in *Drosophila*, but they do not clarify Datlastin cellular role.

Immunohistochemistry and electron microscopy studies carried out in our laboratory, showed that Datlastin is specifically localized to endoplasmic reticulum membranes but is absent from the Golgi apparatus (Figure 4).

Transgenic lines were therefore generated to analyse potential consequences of altering Datlastin expression levels on ER structure and function.

Ubiquitous downregulation of Datlastin levels by RNAi interference results in lethality with few escapers which display small body size and shorter life span. At the subcellular level, loss of Datlastin induces fragmentation of the ER tubular network: in control neurons the ER is organized in long tubular structures, in neurons lacking Datlastin ER profiles are severy undersized (Figure 6) However, in the absence of Datlastin Golgi morphology is not affected and vesicle trafficking is normal.

Moreover, electron microscopy analyses revealed that overexpression of Datlastin also disrupts the ER network. Tubular ER profiles normally seen in controls are absent in motor neurons overexpressing Datlastin where ER membranes appear to be fused forming expanded cisternae (Figure 5). Such disruption of ER architecture strongly impacts ER function resulting in impairment of transport out of the ER. Because loss of Datlastin causes ER fragmentation, whereas overexpression appears to induce excess fusion of ER membranes, these results suggest that Datlastin may be involved in a process termed homotypic fusion of ER membranes.

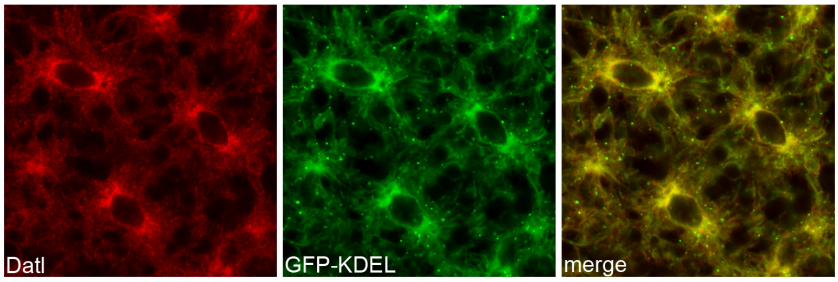

Figure 4 Datlastin is localized on ER membranes

In syncitial blastoderm embryos anti-Datlastin immunofluorescence (red) overlaps with that of the ER reporter GFP-KDEL (green).

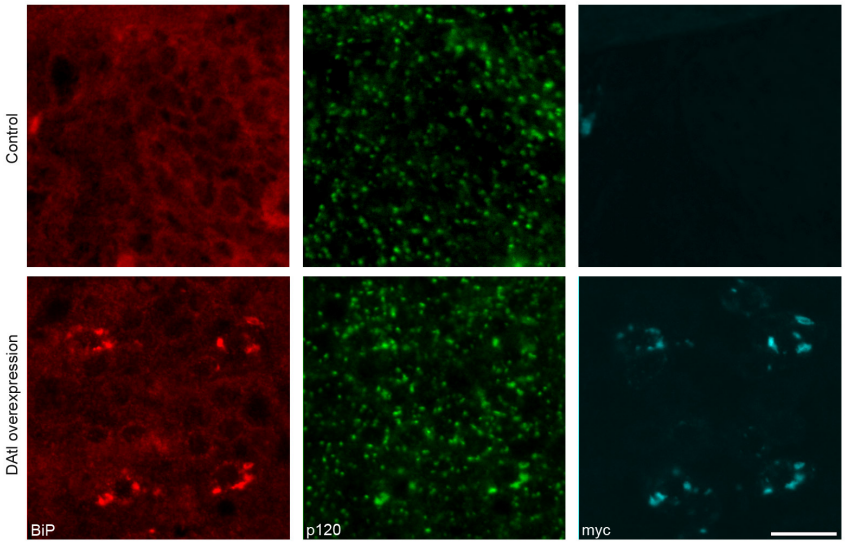

Figure 5 Datlastin overexpression induces phenotypes consistent with hyperfusion of ER membranes

Control and D42-Gal4/+;UAS-Datlastin-Myc/+ third instar larva ventral ganglia were labeled with anti-Myc to detect transgenic Datlastin, anti-BiP and anti-p120 antibodies to visualize ER and Golgi, respectively. High magnification confocal images show that overexpression of Datlastin-Myc in motor neurons induces the formation of cytoplasmic bodies with ER identity, as indicated by labeling both with Myc and BiP. These ER bodies are never found in control neurons. Scale bar 10 um.

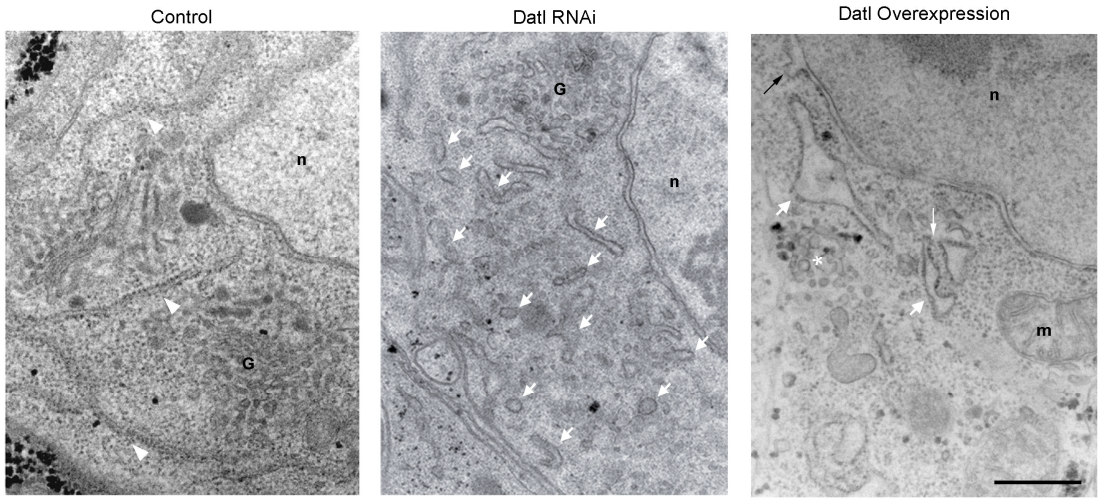

Figure 6 Effects on ER morphology due to Datlastin loss or overexpression

Morphology of the endoplasmic reticulum in motoneurons was evaluated by electron microscopy. In control neurons ER profiles display the typical tubular structure (arrows), while loss of Datlastin in tubulin-Gal4/+;UAS-Datlastin-RNAi/+ causes fragmentation of the ER resulting in shorter profiles (arrows). Golgi apparatus morphology was not affected by loss of Datlastin.

Datlastin overexpression in D42-Gal4/+;UAS-Datlastin-myc/+ motor neurons produces expanded ER elements (arrows), identifiable by the presence of ribosomes as well as dilation of the nuclear envelope (black arrow) suggesting excess membrane fusion. Scale bar 0.5 um (G, Golgi; m, mitochondrion; n, nucleus).

1.5 The dynamin superfamily

Dynamins are large GTPases that belong to a protein superfamily that, in eukaryotic cells, includes classical dynamins, dynamin-like proteins, OPA1, Mx proteins, mitofusins and guanylate-binding proteins/atlastins. They are involved in many processes such as membrane tubulation and/or fission including budding of transport vesicles, division of organelles, cytokinesis and pathogen resistance.

Dynamins are generally classified as 'large GTPases'. This is to distinguish them from the small Ras-like and other regulatory GTPases. In addition to having a larger GTPase domain, dynamin and dynamin-related proteins are distinguished from other GTPases by their oligomerization-dependent GTPase activation, their low GTP-binding affinities and the ability of many members of the dynamin family to interact with lipid membranes.

1.5.1 Overall architecture

The minimal distinguishing architectural features that are common to all dynamins and are distinct from other GTPases are the structure of the large GTPase domain (~300 amino acids) and the presence of two additional domains; the middle domain and the GTPase effector domain (GED), which are involved in oligomerization and regulation of the GTPase activity (Figure 7). The GTPase domain contains the GTP-binding motifs (G1–G4) that are needed for guanine-nucleotide binding and hydrolysis. The conservation of these motifs is absolute except for the G4 motif in guanylate-binding proteins (GBPs). The GTPase catalytic activity can be stimulated by oligomerization of the protein, which is mediated by interactions between the GTPase domain, the middle domain and the GED. In many of the dynamin-superfamily members, this basic set of domains is supplemented by targeting domains, such as: PLECKSTRIN-HOMOLOGY (PH) DOMAINS; proline-rich domains (PRDs) that bind to SRC-HOMOLOGY-3 (SH3) DOMAINS; or by sequences that target dynamins to specific organelles, such as mitochondria and chloroplasts.

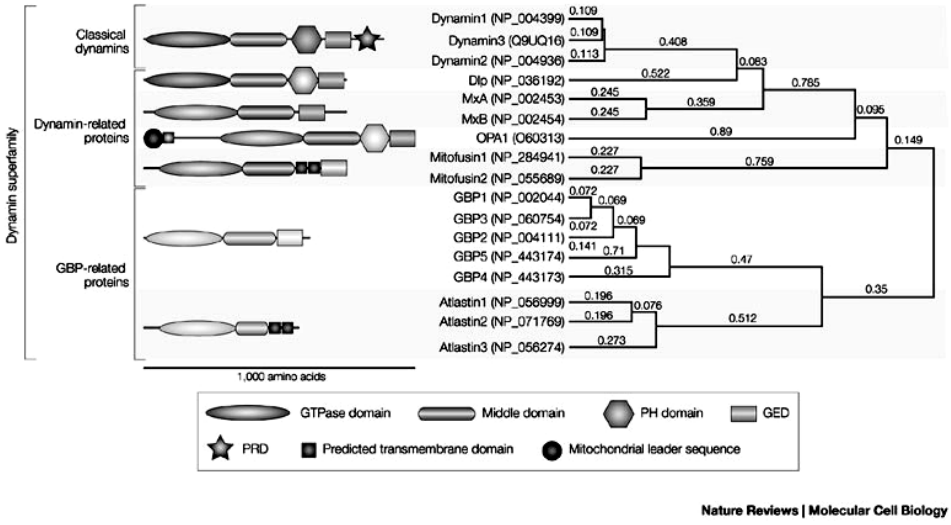

Figure 7 Domain structure of the human dynamin superfamily[2]

1.5.2 Biochemical activities of dynamins

1.5.2.1 GTPase activity

The conserved core of all related GTPbinding proteins is the GTPase domain of ~160 aminoacid residues, which consists of a mixed six-stranded β-sheet that is surrounded by five α-helices. The Ras protein, which has 184 amino-acid residues, is considered to be the minimal GTP-binding protein. The biochemical properties and biological functions of many GTP-binding proteins are influenced by insertions in their GTPase domain. In the dynamin family, the GTPase domain is extended to ~300 amino-acid residues, the structure of which has been solved by Niemann and colleagues (Niemann,

[2] All dynamins contain a GTPase domain that binds and hydrolyses GTP, a middle domain and a GTPase effector domain (GED) that are involved in oligomerization and stimulation of GTPase activity. Additionally, most dynamins contain a domain for interactions with lipid membranes. This can be a pleckstrin-homology (PH) domain, a transmembrane domain or a sequence for lipid attachment. Classical dynamins contain a proline-rich domain (PRD) at the carboxyl terminus that interacts with Src-homology-3 (SH3) domains. Human dynamin-superfamily members have been grouped according to their domain structure and accession numbers are shown. The family tree was calculated in MacVector using the tree building method with Poisson-corrected distances. DLP, dynamin-like protein 1; GBP1, guanylate-binding protein 1; OPA1, optic atrophy 1. (from Nature, 146, February 2004, volume 5).

Knetsch et al. 2001). Dynamins are characterized by their low affinity for GTP and their even lower affinity for GDP. Under physiological conditions, the protein is predicted to be constitutively loaded with GTP, but the protein will also be very sensitive to the energy status of the cell (Krishnan, Rikhy et al. 2001). This contrasts with the Ras-like GTPases, which have a high affinity for GTP and GDP and require guanine nucleotide-exchange factors (GEFs) to catalyse nucleotide exchange.

1.5.2.2 Oligomerization-dependent GTPase activity

Dynamins are different from Ras-like GTPases in that oligomerization stimulates the GTPase activity once a 'critical mass' is reached, and the resulting GTPase activity resembles a chain reaction (there is cooperativity in the GTP hydrolysis). Ras-like regulatory GTPases do not oligomerize: their GTPase activity is stimulated by the binding of GTPase-activating proteins (GAPs). For the oligomerized (assembled) form of dynamin, dynamin itself is the GAP.

1.5.2.3 Membrane binding that precedes oligomerization dependent GTPase activity

Ras GTPase activity is controlled by GAPs, whereas the GTPase activity of dynamin is controlled by self-oligomerization. Fortunately for the cell, futile cycles of dynamin GTP hydrolysis are prevented, as the oligomerization is regulated by membrane recruitment of dynamin to its sites of action. The PH domain of classical dynamins is responsible for their interaction with negatively charged lipid membranes. The affinity of a single PH domain for head groups is low (about 1 mM for inositol-1,4,5-trisphosphate) compared to other PH domains (Klein, Lee et al. 1998; Lemmon and Ferguson 2000). So the strong binding of dynamin to lipids relies on high avidity caused by the oligomerization of the protein. This low affinity of unassembled dynamin for lipids and its oligomerization after lipid binding ensures that there is tight control of GTPase activation. This feature of 'oligomerization dependent GTPase activity on membrane binding' can probably be extended to the dynamin superfamily.

1.5.2.4 Main functions of the dynamin superfamily

The dynamin superfamily is subdivided into 'classical dynamins' and 'dynamin-related proteins'. Classical dynamins are typified by the dynamin proteins that function in the

budding of clathrin-coated vesicles (CCVs) at the plasma membrane, cleavage furrow, Golgi and endosome, but also in nonclathrin-mediated budding events at caveolae and phagosomes.

Dynamin-related proteins cover a much wider range of dynamin homologues. Dynamin-like proteins are involved in division of organelles such as mitochondria and peroxisomes. The OPA1 (optic atrophy 1,) and mitofusin families are also involved in mitochondrial fusion, and therefore antagonize the function of Dlp. The Mx family are induced by interferons and confer resistance against RNA viruses. Human MxA localizes to the smooth endoplasmic reticulum and also interacts with viral ribonucleoproteins. Plants contain many different dynamin proteins. Some of them have similar functions to those in animals (for example, budding of CCVs), but others have functions that are unique to plants, such as formation of the cell plate or chloroplast division (Praefcke and McMahon 2004).

1.6 Membrane fusion

Membrane fusion is the process whereby two separate lipid bilayers merge to become one. It is essential for communication between membrane-delineated compartments in all eukaryotic cells. The best-studied process involving membrane fusion is exocytosis, whereby vesicles fuse with the limiting membrane of a cell in order to release their contents (for example, hormones or neurotransmitters) into the extracellular milieu, or to deposit receptors, transporters, channels or adhesion molecules into the limiting membrane. However, large numbers of membrane-fusion events occur between intracellular compartments, and these events often involve vesicular or tubular intermediates.

Fusion can either be heterotypic (when a membrane fuses with a dissimilar type of compartment; for example, synaptic vesicle exocytosis) or homotypic (when the same compartment fuses with itself, for example endosome–endosome fusion). More enigmatic processes involve the fusion of larger membrane-bound compartments, including whole cells in the case of syncytium formation. Furthermore, enveloped viruses gain entry into the cytosol by fusing their limiting membranes with host cell membranes.

It is now believed that most, if not all, biological membrane fusion proceeds through a hemifusion intermediate (Figure 8). According to this mechanism, an intermediate stage of membrane fusion is the merger of only the outer monolayers, with full fusion resulting in complete bilayer merging. Membrane-fusion intermediates are regulated by cellular proteins that manifest their activity through the promotion of membrane–membrane proximity, by bending and remodelling membranes, or by acting upstream to regulate the lipid or protein composition of the respective lipid bilayers.

Several energy barriers have to be overcome for fusion to occur. One energetically demanding process is to bring about the close apposition of two membranes, which requires protein clearance and the bringing together of repulsive membrane charges. The energy barriers related to curvature deformations during hemifusion-stalk and fusion-pore formation and expansion must also be overcome. The role of fusion proteins is to lower these barriers at the appropriate time and place to allow the regulation of the fusion process.

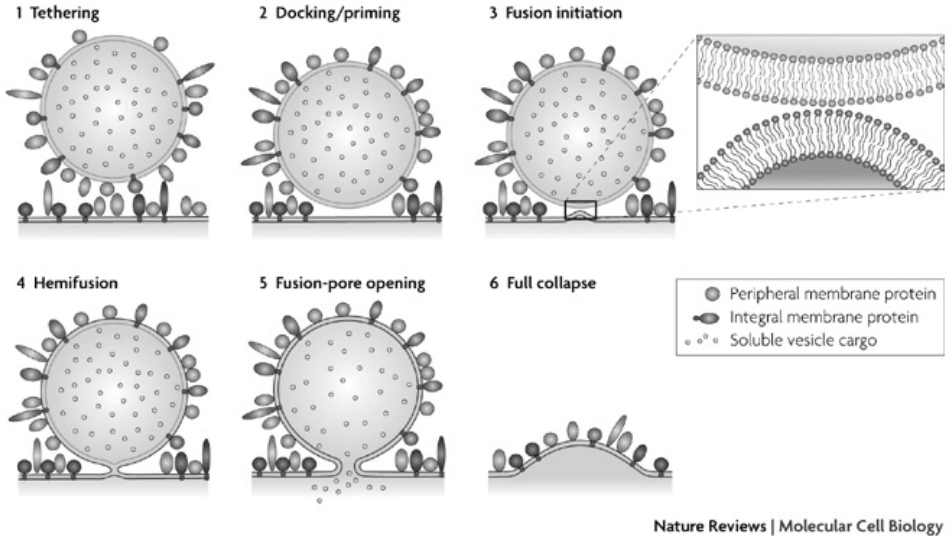

Figure 8 Proposed steps in synaptic vesicle fusion with the plasma membrane. Most membrane-fusion events are likely to follow a similar sequence[3].

[3] Proposed steps in synaptic vesicle fusion with the plasma membrane. Most membrane-fusion events are likely to follow a similar sequence. Steps might not be as temporally delineated as indicated, but the stepwise depiction helps to conceptualize the process. All the steps indicated are regulated by cellular proteins. In step 1, the vesicle is transported and tethered to the appropriate membrane by specific tethering factors, which mediate the long-range recognition between the membranes. In step 2, the loosely tethered state is converted to a tightly docked state, bringing the membranes into closer proximity. In some specialized cells docking is followed by a priming step, during which the fusion machinery is assembled such that it can rapidly respond to a trigger (for example, changes in the Ca^{2+} concentration). Docking should also entail the generation of protein-denuded membranes. In step 3, the high-energy barrier must be lowered to initiate membrane fusion and some membrane stress, such as curvature stress, probably facilitates the reaction. In addition, the distance between the two membranes has to be further decreased in order to bring the membranes into direct contact. Indeed, bilayers have been proposed to fuse when they are separated by ~1 nm. In step 4, hemifusion occurs. Hemifusion is the defining step of this fusion model; in it apposing monolayers merge, whereas distal monolayers do not. In step 5, fusion-pore opening results from the further merger of the two distal monolayers and the release of vesicle content is initiated. In step 6, as a consequence of fusion-pore expansion, the vesicular membrane collapses into the plasma membrane and loses its identity. Martens, S. and H. T. McMahon (2008). "Mechanisms of membrane fusion: disparate players and common principles." Nat Rev Mol Cell Biol **9**(7): 543-56.

Numerous membrane-fusion processes have been extensively studied and many molecules that are involved in fusion have been identified (Figure 9). From these studies it is clear that there are distinct and structurally unrelated membrane-fusion molecules. Despite this, there are general principles that operate in all fusion events.

Membrane-fusion events generally require molecules that tether and dock membranes and bring them into close proximity, molecules that locally disturb the lipid bilayers (for example, by the induction of extreme membrane curvature) in order to reduce the energy barriers for fusion, and molecules that give directionality to the process. The driving force for membrane fusion can come from many sources — for example, from the energy that is derived from protein–lipid interactions or from protein–protein interactions, and ultimately these reactions will have been primed by ATP. Directionality might be achieved by fusion protein folding. In addition, curvature stress that promotes fusion-stalk formation will be relieved during fusion-pore opening and expansion, again giving directionality to the process from the beginning. The different activities listed above do not have to be handled by different proteins, so the same molecules that promote hemifusion-stalk formation might promote fusion-pore expansion. The membrane fusion events are divided into SNARE dependent membrane-fusion and SNARE independent membrane-fusion (viral fusion, mitochondria fusion and cell-cell fusion).

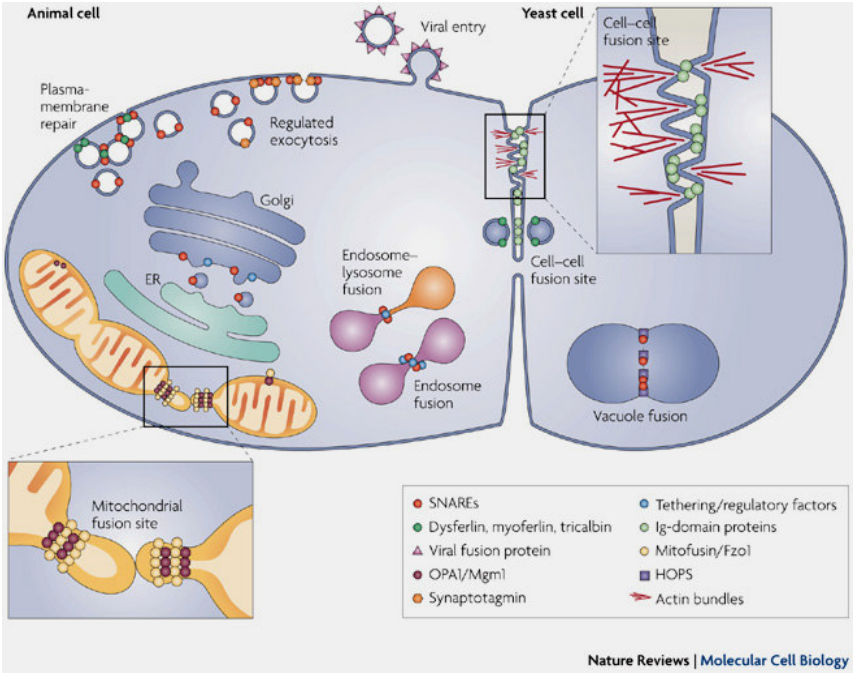

Figure 9 Cell membrane fusion events[4]

---

[4] Membrane fusion in the secretory pathway and in the endosomal and lysosomal systems depends on SNAREs, which are assisted by tethering and regulatory factors that are generally required for efficient SNARE function. During Ca^{2+}-dependent exocytosis the SNAREs are assisted by synaptotagmins, and in endosome fusion they are assisted by the Rab5 effector EEA1. SNAREs and tethering/regulatory factors are replaced by viral fusion proteins in enveloped viruses and by immunoglobulin (Ig)-domain-containing proteins in many cell–cell fusion events. The actin cytoskeleton has also been implicated in membrane fusion and in particular in cell–cell fusion, where it might stabilize the microvilli. Furthermore, multiple-C2-domain (MC2D) proteins such as tricalbin in yeast and myoferlin in mammals have been proposed to function during plasma-membrane repair during leaky cell–cell fusion. Yeast vacuole fusion requires SNAREs and the tethering factor HOPS (homotypic fusion and vacuole protein sorting). Mitochondrial fusion is mediated by the large GTPases mitofusin and OPA1 of the dynamin superfamily. Mgm1 and Fzo1 are the yeast orthologues of OPA1 and mitofusin, respectively. Plasma-membrane repair is initiated by the influx of Ca^{2+} into the cytoplasm and is mediated by the rapid and local fusion of small vesicles with each other and with the plasma membrane. The MC2D protein dysferlin has been shown to be required for this fusion. The involvement of SNAREs in plasma-membrane repair has not been explicitly shown. ER, endoplasmic reticulum (Martens S. and H. T. McMahon, 2008).

Ibid.

1.6.1 SNARE dependent membrane-fusion

SNARE superfamily proteins are essential for many intracellular membrane-fusion events.

Most SNAREs are small type II membrane proteins. The majority of the SNARE protein is exposed in the cytoplasm, followed by a single membrane-spanning region and few amino acids, facing either the lumen of an intracellular compartment or the extracellular side. Some SNAREs lack a membrane-spanning region, but are attached to the membrane by posttranslational acyl modifications.

According to their function, SNAREs have been classified as v- and t- SNAREs, because they operate on opposing membranes, usually on a transport vesicle and a target membrane. Distinct trafficking steps employ different v-/t-SNARE complexes, thus the intracellular distribution of SNAREs provides a rodmap for membrane trafficking (for review (Malsam, Kreye et al. 2008; Martens and McMahon 2008). The assembly of cognate v-/t- SNAREs between two membranes generates trans-SNARE complexes or SNAREpins, which bring the lipid bilayer in close proximity and drive membrane fusion. The structural mechanism underlying SNAREpin formation is the assembly of a highly stable four-helix bundle. The helix-forming units are so-called SNARE motifs. Each SNARE motifs (streches of 60-70 amino acids containg heptad repeats) contributes one helix to the four-helix bundle and the helices are all aligned in parallel. The folding of this bundle is thought to drive the fusion reaction.

v- and t-SNARES are “consumed” during the fusion reaction, but are reused-recycle for repetitive rounds of transport. Recycling is mediated by a molecular machinery that dissociates the extremebly stable v-/t- SNAREs complexes residing in a single lipid bilayer. SNAPs and NSF are cytosolic proteins which target cis-SNARE complexes at all transport event. SNAPs function as adaptors between SNAREs and NSF. NSF is an ATPase. ATP-hydrolisys by NSF dissociates the SNAP-SNARE complex and the four helix SNARE bundle.

The reconstitution of SNAREs into liposomes and the expression of flipped SNAREs on the cell surface have shown that cogante v- and t-SNAREs are sufficient to fuse artificial lipid bilayers (liposomes) and biological membranes (entire cells) (Weber, Zemelman et al. 1998; Hu, Ahmed et al. 2003). However, SNAREs never function

alone, and in ever fusion event that has been analysed in detail, other molecules are required for efficient membrane fusion.

SNAREs protein are responsible for yeast vacuole fusion; homotypic endosomal fusion; heterotypic endosome-lysosome fusion; heterotypic fusion between ER and Golgi and the well characterized synaptic vesicle fusion (Figure 10)

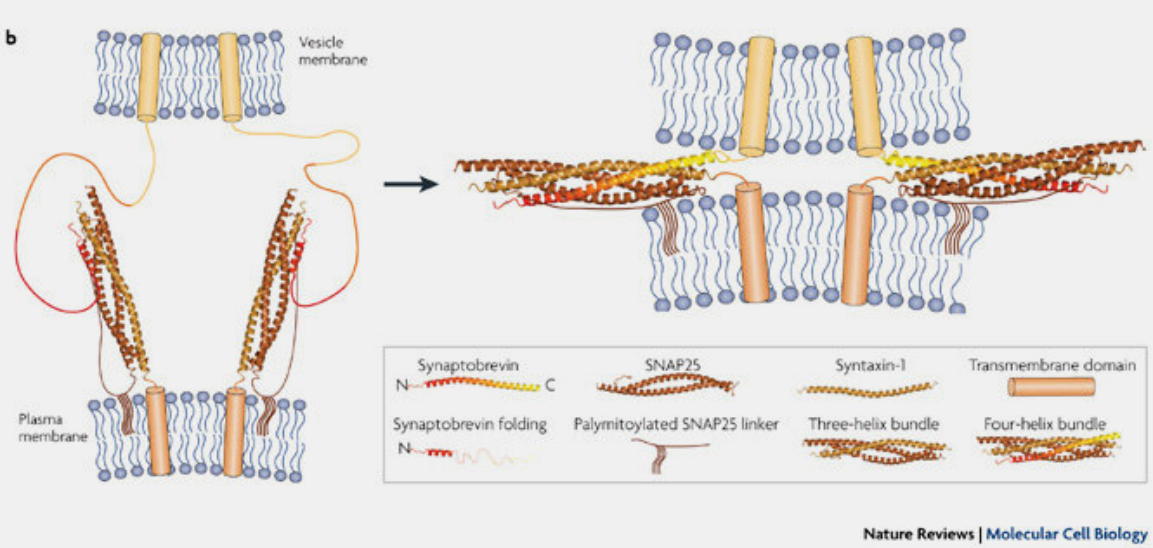

Figure 10 SNARE-dependent membrane fusion[5]

[5] SNARE-dependent membrane fusion involves the final formation of a four-helix bundle with helices contributed by three or four different SNARE proteins. Shown is the formation of the neuronal SNARE complex of vesicular synaptobrevin with plasma-membrane SNAP25 and syntaxin-1. SNAP25 and syntaxin-1 can form a three-helix bundle (the intermediate structure shown on the left has not been structurally determined and so is hypothetical). This can act as the acceptor for synaptobrevin, which is unstructured before assembly and folds from the N terminus to the C terminus (see the initiation of helix assembly on the left) to form the mature SNARE complex. This folding into the fourth strand of the four-helix bundle is proposed to bring the membranes into close apposition (right) (Martens S. and H. T. McMahon, 2008).

1.7 Homotypic ER fusion

The endoplasmic reticulum (ER) is arguably the most complex, multifunctional organelle of eukaryotic cells. Proteins are translocated across the ER membrane, and are folded and modified before they traverse the secretory pathway. The ER also plays a central role in other important processes, including Ca2+ sequestration, signaling and lipid synthesis. It is a complex structure that can have an extremely large surface area (Voeltz, Rolls et al. 2002). It is composed of membrane sheets that enclose the nucleus (the nuclear envelope) and an elaborate interconnected network in the cytosol (the peripheral ER) (Figure 11).

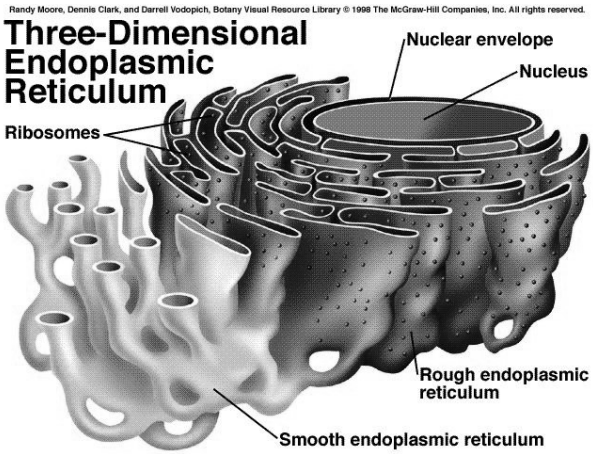

Figure 11 Three-dimensional Endoplasmic reticulum structure

During interphase, the peripheral ER in somatic cells consists of a polygonal network of interconnected tubules and cisternae.

This network appears to emanate from the outer leaflet of the nuclear envelope and spread throughout the cytosol. The fine structure, spatial distribution and abundance of the peripheral ER vary among cell types, reflecting specialized functional requirements. In spite of its continuous appearance, the ER is organized into functionally and morphologically distinct domains. The rough ER, so named for the studded appearance of ribosomes bound to its surface, is involved in the synthesis of secretory and membrane proteins. The smooth ER is ribosome free, and the transitional ER is where carrier vesicles are formed (Baumann and Walz 2001).

The elaborate architecture of the ER reflects its complex roles and maintenance of this architecture is instrumental for proper execution of ER functions. The ER is continuosly rearranged while maintaining its characteristic structure (Voeltz, Rolls et al. 2002) and ER dynamics are the result of movement of tubules along the cytoskeleton (Waterman-Storer and Salmon 1998; Lane and Allan 1999), and homotypic fusion events (Dreier and Rapoport 2000; Voeltz, Prinz et al. 2006; Anderson and Hetzer 2007). Nevertheless, the cytoskeleton is not required for the *de novo* formation of a tubular network *in vitro* (Dreier and Rapoport 2000) and is not necessary for the maintenance of the existing ER network (Terasaki, Chen et al. 1986; Prinz, Grzyb et al. 2000). In contrast, homotypic membrane fusion activity is essential for maintaining the typical structure of the ER (Vedrenne and Hauri 2006) and its failure prevents the formation of the intact ER network (Dreier and Rapoport 2000; Anderson and Hetzer 2007). The fusion of intersecting tubules contributes to the formation of new polygons, whereas the fusion of two junctional tubules results in the net loss of a polygon within the peripheral ER network. The nuclear envelope of most higher eukaryotic cells breaks down during prometaphase, and homotypic membrane fusion is required to reassemble daughter nuclei at the end of mitosis. Analysis of these fusion reactions suggests that the mechanism is similar to that of other membrane fusion reactions. Homotypic fusion of ER membranes depends on GTP hydrolysis and does not require cytosolic protein or ATP (Dreier and Rapoport 2000; Voeltz, Prinz et al. 2006; Anderson and Hetzer 2007), suggesting the involvement of a GTP-dependent fusion machinery associated with the ER membranes. A role in homotypic fusion has been propose for the p97 protein complex (Uchiyama, Jokitalo et al. 2002; Kano, Kondo et al. 2005; Kano, Kondo et al. 2005) and BNIP1 (Nakajima, Hirose et al. 2004), however their involvement is indirect and neither exhibits GTPase activity. Thus, the molecular components of the GTP-dependent activity responsible for homotypic fusion of ER membranes have not yet been identified.

2 Research aim

Mutations of the SPG3a gene, which encodes for the large oligomeric GTPase Atlastin-1, are responsible for the most severe form of Hereditary Spastic Paraplegia (HSP), a group of genetically and clinically heterogeneous neurodegenerative disorders in which the predominant feature is the progressive spasticity associated with mild weakness of the lower limbs. In our laboratory, a *Drosophila* model to study Atlastin-1 cellular role has been created. The presence in the *Drosophila* genome of a single high conserved Atlastin ortholog (Datlastin) combined with the excellent genetic manipulation available in flies and the high conservation of cellular pathways between flies and vertebrates make *Drosophila* a valuable system to investigate Atlastin role. Experiments carried out *in vivo* have shown that Datlastin is required in the process of homotypic fusion of Endoplasmic reticulum membranes. Homotypic fusion activity is critical for both the biogenesis and maintenance of the ER and a proper ER architecture is essential for ER functionality. Datlastin resides exclusively in the ER and in *Drosophila*, Datlastin depletion causes ER fragmentation, while its overexpression results in the formation of expanded ER elements consistent with excessive fusion of ER membranes.

The aim of this work is to analyse the mechanism whereby Datlastin promotes homotypic fusion of ER membranes by combining genetic, biochemical, biophysical and molecular modelling approaches and to propose a model of Datlastin action.

3 Methods

3.1 Molecular biology techniques: generation of constructs

The Datlastin cDNA was previously obtained from *Drosophila* RNA extract and cloned in the pDrive cloning vector (Qiagen): Datlastin/pDrive.

3.1.1 Cloning of the Datlastin cDNA fragment in pcDNA3 Zeo+ plasmid: Datlastin-HA/pcDNA3.1/Zeo(+) and Datlastin-Myc/ pcDNA3.1/Zeo(+)

pcDNA3.1/Zeo(+) is a plasmid designed for high level expression in a variety of mammalian cell lines (see Appendix C 3.10). Two differently tagged Datlastin forms were cloned in the pcDNA3.1/Zeo(+) plasmid: Datlastin-HA and Datlastin-Myc.
To insert the HA epitope in the C-terminus of Datlastin, cDNA was amplified from Datlastin/pDrive vector using the following primers:

Forward

ForAtlATGEcoRI 5'AGCTGAATTCATGGGCGGATCGGCAGTGCAGG3'

Reverse

THM XhoI3' R HA 5'AGCTCTCGAGCTAGCCCGCATAGTCAGGAACATCGTATGG GTATGACCGCTTCACCTTGCCATTG3'

To insert the Myc epitope in the C-terminus of Datlastin, cDNA was amplified from Datlastin/pDrive vector using the following primers:

Forward

ForAtlATGEcoRI 5'AGCTGAATTCATGGGCGGATGGGCAGTGCAGG3'

Reverse

THM XhoI3' R Myc 5'AGCTCTCGAGCTACAGATCTTCTTCAGAAATAAGTTTTTGTT CTGACCGCTTCACCTTGCCATTG3'

To generate each of these two constructs the protocol used was the following:

PCR

Component	Volume/ 50 ul reaction
5X Phusion HF buffer	10 ul
Datlastin/pDrive template (50 ng/ul)	1 ul
Forward (10 uM)	1 ul
Reverse (10 uM)	1 ul
10 mM dNTPs	1 ul
Phusion DNA polymerase (2 U/µl)	0.5 ul
H_2O	add to 50 ul

PCR cycle

Cycle step	Temperature	Time	
Initial denaturation	98°C	30 seconds	
Denaturation	98°C	10 seconds	30 cycles
Annealing	57°C	20 seconds	
Extension	72°C	1 minute	
Final extension	72°C	10 minutes	

Restriction reactions

pcDNA3.1/Zeo(+) plasmid and Datlastin-HA or Datlastin-Myc PCR fragments were digested with EcoRI and XhoI restriction enzymes in the following reactions:

Component	Volume/ 50 ul reaction	Component	Volume/ 50 ul reaction
Datlastin PCR fragment (50ng/ul)	20 ul	pcDNA3.1/Zeo(+) plasmid (100ng/µl)	5 ul
EcoRI (10U/ul)	2 ul	EcoRI (10U/ul)	2 ul
XhoI (10U/ul)	2 ul	XhoI (10U/ul)	2 ul
10X L buffer	5 ul	10X L buffer	5 ul

H_2O	add to 50 ul	H_2O	add to 50 ul

Mixed products were incubated at 37°C for 1 hour and successively separated by electrophoresis through a 1% agarose gel. The bands corresponding to the Datlastin PCR fragment and pcDNA3.1/Zeo(+) plasmid were cut from gel and purified using the QIAquick Gel Extraction Kit Qiagen). Purified DNA products were eluted in 10 µl of elution buffer.

The purified DNA fragments were ligated as follows:

Ligation

Component	Volume/ 10 ul reaction
Purified pcDNA3.1/Zeo(+) plasmid (100ng/ul)	1 ul
Purified Datlastin fragment (50 ng/ul)	4 ul
10X Ligation buffer	1 ul
Ligase enzyme (Invitrogen)	2 ul
H_2O	add to 10 ul

The mixture was incubated at 16°C for 1 hour.

Transformation

Ligation mixture was used for transformation of chemically competent DH5alpha cells (Invitogen). Transformed bacteria were plated on LB–ampicillin agar plates and incubated overnight at 37°C. 10 colonies for each construct were grown in LB medium with ampicillin. Plasmid DNA was successively purified by minipreparation protocol (see Appendix A 3.8.2) and tested by restriction analysis for the right insertion.

Purification of Datlastin-HA/pcDNA3.1/Zeo(+) and Datlastin-Myc/ pcDNA3.1/Zeo(+)

Plasmid DNA were purified from an overnight culture using a "Midi" plasmid purification kit, according to Qiagen Plasmid Midi purification protocols. The final pellets were re-suspended in 50 ul of TE buffer.

3.1.2 Cloning of Datlastin fragments in pcDNA3/Zeo(+) plasmid

Four Datlastin fragments were cloned in pcDNA3.1/Zeo(+) plasmid: Datl$^{1-303}$ encompassing the GTP binding domain, Datl$^{304-422}$ containing the putative coiled-coil, Datl$^{423-541}$ which includes the two transmembrane domains and the short C-terminus sequence, and Datl$^{304-541}$.

For each fragment were generated two constructs: one for the expression of a HA tagged form, and the other for the expression of a Myc tagged form.

The primers used were the following:

Datl $^{1-303}$	Forward	
	ForAtlATGEcoRI	5'AGCTGAATTCATGGGCGGATCGGCAG TGCAGG3'
	Reverse	
	GBP XhoI3'Myc R	5'AGCTCTCGAGCTACAGATCTTCTTCA GAAATAAGTTTTTGTTCGTACTGGATGA GATCGCGGGC3'
	GBP XhoI3'HA R	5'AGCTCTCGAGCTAGCCCGCATAGTCA GGAACATCGTATGGGTAGTACTGGATG AGATCGCGGGC3'
Datl $^{304-422}$	Forward	
	Pfam EcoRI5' F	5'AGCTGAATT**C**CCATAATGTTCCAATC GTACATGAACATC3'
	Reverse	
	Pfam XhoI 3' Myc R	5'AGCTCTCGAGCTACAGATCTTCTTCA GAAATAAGTTTTTGTTCTGTCCGTGCTG CCTTAAAGATG3'
	Pfam XhoI 3' HA R	5'AGCTCTCGAGCTAGCCCGCATAGTCA GGAACATCGTATGGGTATGTCCGTGCT GCCTTAAAGATG3'
Datl $^{423-541}$	Forward	
	THM EcoRI5' F	5'AGCTGAATTCCCATAATGGCACGGAC ACCGGCGGTGTAC3'

	Reverse	
	THM XhoI3' Myc R	5'AGCTCTCGAGCTACAGATCTTCTTCA GAAATAAGTTTTTGTTCTGACCGCTTCA CCTTGCCATTG3'
	THM XhoI3' HA R	5'AGCTCTCGAGCTAGCCCGCATAGTCA GGAACATCGTATGGGTATGACCGCTTC ACCTTGCCATTG3'
Datl $^{304-541}$	Forward	
	PFAM EcoRI5' F	5'AGCTGAATTCCCATAATGTTCCAATC GTACATGAACATC3'
	Reverse	
	THM XhoI3' Myc R	5'AGCTCTCGAGCTACAGATCTTCTTCA GAAATAAGTTTTTGTTCTGACCGCTTCA CCTTGCCATTG3'
	THM XhoI3' HA R	5'AGCTCTCGAGCTAGCCCGCATAGTCA GGAACATCGTATGGGTATGACCGCTTC ACCTTGCCATTG3'

For the generation of each of these constructs, the protocol was the following:

PCR

Component	Volume/ 50 ul reaction
5X Phusion HF buffer	10 ul
Datlastin/pDrive template (50 ng/ul)	1 ul
Forward (10 uM)	1 ul
Reverse (10 uM)	1 ul
10 mM dNTPs	1 ul
Phusion DNA polymerase (2 U/µl)	0.5 ul
H_2O	add to 50 ul

PCR cycle

Cycle step	Temperature	Time	
Initial denaturation	98°C	30 seconds	
Denaturation	98°C	10 seconds	30 cycles
Annealing	57°C	20 seconds	
Extension	72°C	30 sec / 1 Kb	
Final extension	72°C	10 minutes	

Restriction reactions

pcDNA3.1/Zeo(+) plasmid and PCRs of Datlastin fragments were digested with EcoRI and XhoI restriction enzymes in the following reactions:

Component	Volume/ 50 ul reaction	Component	Volume/ 50 ul reaction
PCR Datlastin fragment (50ng/ul)	20 ul	pcDNA3.1/Zeo(+) plasmid (100ng/µl)	5 ul
EcoRI (10U/ul)	2 ul	EcoRI (10U/ul)	2 ul
XhoI (10U/ul)	2 ul	XhoI (10U/ul)	2 ul
10X L buffer	5 ul	10X L buffer	5 ul
Add H_2O	to 50 ul	Add H_2O	to 50 ul

Mixed products were incubated at 37°C for 1 hour and successively separated by electrophoresis through a 1% agarose gel. The bands corresponding to the PCRs of Datlastin fragments and to pcDNA3.1/Zeo(+) plasmid were cut from gel and purified using the QIAquick Gel Extraction Kit (Qiagen). Purified DNA products were eluted in 10 µl of elution buffer and ligated as follows:

Ligation

Component	Volume/ 10 ul reaction
Purified pcDNA3.1/Zeo(+) plasmid	1 ul

(100ng/ul)

Purified Datlastin fragment (50 ng/ul)	4 ul
10X Ligation buffer	1 ul
Ligase enzyme (Invitrogen)	2 ul
H_2O	add to 10 ul

The mixture was incubated at 16°C for 1 hour.

Transformation

Ligation mixture was used for transformation of chemically competent DH5 alpha cells (Invitogen).Transformed bacteria were plated on LB–ampicillin agar plates and incubated overnight at 37°C. 10 colonies for each construct were grown in LB medium with ampicillin. Plasmid DNA was successively purified by minipreparation protocol (see 3.8.2) and tested by restriction analysis for the right insertion.

Plasmid purification

Expression vectors were purified from an overnight culture using a "Midi" plasmid purification kit, according to Qiagen Plasmid Midi purification protocols. The final pellets were re-suspended in 50 ul of TE buffer.

3.1.3 Site specific mutagenesis

To introduce specific nucleotide substitutions in Datlastin cDNA, site-directed mutagenesis was performed using Pfu Ultra HF DNA polymerase (Startagene).

The basic procedure utilizes a supercoiled double-stranded DNA (dsDNA) vector with an insert of interest and two synthetic oligonucleotide primers containing the desired mutation. The oligonucleotide primers, each complementary to opposite strands of the vector, are extended during temperature cycling by the Pfu Ultra DNA polymerase polymerase. Pfu Ultra DNA polymerase replicates both plasmid strands with high fidelity and without displacing the mutant oligonucleotide primers. Incorporation of the oligonucleotide primers generates a mutated plasmid containing staggered nicks. Following temperature cycling, the product is treated with DpnI. The DpnI endonuclease (target sequence: 5´-Gm6ATC-3´) is specific for methylated and

hemimethylated DNA and is used to digest the parental DNA template and to select for mutation-containing synthesized DNA. DNA isolated from almost all *E. coli* strains is dam methylated and therefore susceptible to DpnI digestion. The nicked vector DNA containing the desired mutations is then transformed into XL1-Blue chemiocompetent cells.

PCR reaction

Component	Volume/ 50 ul reaction
10X PfuUltra HF reaction buffer	5 ul
Datlastin-HA/pcDNA3.1/Zeo(+) (50 ng/ul) or Datlastin-Myc/pcDNA3.1/Zeo(+) (50 ng/ul)	1 ul
Forward (10 uM)	1 ul
Reverse (10 uM)	1 ul
10 mM dNTPs	1 ul
Pfu Ultra HF DNA polymerase (2.5 U/ ul)	1 ul
H_2O	add to 50 ul

PCR cycle

Cycle step	Temperature	Time	
Initial denaturation	95°C	1 minute	
Denaturation	95°C	50 seconds	18 cycles
Annealing	52°C	50 seconds	
Extension	68°C	10 minutes	
Final extension	68°C	30 minutes	

Following temperature cycling, the reaction was placed on ice for 2 minutes.

1 µl of the DpnI restriction enzyme (10 U/µl) was added directly to the amplification.

The reaction was mixed by pipetting the solution up and down several times, and immediately incubated at 37°C for 1 hour to digest the parental (i.e., the non mutated) supercoiled dsDNA.

Specific primers used for single and multiple substitutions

Aminoacidic Substitutions		Primers In small letters are indicated the substituted nucleotides
K51A	Forward	5'TTCCGAAAGGgcGCGAGCTTCCTGCTG3'
	Reverse	5'CAGCAGGAAGCTCGCgcCCTTTCGGAA3'
L396P	Forward	5'GAAATTCCGCAAGCAACctGAAGATGATCTTGAG3'
	Reverse	5'CTCAAGATCATCTTCagGTTGCTTGCGGAATTTC3'
L400P	Forward	5'GCAACTGGAAGATGATCcTGAGGAGGTCTTCAC3'
	Reverse	5'GTGAAGACCTCCTCAgGATCATCTTCCAGTTGC3'
F404P	Forward	5'GATCTTGAGGAGGTCccCACCAACTACCAAGC3'
	Reverse	5'GCTTGGTAGTTGGTGggGACCTCCTCAAGATC3'
L396P, L400P, F404P	Forward	5'GCAACctGAAGATGATCcTGAGGAGGTCccCACCAACTACCAAGC3'

Reverse 5'GGTGggGACCTCCTCAgGATCATCTTCag GTTGCTTGCGGAATTTC3'

Transformation

10 µl of each reaction mixture was used for transformation of chemically competent XL1-blue bacteria. Transformed bacteria were plated on LB–ampicillin agar plates and incubated overnight at 37°C.
10 colonies were grown in LB medium with ampicillin. Plasmid DNA was successively purified by minipreparation protocol (see Appendix A 3.8 for procedure).

Plasmid purification

Plasmids were purified from an overnight culture using a "Midi" plasmid purification kit, according to Qiagen Plasmid Midi purification protocols. The final pellets were re-suspended in 50 ul of TE buffer.

Sequencing of mutated Datlastin cDNA

Two clones of each construct have been sequenced to verify the presence of the specific mutations. The DNA clones were sequenced by Bio-Fab Research (http://www.biofabresearch.it/index2.html) using the following primers:

D-ATL Forward 500 5'AGCACCTGCAGCTCTTCACT3'

T7 universal primer 5'TAATACGACTCACTATAGGG3'

PfamEcoRI5' Forward 5'AGCTGAATTCCCATAATGTTCCAATCGTACATGAA CATC3'

3.1.4 Cloning the K51A Datlastin cDNA in pUAST plasmid

pUAST plasmid (Appendix C 3.10) and Datlastin cDNA carrying the K51A mutation in pcDNA3.1/Zeo(+) were digested with EcoRI and XhoI restriction enzymes in the following reactions:

Component	Volume/ 50 ul reaction	Component	Volume/ 50 ul reaction
K51A Datlastin cDNA/ pcDNA3.1/Zeo(+) (50ng/ul)	20 ul	pUAST plasmid (100ng/µl)	5 ul
EcoRI (10U/ul)	2 ul	EcoRI (10U/ul)	2 ul
XhoI (10U/ul)	2 ul	XhoI (10U/ul)	2 ul
10X L buffer	5 ul	10X L buffer	5 ul
Add H_2O	to 50 ul	Add H_2O	to 50 ul

Mixed products were incubated at 37°C for 1 hour and successively separated by electrophoresis through a 1% agarose gel. The bands corresponding to the mutated K51A Datlastin cDNA and pUAST plasmid were cut from gel and purified using the QIAquick Gel Extraction Kit (Qiagen). Purified DNA products were eluted in 10 µl of elution buffer.

The two purified DNA fragments were ligated as follows:

Component	Volume/ 10 ul reaction
Purified pUAST plasmid (100ng/ul)	1 ul
Purified K51A Datlastin cDNA fragment (50 ng/ul)	4 ul
10X Ligation buffer	1 ul
Ligase enzyme (Invitrogen)	2 ul
H_2O	add to 10 ul

The mixture was incubated at 16°C for 1 hour.

Transformation

Ligation mixture was used for transformation of chemically competent DH5 alpha cells (Invitogen). Transformed bacteria were plated on LB–ampicillin agar plates and incubated overnight at 37°C.

10 colonies were grown in LB medium with ampicillin. Plasmid DNA was successively purified by minipreparation protocol (Appendix A 3.8) and tested by restriction analysis for the right insertion.

Plasmid purification

K51A Datlastin/pUAST plasmid was purified from an overnight culture using a "Midi" plasmid purification kit, according to Qiagen Plasmid Midi purification protocols. The final pellet was re-suspended in 50 ul of TE buffer.

3.2 Cellular biology

3.2.1 HeLa cell culture

HeLa cell culture was derived from a cervical carcinoma of a 31 years old african-american woman. This was the first aneuploid line derived from human tissue maintained in continuous cell culture.

3.2.1.1 Propagation and subculturing

HeLa cells were grown in complete DMEM medium (see Appendix B 3.9) with 10% FBS serum and antibiotics, at 37°C in a CO_2 incubator.

Cells were passaged when growing logarithmically (at 70 to 80 % confluency) as follows:

- The cell layer was briefly washed twice with PBS to remove all traces of serum, then trypsin solution (see Appendix B 3.9) was added to flask and cells were observed under an inverted microscope until cell layer was dispersed (usually within 5 minutes).
- Complete growth medium was added to stop trypsin action, cells were aspirated by gently pipetting and diluted 1:10 into a new flask with new complete medium.
- For cell count, an aliquot of the cell suspension, before plating, was mixed 1:1 with a solution of 0.1% Trypan blue (Sigma) in PBS. Trypan blue is a vital stain used to selectively colour dead cells. In a viable cell Trypan blue is not absorbed, however it traverses the membrane in a dead one. Hence, dead cells are shown as a distinctive blue colour under a microscope. 10 ul of the above mixture was charged on a counting chamber and viable cells in the "counting squares" were counted. The cells density was calculated as follows: average of counted cells/ counting square X 10^4 X dilution factor (=2) = number of cells/ml

3.2.2 Plasmid DNA Transfection

To introduce expression plasmids into HeLa cells Lipofectamine™ 2000 Transfection Reagent (Invitrogen) was used. Lipofectamine™ 2000 Transfection Reagent is a mix of cationic lipids. The basic structure of cationic lipids consists of a positively charged head group and one or two hydrocarbon chains. The charged head group governs the interaction between the lipid and the phosphate backbone of the nucleic acid, and facilitates DNA condensation. The positive surface charge of the liposomes also mediates the interaction of the nucleic acid and the cell membrane, allowing for fusion of the liposome/nucleic acid ("transfection complex") with the negatively charged cell membrane. The transfection complex is thought to enter the cell through endocytosis. Once inside the cell, the complex must escape the endosomal pathway, diffuse through the cytoplasm, and enter the nucleus for gene expression.

Protocol

In a six-well, one day before transfection, 4 x 10^5 cells were plated in 1,5 ml of DMEM medium without antibiotics so that cells were 90-95% confluent at the time of transfection.

For each transfection sample, the complexes were prepared as follows:

- DNA (2-3ug) was diluted in 250 µl of DMEM medium without antibiotics and serum and mixed gently.
- Lipofectamine™ 2000 was mixed gently before use, then 8ul were diluted in 250 µl of DMEM medium without antibiotics and serum. The sample was incubated for 5 minutes at room temperature.
- After the 5 minute incubation, the diluted DNA was combine with the diluted Lipofectamine™ 2000 (total volume = 500 µl), mixed gently and incubated for 20 minutes at room temperature.

The 500 µl of complexes were added to each well containing cells and medium.

Cells were incubated at 37°C in a CO_2 incubator for 24 hours prior to testing for transgene expression. Medium with transfection complexes was changed after 5 hours.

3.2.3 Immunocytochemestry (ICC)

For immunocytochemistry, the day before transfection cells were plated on a glass coverslip previously sterilized with ethanol.
The procedure used is divided into the below steps:

Fixation

One day after transfection, the cells were fixed in 4% paraformaldehyde in PBS pH 7.4 for 10 minutes at room temperature. The cells were then washed tree times with PBS to eliminate paraformaldehyde.

Permeabilization

To permeabilize cell membranes and improving the penetration of the antibody, the cells were incubated for 10 minutes with PBS containing 0.1% Triton X-100 (Applichem).

Blocking and Incubation

Cells were incubated with 10% serum in PBS for 10 minutes to block non specific binding of the antibodies.
Primary antibodies, diluted in PBS with 5% serum, were applied for 1 hour in a humidified chamber at 37°C. Cells were washed three times with PBS and then secondary antibodies, diluted in PBS, were applied for 1 hour in a humidified chamber at 37°C.

Mounting and analysis

Coverslips were mounted with a drop of the mounting medium Wowiol (Sigma). Images were collected with a Nikon C1 confocal microscope and analysed using either Nikon EZ-C1 (version 2.1) or NIH ImageJ (version 1.32J) softwares.

Primary antibodies used	**Dilution**
Anti c-Myc rabbit (Sigma)	1:120

Anti PDI mouse (BD biosciences)	1:200
Anti GM130 mouse (BD biosciences)	1:200

Secondary antibodies used	**Dilution**
Alexa fluor 488 anti mouse (Invitrogen)	1:1000
Alexa fluor 555 anti rabbit (Invitrogen)	1:1000

3.3 Biochemical techniques

3.3.1 Co-Immunoprecipitation (co-IP)

Co-immunoprecipitation (co-IP) is a common technique for protein interaction discovery.

An antibody for the protein of interest, linked to a support matrix, is incubated with a cell extract so that the antibody will bind the protein in solution. The antibody/antigen complex will then be pulled out of the sample: this physically isolate, from the rest of the sample, the protein of interest and other proteins potentially bound to it. The sample can then be separated by SDS-PAGE for Western blot analysis.

In co-IP experiments, anti-c-Myc agarose conjugate (Sigma) was used. Anti-c-Myc agarose conjugate is prepared with an affinity purified anti-c-Myc antibody coupled to cyanogen bromide-activated agarose. The purified antibody is immobilized at 1.0 to 1.5 mg antibody per ml agarose. Anti-c-Myc antibody is developed in rabbit using a peptide corresponding to amino acid residues 408-425 of human c-Myc as the immunogen.

Anti-c-Myc antibody recognizes the epitope located on c-Myc tagged fusion proteins and it reacts specifically with N- and C terminal c-Myc-tagged fusion proteins.

The co-immunoprecipitation procedure used the following:

- 10^6 cells, plated on a six wells plate, were harvested using 0.5% Triton X-100 (Applichem) in PBS, incubated in ice for 15 minutes and then centrifuged at 16000g for 15 minutes.
- 30 ul of anti-c-Myc agarose conjugate suspension was added to a microcentrifuge tube and washed 5 times with PBS by a short spin.

- Cell extract (lysate) was added to the resin and incubated for 2 hours on an orbital shaker at room temperature.
- At the end of incubation time, the supernatant was recovered and the resin was washed 5 times with PBS.
- After the final wash, 70 ul of 1X Laemmli buffer (see Appendix B 3.9) were added to the resin and incubated at 95°C for 5 minutes.
- After boiling, the sample was vortexed and then centrifugated for 5 seconds (pellet).
- The presence of the c-Myc tagged protein and of other proteins potentially bound to it was detected in lysate, supernatant and pellet by Western blotting.

3.3.2 Immunoisolation of membrane vesicles and membrane fractionation

To obtain harbouring vesicles, the sample were prepared as follows:

- 10^6 transfected cells, plated on a six wells plate, were suspended in homogenization buffer (10 mM HEPES-KOH buffer pH 7.4 containing 0.22 M mannitol, 0.07 M sucrose and protease inhibitors) and homogenized using a syringe with a 26-gauge needle.
- Homogenate was sonicated and the supernatant containing vesiculated membranes recovered by centrifugation at 4000g for 5 minutes at 4°C in order to remove unbroken organelles.
- When required, the vesiculated membranes were mixed with another pool of harbouring vesiscles and incubated at 30°C for 1 hour.
- After incubation, immunoprecipitation of the harbouring vesicles was performed as described above (3.3.1).
- The remaining supernatants containing vesiculated membranes were centrifugated at 120000 g for 60 minutes to separate a membrane fraction (pellet) and a soluble fraction (supernatant).
- Supernatant and pellet derived from the immunoprecipitation and 100000 g centrifugation were analysed by western blotting.

3.3.3 SDS PAGE

SDS-PAGE stands for Sodium dodecyl sulfate (SDS) polyacrylamide gel electrophoresis (PAGE) and is a method used to separate proteins according to their size. Since different proteins with similar molecular weights may migrate differently due to their differences in secondary, tertiary or quaternary structure, SDS, an anionic detergent, is used in SDS-PAGE to reduce proteins to their primary (linearized) structure and coat them with uniform negative charges: proteins having identical charge to mass ratios are fractionated by size.

Gel making

The resolving gel was prepared with a 10% polyacrylamide content, while the stacking gel had a 5% acrylamide concentration.

Components	Resolving gel	Stacking gel
Acrylamide solution (Fluka)	10% (v/v)	5% (v/v)
Tris-HCl pH 8.8	0.37M	
Tris-HCl pH 6.8		0.125M
Ammonium persulphate	0.1% (w/v)	0.1% (w/v)
SDS	0.1% (w/v)	0.1% (w/v)
TEMED	0.02% (v/v)	0.02% (v/v)

Sample preparation

Samples were diluted in Laemli buffer (Appendix B 3.9) and then boiled at 95°C for 5 minutes.

Running the electrophoresis

The amperage applied was 15mA/gel until the proteins reached the resolving gel, then it was increased to 25mA/gel.

Western blotting

After the electrophoresis, the proteins were transferred from gel to PVDF membrane (Amersham Biosciences).

The membrane was blocked with a solution of 10% milk in TBS-T (Appendix B 3.9) for 15 minutes at room temperature on a shaking platform.

The membrane was then incubated with the primary antibody diluted to the appropriate concentration in TBS-T and milk 2%, at 4°C O/N.

The secondary antibody diluted to the appropriate concentration in TBS-T was added and incubated for 1 hour at room temperature.

The membrane detection was performed by ECL plus kit (Amersham Biosciences).

Primary antibodies used	**Dilution**
Anti c-Myc mouse (Sigma)	1:1000
Anti HA mouse (Cell Signalling)	1:1000
Anti PDI mouse (BD biosciences)	1:500
Anti calnexin rabbit (Millipore)	1:1000

Secondary antibodies used	**Dilution**
Anti mouse-HRP (Dako)	1:10000
Anti rabbit-HRP (Dako)	1:10000

3.4 Computational Methods

3.4.1 Databases

The amino acid sequence of *Drosophila* atlastin (Datlastin) was retrieved from the protein sequence database at NCBI http://www.ncbi.nlm.nih.gov. The 3-D structures of proteins were obtained from the protein data bank (Berman, Westbrook et al. 2000).

3.4.2 Software and hardware.

BioEdit (Hall TA, 1999) and Molecular Operating Environment (MOE ver.2007.09 http://www.chemcomp.com.) suite were used for display and manipulation of sequences.

MOE was also used to visualization and/or rendering, for homology modeling the 3-D structures, and for the stereochemical quality of the generated models. All the software were run on a 16 CPU (Intel Core^{TM}2 Quad CPU 2.40 GHz) linux cluster. Default values were used for all the parameters, unless specified otherwise.

3.4.3 Sequence alignment

Sequence alignments were performed using Blom62 similarity matrix implemented by MOE.

3.4.4 Template searching

MOE-SearchPDB was used to identify all possible homologous to the query sequence. The search is performed on a database of protein structures and sequences that have been clustered into families.

3.4.5 Homology modelling

The homology model of the 1-419 domain of *Drosophila* atlastin (D-atlastin) was assembled based on the x-ray structures of three different templates. Domain 1 (1-315): the GTP-binding domain has been model based the similarity with the N-terminal GTPase domain of human guanylate binding protein 1 (hGBP1, pdb code: 2BC9); domain 2 (315-382): this region has been constructed based on the similarity with the crystal structure of the of the receptor-binding (Ig V-type) domain of human B7-2 (pdb code: 1NCN); and domain 3 (383-419): this region has been built up based on the similarity with the N-terminal region of myosin`s rod-like subfragment (pdb code: 3BAS).

An ensemble of 25 model structures was generated. These were ranked by analysis of their packing score and contact energy, using the "Homology Modeling" tool implemented by MOE. The analysis of homology models stereochemistry has been carried out using the "Protein Geometry" tools implemented by MOE.

3.5 Circular dichroism spectroscopy (CD)

The phenomenon of circular dichroism is very sensitive to the secondary structure of polypeptides and proteins. Circular dichroism (CD) spectroscopy is a form of light

absorption spectroscopy that measures the difference in absorbance of right- and left-circularly polarized light (rather than the commonly used absorbance of isotropic light) by a substance. Linearly polarized light is polarized in a certain direction (that is, the magnitude of its electric field vector oscillates only in one plane, similar to a sine wave). In circularly polarized light, the electric field vector has a constant length, but rotates about its propagation direction. Hence it forms a helix in space while propagating. If this is a left-handed helix, the light is referred to as left circularly polarized, and vice versa for a right-handed helix. The electric field of a light beam causes a linear displacement of charge when interacting with a molecule, whereas the magnetic field of it causes a circulation of charge. These two motions combined result in a helical displacement when light impinges on a molecule. Since circularly polarized light itself is "chiral", it interacts differently with chiral molecules. That is, the two types of circularly polarized light are absorbed to different extents. In a CD experiment, equal amounts of left and right circularly polarized light are radiated into a (chiral) solution. One of the two polarizations is absorbed more than the other one, and this wavelength-dependent difference of absorption is measured, yielding the CD spectrum of the sample.

3.5.1 Determination of Protein Secondary Structure by Circular dichroism

Secondary structure can be determined by CD spectroscopy in the "far-uv" spectral region (190-250 nm). At these wavelengths the chromophore is the peptide bond, and the signal arises when it is located in a regular, folded environment.

Alpha-helix, beta-sheet, and random coil structures each gives rise to a characteristic shape and magnitude of CD spectrum. This is illustrated by Figure 12 which shows standard spectra of poly-Lysine in these three different conformations. The approximate fraction of each secondary structure type present in a protein can thus be determined by analyzing its far-uv CD spectrum as a sum of fractional multiples of such reference spectra. Like all spectroscopic techniques, the CD signal reflects an average of the entire molecular population. Thus, while CD can determine that a protein contains about 50% alpha-helix, it cannot determine which specific residues are involved in the alpha-helical portion.

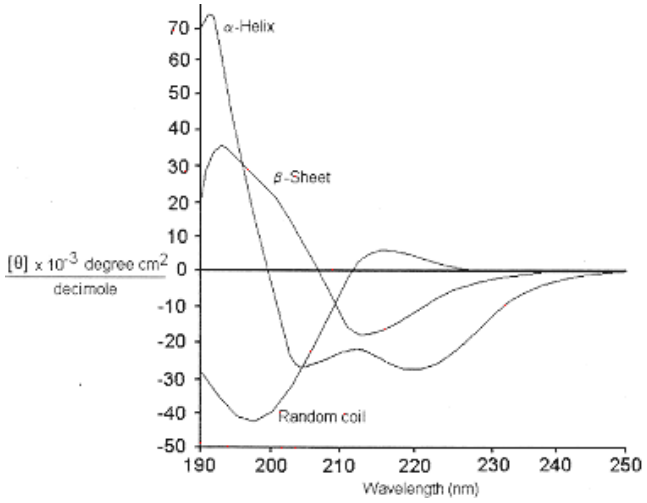

Figure 12 CD reference spectrum of poli-Lysine.[6]

3.5.2 CD experimental conditions

Datl-coil peptide corresponding to the Datlastin Met 383-Ala 419 region was synthesized by the German company BioGenes.

CD experiments were carried out on Jasco J-715 spectropolarimeter. The CD spectra were acquired at room temperature using a 0.01-cm cell, and elaborated by using Jasco Spectra Manager Software version 1.04.00.

The recordings were performed in phosphate buffer (50mM K_2PO_4; KCl 50mM) pH 7 with or without TFE; or in Dodecil-Phosphate-Coline (DPC) solution to simulate a membrane environment.

DPC is an amphiphilic molecule composed by a long hydrocarbon "tail" and a hydrophilic "head". Like the other surfactants, in diluted aqueous solution DPC exits mainly as solvated monomeric species. When a sufficient amount of DPC is dissolved in water, several bulk solution properties are significantly changed, particularly the surface tension and the ability of the solution to solubilise hydrocarbons. These changes

---

[6] Alpha helix characteristic spectrum presents a positive maximum point at 192 nm and two minimum points around 208 nm and 222 nm.

Beta-sheet CD spectrum presents a positive maximum point around 195 nm and a minimum point around 218 nm.

The random coil spectrum has an intense minimum point around 200 nm and a weak band, negative or positive, at greater wavelengths.

do not occure until a minimum bulk DPC concentration is reached: the critical micelle concentration (CMC). At the CMC the monomers undergo self-assembly to form roughly spherical structures known as micelle.

3.6 *Drosophila* transformation

3.6.1 *Drosophila melanogaster* life cycle

Fruit flies begin their lives as an embryo in an egg. This stage lasts for about one day. During this time, the embryo develops into a larva. The first instar larva hatches out of the egg, crawls into a food source, and eats. After a day, the first instar larva molts and becomes the second instar larva. After two days in this stage, the larva molts again to become the third instar larva. After three days of eating in this stage, the larva crawls out of the food source and molts again. Following this molt, the larva stops moving and forms a pupa. *Drosophila* stays in the pupa for about five days. During this time, the metamorphosis, or change, from larva to adult is occurring. Adult structures like wings, legs, and eyes develop. When the adults emerge from the pupa they are fully formed. They become fertile after about ten hours, copulate, the females lay eggs, and the cycle begins again. The whole life cycle takes about 12-14 days (Figure 13)

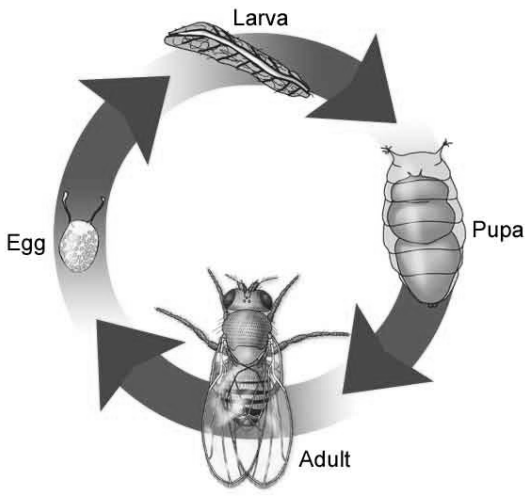

Figure 13 ***Drosophila melanogaster*** **life cycle**

3.6.2 Microinjection

Preparing the DNA for microinjection

Injection mix	Final concentration
Construct plasmid	3 µg/µl
Helper plasmid	1 µg/µl
10XMicroinjecting buffer (Appendix B 3.9)	1X

The mix is filtered through a 0.2 µm filter.

The helper plasmid is a source of P-element transposase that allows the insertion of DNA construct into the fly genome.

Fly strains

A white mutant strain, w1118 (phenotype white eyes) was used in this protocol to allow detection of transgenic flies carrying white gene (phenotype red/orange eye). These flies were used both as a source of embryos for the injection and as a backcross stock to amplify the transformants.

Needles Preparation

The quality of the needles is critical for high through-put. Needles should be pulled on any horizontal puller of the Sutter brand series using 1.0 mm OD borosilicate capillaries with omega dot fiber (WPI). The settings will be different for each machine and will need to be updated each time the heating filament is replaced or re-shaped, or a new type of capillaries is used. Several parameters influence the shape and properties of the needle and the effect produced by changing any of them (heat, velocity of pull, pressure of gas flow, number of steps) is difficult to predict. However, a paper by (Miller, Holtzman et al. 2002) is a very useful guideline for designing suitable needles. The needle should be progressively but shortly tapered and have no discontinuity or step. Needles that are too elongated will bend and brake when impaling the chorion. The condition used for our contruct microinjection are: Heat=414 Pull=200 Vell=250 Time=150

Embryo collection

Embryos must be injected before blastoderm cellularization, a developmental stage that begins 45-50 minutes after eggs are laid at 22°C. Cellularization is easily visible at the microscope, and such old embryos should not be injected. They should be killed by piercing them with the injection needle. Injections should be performed during the first 45 minutes after egg laying.

Preparing the embryos

Clean embryos were transferred in a small quantity of water to the centre of the coverslip with a clean thin pointed brush. 100 moist embryos were lined up with the dissection needle, one at a time, near one edge of the coverslip, with the posterior pole pointing to the edge. Embryos were let to dry for a few minutes to attach them firmly to the coverslip and then covered with as little halocarbon oil mix as possible. After 5-10 min the oil has penetrated between the chorion and the vitelline membrane clearing the embryo and allowing a rough staging under the dissecting scope.

Microinjection

The injection set-up consists of two parts: an inverted microscope (Nikon) equipped with a 20X lens and a micromanipulator InjectMan (Eppendorf) linked to the FemtoJet air-pressure injecting device (Eppendorf) connected to the needle holder. A set-up was installed in a cool room (18˚/20°C) to give more time flexibility as the embryos develop more slowly and the appropriate stage for injection lasts longer. The microinjection of the embryos was completely automatic, the needle was inserted quickly in the centre of the posterior pole were the germ cells will form, and pulled out quickly to avoid any leakage.

After the injection

Most of oil was drained off the coverslip and it was transferred to a food vial, placing the edge with the embryos against the food. The vials were kept at 18° C for two days then larvae were collected and transferred in vials of standard food and maintained at room temperature until adults hatched.

Back-crossing the injected flies

Hatching adults (F0) were separated by sex. Each male was crossed to 2 virgin w1118 females and each female, even if obviously not virgin, to 2 or more w1118 males. Crosses were performed in separate vials of standard food. When at least 20-50 adult F1 flies hatched in each vial they were screened to look for transformants individual. Transgenic flies (red eyes individuals) were crossed again with w1118 flies and with balancer lines.

Characterization of transgenic lines

F1 individuals may bear one transgene insertion on any of the chromosomes: X, II or III. Transgenes inserted on the fourth chromosome are very rare as this chromosome is rather small and essentially heterochromatic.

The transgene should be immediately placed in front of a balancer chromosome, to avoid its loss.

If the insertion lays on the second chromosome the fly is crossed with the Sm6/TfT balancer stock (carrying the dominant morphological marker curly wing) as the schema reported below.

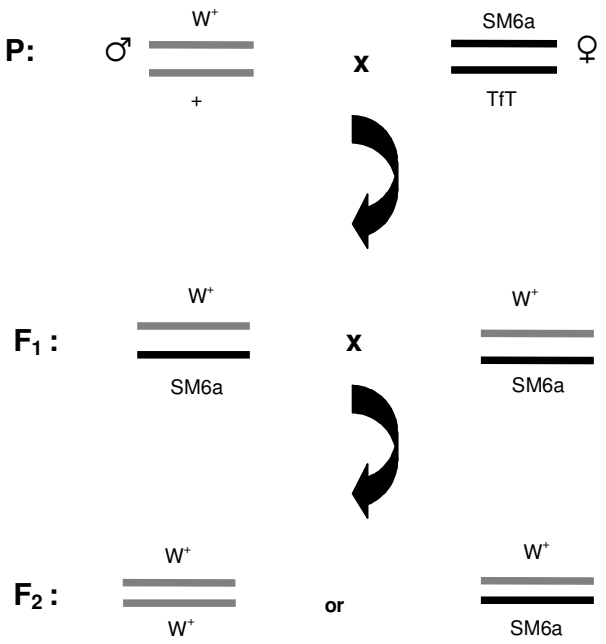

Figure 14 Cross with II chromosome balancer

If in F2 progeny there are individuals with white eyes the insertion is localized on another chromosome.

If the insertion lays on the third chromosome, the fly is crossed with the TM3/TM6 balancer stock (carrying the dominant morphological marker stubble hairs) as the schema reported below.

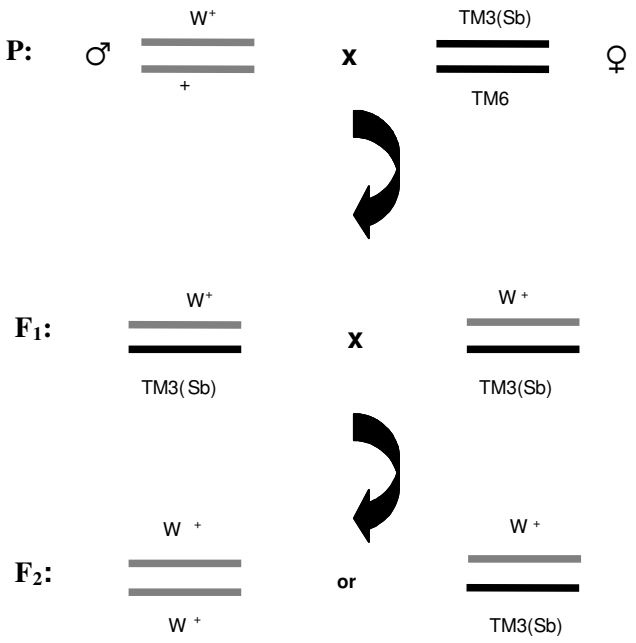

Figure 15 Cross with III chromosome balancer

If in F2 progeny there are individuals with white eyes the insertion is localized on another chromosome.

If the insertion lays on the X chromosome the fly is crossed with the Fm7/Sno balancer stock (carrying the dominant morphological marker heart- shaped eyes) as the schema reported below.

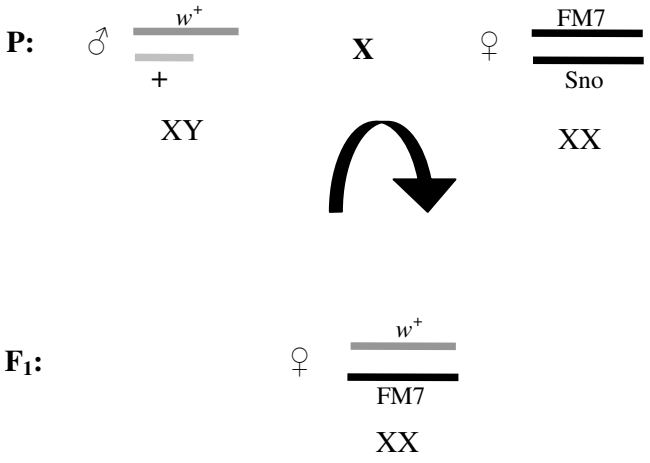

Figure 16 Cross with X chromosome balancer

If the insertion is occurred in the X chromosome, all the F1 females have w^+/FM7 phenotype.

3.7 Techniques for phenotypic analysis

3.7.1 Immunohistochemistry

Immunostaining was performed on wandering third instar larvae reared at 25°C.

Larvae dissection

Wandering third instar larvae were raised at 25°C. After harvesting larvae, they were dissected dorsally in standard saline and fixed in 4% paraformaldeyde for 45 min. Preparations were subsequently washed in phosphate-buffered saline (PBS) containing 0.5% bovine serum albumin.

Antibodies

Primary antibodies were applied overnight at 4°C, while secondary antibodies were incubated with dissections for approximately 2 hr at room temperature.

Primary antibodies used	**Dilution**
Anti-BiP rat (Babraham)	1:50
Anti-p120 mouse (Calbiochem)	1:600
Anti-myc mouse (Cell Signaling)	1:500
Anti Datlastin guinea pig	1:1000

The anti-D-atlastin antibody was previously produced. The process of immunization was performed with a synthetic peptide designed on the proteic sequence of D-atlastin AVGGGAASYRSQTSVNASNGKVK and it was outsourced to the German company BioGenes.

Secondary antibodies used	**Dilution**

Alexa fluor 488 anti mouse (Invitrogen)	1:1000
Cy5 anti mouse (Jackson laboratories)	1:500
Cy5 anti rat (Jackson laboratories)	1:500
Alexa fluor 555 anti guinea pig (Invitrogen)	1:1000

Image analysis

Images were collected with a Nikon C1 confocal microscope and analyzed using either Nikon EZ-C1 (version 2.10) or NIH ImageJ (version 1.32J) softwares.

3.7.2 *Drosophila* Driver lines

Datlastin K51A transgenic lines were tested using different Gal4 driver lines.
The Gal4 activator lines used in this study were GMR-Gal4, Tubulin-Gal4, Elav-Gal4, MEF2-Gal4 and D42-Gal4 (Bloomington Stock Center, Indiana University). All experimental crosses were performed at 25°C.

3.8 Appendix A: General protocols

3.8.1 Transformation of chemiocompetent cells

- Gently thaw the chemiocompetent cells on ice.
- Add ligation mixture to 50 µl of competent cells and mix gently. Do not mix by pipetting up and down.
- Incubate on ice for 30 minutes.
- Heat-shock the cells for 30 seconds at 42°C without shaking.
- Immediately transfer the tube to ice.
- Add 450 µl of room temperature S.O.C. medium.
- Cap the tube tightly and shake the tube horizontally (200 rpm) at 37°C for 1 hour.
- Spread 20 µl and 100 µl from each transformation on prewarmed selective plates and incubate overnight at 37°C.

3.8.2 Preparation of plasmid DNA by alkaline lysis with SDS: minipreparation

Plasmid DNA may be isolated from small-scale (1-3 ml) bacterial cultures by treatment with alkali and SDS.

- Inoculate 3 ml of LB medium (Appendix B 3.9) containing the appropriate antibiotic with a single colony of transformed bacteria. Incubate the culture overnight at 37°C with vigorous shaking.
- Pour 1.5 ml of the culture into a microfuge tube. Centrifuge at maximum speed for 30 seconds in a microfuge. Store the unused portion of the original culture at 4°C.
- When centrifugation is complete, remove the medium by aspiration, leaving the bacterial pellet as dry as possible.
- Resuspend the bacterial in 100 µl of ice-cold Alkaline lysis solution I (Appendix B 3.9) by vigorous vortexing.
- Add 200 µl of freashly prepared Alkaline lysis solution II (Appendix B 3.9) to each bacterial suspension. Close the tube tightly, and mix the contents by inverting the tube rapidly five time. Do not vortex. Store the tube on ice.
- Add 150 µl of ice-cold Alkaline lysis solution III (Appendix B 3.9). Close the tube and disperse Alkaline lysis solution III through the viscous bacterial lysate by inverting the tube several times. Store the tube on ice 3-5 minutes.
- Centrifuge the bacterial lysate at maximum speed for 5 minutes at 4°C in a microfuge. Transfer the supernatant to a fresh tube.
- Precipitate nucleic acids from the supernatant by adding 2 volumes of ethanol at room temperature. Mix the solution by vortexing and then allow the mixture to stand 2 minutes at room temperature.
- Collect the precipitate of nucleic acid by centrifugation at maximum speed for 10 minutes at 4°C in a microfuge.
- Remove the supernatant by gentle aspiration. Stand the tube in an inverted position on a paper towel to allow all of the fluid to drain away. Use a pipette tip to remove any drops of fluid adhering to the walls of the tube

- Add 2 volumes of 70% ethanol to the pellet and invert the closed tube several times. Recover the DNA by centrifugation at maximum speed for 5 minutes at 4°C in a microfuge.
- Again remove all the supernatant by gentle aspiration.
- Dissolve the nucleic acids in 50 ul of TE buffer (pH 8.0) or distillated autoclavated water containing 20 ug/ml DNase-free RNase A (pancreatic RNase). Vortex the solution gently for a few seconds. Store the DNA solution at -20°C.

3.9 Appendix B: Stocks and solutions

LB Medium (Luria-Bertani Medium)

Bacto-tryptone	10g
Yeast extract	5g
NaCl	10g
H_2O	to 1 Liter

Autoclave.

LB Agar

Bacto-tryptone	10g
Yeast extract	5 g
NaCl	10 g
Agar	20g
H_2O	to 1 Liter

Adjust pH to 7.0 with 5 N NaOH. Autoclave.

LB–Ampicillin Agar

Cool 1 Liter of autoclaved LB agar to 55° and then add 10 ml of 10 mg/ml filter-sterilized Ampicillin. Pour into petri dishes (~25 ml/100 mm plate).

SOC medium

Bacto-tryptone	20g
Yeast extract	5 g
NaCl	0,5 g
KCl 1M	2,5 ml
H_2O	to 1 Liter

Adjust pH to 7.0 with 10N NaOH, autoclave to sterilize, add 20 ml of sterile 1 M glucose immediately before use.

Alkaline lysis solution I

Glucose 50 mM

Tris HCl 25 mM (pH 8.0)

EDTA 10 mM (pH 8.0)

Solution I can be prepared in batches of approximately 100 ml, autoclaved for 15 minutes and stored at 4 °C.

Alkaline lysis solution II

NaOH 0.2 N (freshly diluted from a 10 N stock)

SDS 1% (w/v)

Alkaline lysis solution III

Potassium acetate 3 M

Glacial acetic acid 11.5% (v/v)

TE Buffer

Tris-HCl 10 mM (pH 7.5)

EDTA 1 mM

DMEM complete medium

DMEM 4.5g/L Glucose with L-Glutamine (Lonza)

FBS 10% (v/v)

Penicillin-Streptomycin mixture 100X (Lonza, contains 5000 units potassium penicillin and 5000 ug streptomycin sulfate)

Phoshate Buffered Saline (PBS)

KH_2PO_4	1444 mg/L
NaCl	9000 mg/L
Na_2HPO_4	795 mg/L

Trypsin solution

Trypsin 2,5% 10X (Lonza)

Running buffer 1X

Tris 25mM

Glycine 250mM

SDS 0.1%

In deionized H_2O

Transfer buffer 1X

Tris 25mM

Glycine 192mM

In deionized H_2O

TBS-T buffer 1X

Tris 100mM

NaCl 1,5M

Tween-20 1%

In deionized H_2O

Laemmli buffer 2X

SDS 4%

Glycerol 20%

2-mercaptoethanol 10%

Bromphenol blue 0,004%

Tris HCl 125mM

The solution has a pH of approximately 6.8

10X injection buffer:

Sodium Phosphate Buffer pH 6.8 0.1M

KCl 5mM

***Drosophila'*s food**

Agar	15 g
Yeast extract	46.3 g
Sucrose	46.3 g
H_2O	to 1 Liter

Autoclave and then add 2 g of Nipagine dissolved in 90% ethanol.

Egg laying food

Agar	6 g
Sucrose	6.6 g
Fruit juice	66 ml
H_2O	to 200ml

3.10 Appendix C: plasmids

3.10.1 pDrive cloning vector (Qiagen)

The pDrive Cloning Vector provides superior performance through UA-based ligation and allows easy analysis of cloned PCR products.

This vector allows ampicillin and kanamycin selection, as well as blue/white colony screening. The vector contains several unique restriction endonuclease recognition sites around the cloning site, allowing easy restriction analysis of recombinant plasmids.

The vector also contains a T7 and SP6 promoter on either side of the cloning site, allowing *in vitro* transcription of cloned PCR products as well as sequence analysis using standard sequencing primers. In addition, the pDrive Cloning Vector has a phage f1 origin to allow preparation of single-stranded DNA (Figure 17).

3.10.2 pcDNA3.1/Zeo(+) (Invitrogen)

pcDNA3.1/Zeo (+) is an expression vector, derived from pcDNA3.1, designed for high-level stable and transient expression in a variety of mammalian cell lines.

To this aim, it contains Cytomegalovirus (CMV) enhancer-promoter for high-level expression; large multiple cloning site; Bovine Growth Hormone (BGH) polyadenylation signal; transcription termination sequence for enhanced mRNA stability and Zeocin resistance coding region (Figure 18).

3.10.3 pUAST vector

pUAST is a P-element based vector that allows one to place the gene of interest under GAL4. pUASt consists of five tandemly arrayed optimized GAL4 binding sites followed by the hsp70 TATA box and transcriptional start, a polylinker containing unique restriction sites and the SV40 small T intron and polyadenylation site. These features are included in a P-element vector (pCaSpeR3) containing the P-element ends (P3' and P5') and the white gene which acts as a marker for successful incorporation into the *Drosophila* genome (Figure 19).

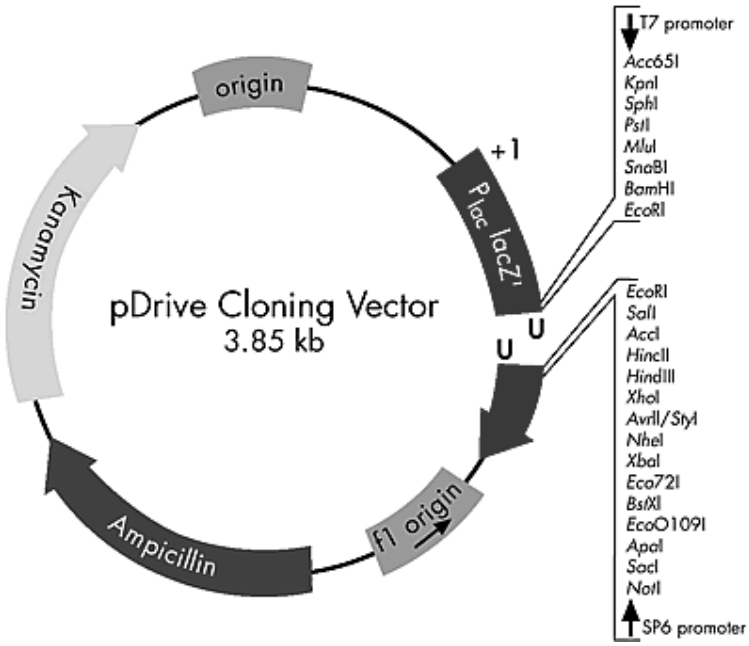

Figure 17 pDrive Cloning vector map

pcDNA3.1/Zeo(+) **Code: PMC 006**

Comments for pcDNA3.1/Zeo (+)
5015 nucleotides

CMV promoter: bases 209-863
T7 promoter priming site: bases 863-882
Multiple cloning site: bases 895-1010
BGH reverse priming site: bases 1022-1039
BGH polyadenylation signal: bases 1021-1235
f1 origin: bases 1298-1711
SV40 promoter and origin: bases 1776-2101
EM7 promoter: bases 2117-2183
Zeocin™ resistance gene: bases 2184-2558
SV40 polyadenylation: bases 2688-2817
pUC origin: bases 3201-3874 (C)
bla promoter: bases 4880-4978 (C)
Ampicillin (*bla*) resistance gene: bases 4019-4879 (C)

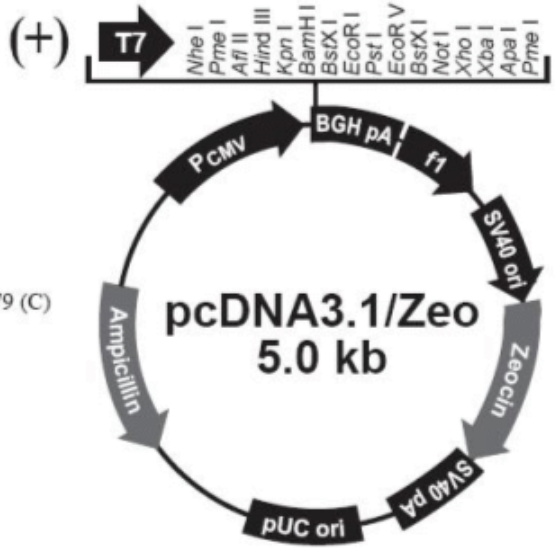

Figure 18 pcDNA3.1/Zeo(+) map

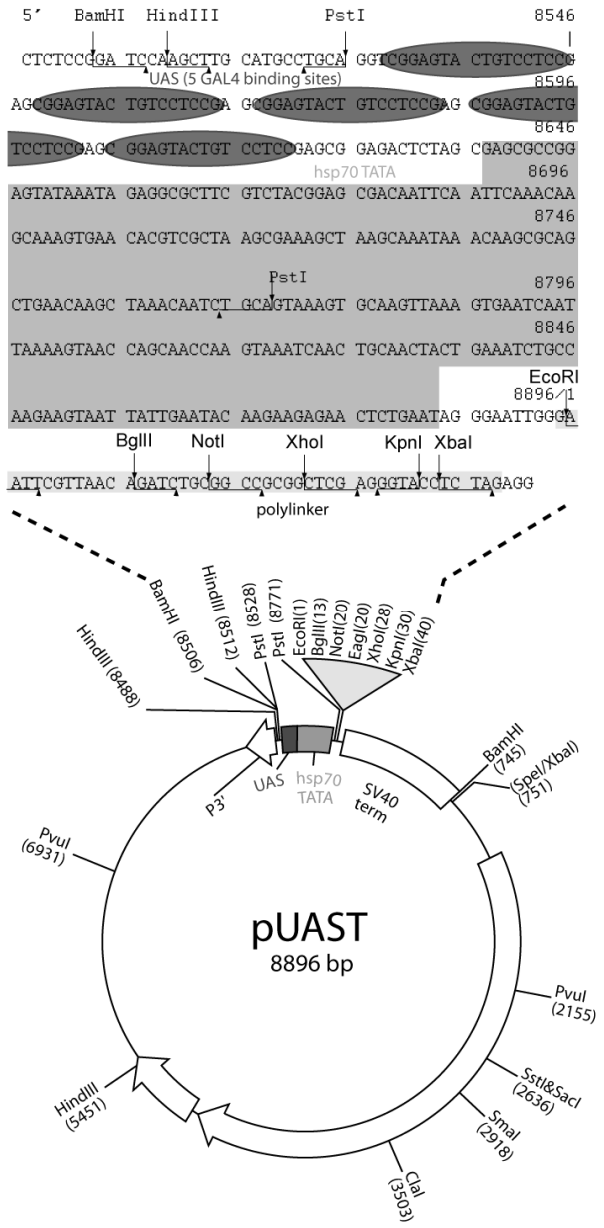

Figure 19 pUAST map

4 Results

4.1 Datlastin is capable of homo-oligomerization and mediates tethering of ER membranes

Recent studies from our laboratory indicate that Datlastin, the *Drosophila* homologue of human atlastin-1, whose mutation causes a form of HSP, is involved in the homotypic fusion of ER membranes.

Datlastin specifically localizes to the ER membranes and experiments carried out *in vivo* in *Drosophila* revealed that Datlastin depletion causes ER fragmentation, while its overexpression results in the formation of expanded ER elements consistent with excessive fusion of ER membranes (see Introduction 1.4.3).

Human and *Drosophila* atlastin proteins belong to the dynamin superfamily. A common feature of the members of this family is their capacity to homo-oligomerize (see 1.5). Because human atlastins have been shown to self-assemble into oligomeric complexes (Zhu, Patterson et al. 2003; Rismanchi, Soderblom et al. 2008), we tested whether Datlastin might also be capable of self-association using co-immunoprecipitation experiments.

Co-immunoprecipitation (co-IP) is a common technique used for protein interaction discovery. An antibody for the protein of interest, linked to a support matrix, is incubated with a cell extract so that the antibody will bind the protein in solution. The antibody/antigen complex will then be pulled out of the sample (precipitation): this physically isolates, from the rest of the sample, the protein of interest and other proteins potentially bound to it (co-immunoprecipitation). Finally, components of the immuno complex (antibody, antigen and co-immunprecipitated proteins) are analyzed by SDS-PAGE and Western blot.

To test Datlastin self-assembling ability, HeLa cells were co-transfected with Datlastin-HA and Datlastin-Myc expression constructs (Methods 3.1.1). Lysates prepared from these cells were immunoprecipitated using anti-Myc antibodies. The immunoprecipitate was analyzed by western blotting with both anti-Myc and anti-HA antibodies. The presence of both Myc and HA signals in the immunoprecipitate showed that immunoprecipitation of Datlastin-Myc pulled down also Datlastin-HA thus

demonstrating that Datlastin molecules are capable of self-association (Figure 20). In a control experiment, a lysate obtained from HeLa cells expressing only Datlastin-HA was immunoprecipitated using anti-Myc antibody: the absence of anti-HA signal in the immunoprecipitation pellet showed that Datlastin oligomerization was not due to non specific binding of Datlastin-HA to anti-Myc beads (Figure 20).

To analyze if Datlastin molecules could homo-oligomerize when localized on distinct ER membranes, we devised a membrane vesicle immunoprecipitation assay (3.3.2). HeLa cells were separately transfected with Datlastin-HA or Datlastin-Myc constructs to obtain cells with ER membranes containing only one of the two differentially tagged Datlastin forms. Because Datlastin is an integral membrane protein, to preserve its localization on ER membranes transfected cells were homogenized in the absence of detergent and fragmented membranes were vesiculated by sonication. The two pools of Datlastin-harbouring ER vesicles, one containing Datlastin-Myc and the other Datlastin-HA, were then mixed and immunoprecipitated. We found that when anti-Myc antibodies were used to precipitate Datlastin-Myc harbouring vesicles, Datlastin-HA co-immunoprecipitated too. In control experiments, anti-Myc beads were unable to pull down Datlastin-HA when incubated with a lysate obtained from cells expressing only Datlastin-HA (Figure 21).

Vesicles were subjected to centrifugation in order to separate a membrane fraction (pellet) and a soluble fraction (supernatant) which were tested for the presence of Datlastin. In agreement with a previous report on human atlastin-1 (Zhu, Patterson et al. 2003), Datlastin and the ER resident integral membrane protein calnexin partitioned exclusively to the membrane fraction, while the ER-lumenal protein PDI (protein disulfide isomerise) remained in soluble fraction (Figure 21). This demonstrated that under these experimental conditions, Datlastin was exclusively associated with membranes and was not released in the cytosol during the lysis step. Therefore binding between Datlastin-Myc and Datlastin-HA occurred between molecules localized on distinct vesicles.

These data indicate that Datlastin has the ability to self-associate and can mediate the formation of a complex in *trans* between Datlastin molecules localized on adjacent ER membranes. Formation of Datlastin trans-complexes could be responsible for the initial tethering of ER membranes required for full fusion.

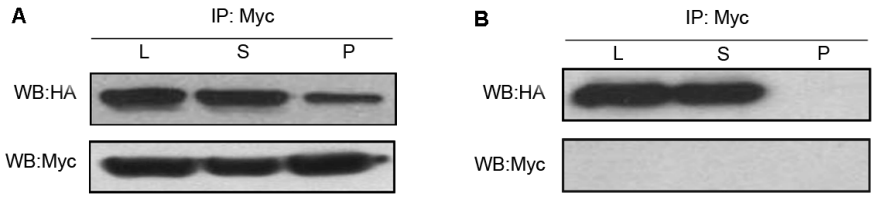

Figure 20 Datlastin is capable of homo-oligomerization

(**A**) HeLa cells were co-transfected with Datlastin-Myc and Datlastin-HA constructs. Lysates prepared from these cells were immunoprecipitated using anti-Myc antibodies. Immunoprecipitates were analyzed by western blot with both anti-HA and anti-Myc antibodies. The ability of anti-Myc to co-immunoprecipitate Datlastin-HA demonstrates that Datlastin forms oligomers. (**B**) In a control experiment HeLa cells were transfected with Datlastin-HA and the lysate immunoprecipitated with anti-Myc antibody. L, lysate; S, supernatant; P, pellet.

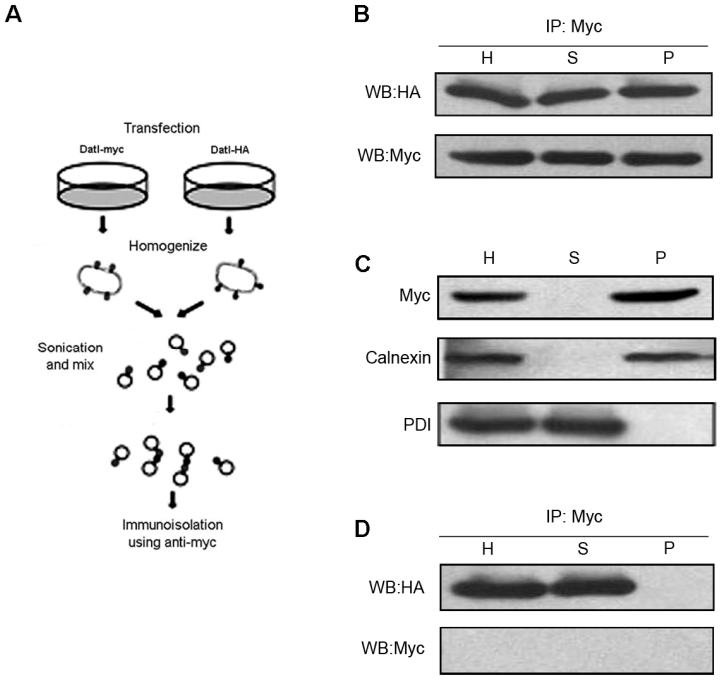

Figure 21 Datlastin mediates tethering of ER membranes

(**A**) Schematic representation of the membrane vesicle immunoprecipitation assay. (**B**) Cleared homogenates from HeLa cells expressing Datlastin-HA or Datlastin-Myc were sonicated, mixed and incubated. The reaction mixture was subjected to immunoprecipitation using anti-Myc antibody. The immunoprecipitate was analyzed by western blotting with anti-Myc and anti-HA antibodies. The ability of anti-Myc to co-immunoprecipitate Datlastin-HA demonstrates the ability of Datlastin to self-associate

through the formation of a complex in *trans* between Datlastin molecules localized on adjacent ER membranes. (**C**) Western blot analysis of the soluble and membrane fractions obtained by ultracentrifugation of cell homogenates demonstrates that Datlastin fractionates exclusively with the membrane pellet together with the ER membrane protein calnexin, while the ER-lumenal protein PDI is found in the soluble cytosolic fraction. (**D**) In a control experiment HeLa cells were transfected with Datlastin-HA and membrane vesicles, prepared as explained, were immunoprecipitated with anti-Myc antibody. H, cell homogenate; S, supernatant; P, pellet.

4.2 Datlastin molecular modelling

In collaboration with the Molecular Modelling Section of the Department of Pharmaceutical Sciences of the University of Padova, a molecular modelling approach was used to identify the domains of Datlastin potentially responsible for homo-oligomerization.

A homology model of the extended cytoplasmic domain of Datlastin (1-419), without the C terminal transmembrane region, was constructed. Using a multiple template-driven homology modelling approach, three suitable templates covering the entire length of the Datlastin 1-419 domain were identified (Figure 22).

The region corresponding to the GTPase domain (1-328) has been modelled based on the X-ray structure of the N-terminal GTPase domain of hGBP1 (pbd code: 2BC9). The region between aminoacid 329-382 has been constructed based on the sequence similarity with the crystal structure of the receptor-binding (Ig V-type) of human B7-2 (pbd code: 1NCN).

Importantly, the domain comprised between aminoacid 383 and 419 has been modelled based on its sequence similarity (33% identity) with the helicoidal structure of a myosin heavy chain/GCN4 bZIP domain chimera (pdb code: 3BAS) (Brown et al. 2008). In addition, other two helicoidal structures have been identified during template searching: the GCN4 domain of the bZIP protein (pbd code: 2DGC; 32% of identity) (Keller, Konig et al. 1995), indicating that sequence homology with the 3BAS peptide depends on the GCN4 portion of the chimera, and the heptad repeat region (HR2) domain of mitofusin (pbd code: 1T3J; 10% of identity). All recovered templates correspond to well established coiled-coil domains, in particular the leucine zipper of the yeast transcriptional activator GNC4 is the best-characterized coiled coil and the heptad repeat region (HR2) of mitofusin, an integral mitochondrial membrane protein,

mediates its oligomerization providing a mechanism for organelle tethering. The significant high sequence similarities of the 383-419 region of Datlastin with these helicoidal domains is the first indirect evidence of the possible presence of a putative coiled-coil in Datlastin.

Coiled-coil domains are protein-protein interaction motifs which mediate subunit oligomerization of a large number of proteins. Coiled-coil domains play a central role in membrane fusion mediated by SNARE proteins, viral envelope glycoproteins and mitofusins because they contribute to the membrane tethering (Eckert and Kim 2001; Bonifacino and Glick 2004; Koshiba, Detmer et al. 2004). Therefore, the 383-419 region is likely to represent the Datlastin oligomerization interface.

Coiled-coils consist of two or more alpha helices (up to seven) that twist around each other to form a supercoil. The sequence of coiled coil domain shows a heptad repeat in the chemical nature of sidechains. Schematically, if these seven structural positions are labelled a-g, **a** and **d** are hydrophobic and form the helix interface, while **b**, **c**, **e** and **f** are hydrophilic and form the solvent-exposed part of the coiled coil (Lupas 1996).

The primary sequence of the predicted Datlastin coiled coil region does not correspond to a canonical heptad repeat whose preservation requires the introduction of a single residue gap (Figure 23). In literature, it is documented that these discontinuities in the periodicity of heptad repeats could be compensated for by small distortions of the helix structure around its axis, that leave the core interactions largely unperturbed (Lupas 1996; Mason and Arndt 2004).

Hydrophobic interactions are the primary driving force of the oligomerization process involved in the bundling of alpha helices into coiled-coils. A cluster of six hydrophobic residues (Phe 388, Phe 392, Leu 396, Leu 400, Val 403 and Phe 404) has been identified as a crucial part of the putative Datlastin coiled-coil.

A comparative analysis revealed that analogous coiled-coil segments are present in human atlastin-1 and also in the other two members of atlastin family: atlastin-2 and -3 (Figure 24).

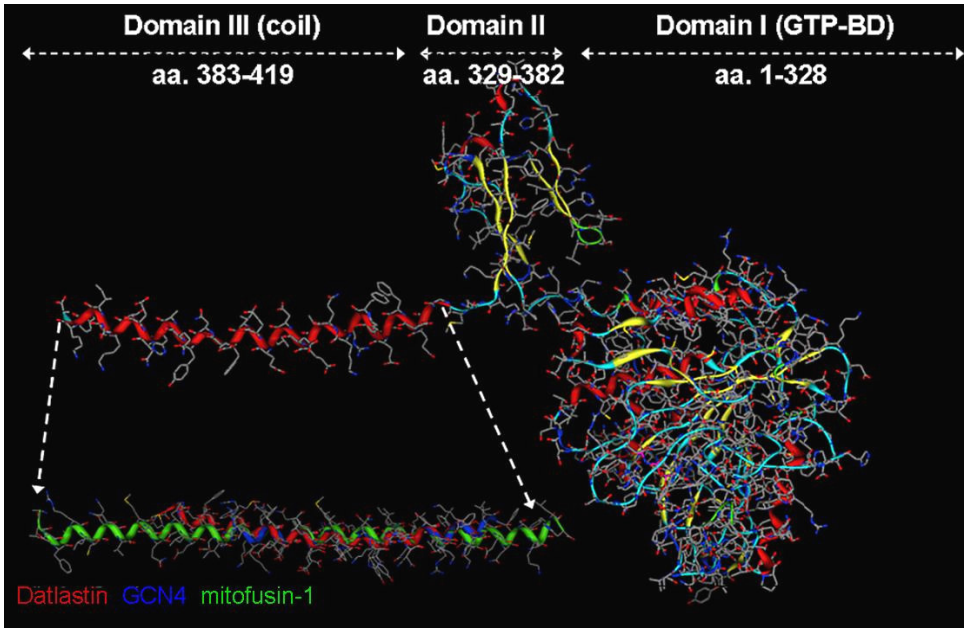

Figure 22 Molecular modelling of Datlastin extended cytoplasmic domain (1-419)

```
GCN4                    KQLEDKVEELLSKNYHLENEVARLKKL
Datl 383 MGGEEFTEKFRKQLEDDLEEVFT-NYQAHNESKNIFKA 419
                        d   a   d   a   d   a   d
```

Figure 23 Alignment between Datlastin and GCN4 coiled-coil domains

The primary sequence of the predicted Datlastin coiled coil region (Met 383-Ala 419) does not correspond to a canonical heptad repeat, but its preservation requires the introduction of a single residue gap. Residues in positions **a** and **d** are highlighted in grey. Identical residues are highlighted in red.

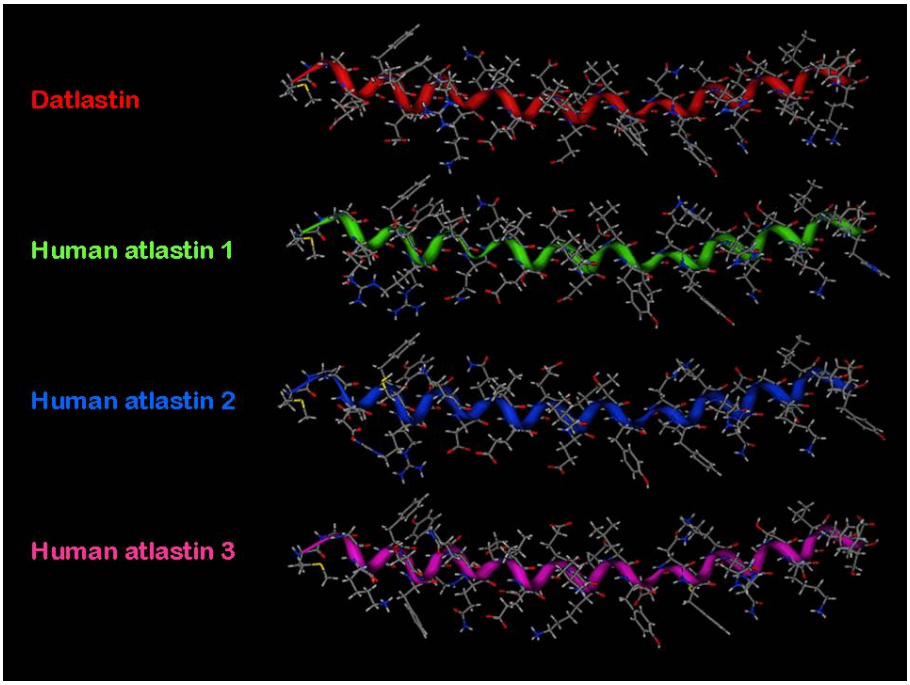

Figure 24 Comparison between coiled-coil segments present in Datlastin and in Atlastin-1,-2,-3

4.3 Datlastin coiled-coil region

4.3.1 Coiled-coil secondary structure prediction

Coiled-coils are characterized by an alpha helical secondary structure. The propensity of the putative Datlastin coiled-coil region (Met 383- Ala 419) to fold into alpha helix was calculated using two different programs: JPRED3 and AGADIR.

JPRED3 software (http://www.compbio.dundee.ac.uk/~www-jpred/) predicts the propensity of a peptide to structure into an alpha helix in the context of the whole protein. JPRED3 indicated that Datlastin 383-419 region could form a stable alpha-helix with an alpha helical content of 65%.

AGADIR algorithm considers a protein region as an isolated peptide in an aqueous environment for predicting its secondary structure behaviour. AGADIR program uses statistical mechanics to consider short range interaction between residues at different pH and temperature (Munoz and Serrano 1997). Datlastin 383-419 was predicted, by this program, to be unstructured, with only 10% of alpha helical content. Taken together, these data suggested that the peptide can potentially adopt an α -helical structure, but only in the context of the intact protein.

The propensity of the peptide to adopt a coiled-coil conformation was estimated by using PCOILS program (Gruber, Soding et al. 2006). PCOILS software compares the sequence of interest to a database of known parallel two-stranded coiled-coils and derives a similarity score. By comparing this score to the distribution of scores in globular and coiled-coil proteins, the program then calculates the probability that the sequence will adopt a coiled-coil conformation.

PCOILS found for Datlastin 383-419 region a propensity to form coiled-coil structure especially in the central part which shows greater homology with the well characterized coiled coil region of yeast transcriptional activator GCN4 (Figure 23).

4.3.2 Circular dichroism analysis

To study the secondary structure of the predicted coiled-coil, a synthetic peptide corresponding to the Met 383 and Ala 419 region (Datl-coil) was synthesized and analyzed by circular dichroism spectroscopy (CD).

Circular dichroism (CD) spectroscopy is a form of light adsorption spectroscopy very sensitive to the secondary structure of a peptide: alpha-helix, beta-sheet, and random coil structures each gives rise to characteristic shapes and magnitudes of CD spectrum (see methods 3.5).

In aqueous or phosphate buffered medium (K_2HPO_4 50mM, KCl 50mM pH 7) the peptide was unstructured and neither increasing peptide concentration, nor changing PH, ionic strength or divalent cation concentration increased the α–helical content. This behaviour for the isolated peptide was consistent with the prediction of the AGADIR algorithm (4.3.1). Typical single-stranded polypeptides generally do not form stable α–helices in aqueous solution and required the additional stabilization of less polar solvents (Brown and Klee 1971; Bierzynski, Kim et al. 1982). For this reason, the peptide was suspended in phosphate buffer with TFE (trifluoroethanol), a helix-promoting hydrophobic solvent widely used to stabilize marginally stable α–helical structures in potentially α–helical peptides (Nelson and Kallenbach 1986; Hodges, Zhou et al. 1990; Dyson, Merutka et al. 1992; Dyson, Sayre et al. 1992).

In the presence of TFE the peptide folded into α–helix and increasing concentration of TFE resulted in a significant increase of the α–helical content (Figure 25). The minimal concentration of TFE at which the peptide underwent a transition from mostly

unstructured to partially folded was approximately 10%. A 60uM Datl-coil solution containing 10% TFE displayed a α–helical content around 40% (the α–helical content is calculated by the molecular ellipticity value at 222 nm/ 32500 which is the ellipticity value of a standard 100% alpha-helix poli-Lysine peptide at 222nm (Greenfield and Fasman 1969).

TFE increases the α–helical content while it disrupts tertiary and quaternary structures stabilized by hydrophobic interactions (Lau, Taneja et al. 1984). Therefore for studying the relationship between peptide concentration and α–helical content, a TFE concentration of 10% was chosen because it was low enough to stabilize the secondary structure of monomeric peptide while still allowing strong intermolecular interactions. Disrupting effects of TFE on the peptide-peptide interactions producing stable oligomers have been documented at concentrations of TFE as high as 50% (Vinogradov, Mari et al. 1996).

Whereas spectra were independent of peptide concentration in aqueous solution, in the presence of 10% TFE the increase in peptide concentration resulted in a concomitant increase in α–helical content, as indicated by the increase in negative ellipticity at 222 nm (Figure 25). Ellipticity increased from 58% to 86% when peptide concentration increased from 300uM to 600uM. This is consistent with the fact that peptides with α–helical structures that are dependent on dimerization or oligomerization show an augmentation of α–helical content as the peptide concentration is increased. This presumably arises because the equilibrium between monomeric peptide (in the form of random coil) and coiled-coil dimer is shifted toward the formation of the coiled-coil dimer, which increases the α–helical content of the peptide (Adamson, Zhou et al. 1993). Because only 4 aminoacid residues separate the coiled-coil region from the first transmembrane domain in the intact Datlastin protein, we tested if the peptide could adopt an α–helical structure in a membrane mimetic environment generated by using dodecil-phosphate-coline (DPC) micelle (see 3.5.2). When Datl-coil was solubilised in the presence of DPC micelles (used at concentration higher than its critical micelle concentration CMC), we found that the peptide folded into alpha-helix (Figure 25). This observation suggests that within native Datlastin the position of the coiled coil region in close proximity of the ER membranes may be important for proper folding of this domain into alpha helix.

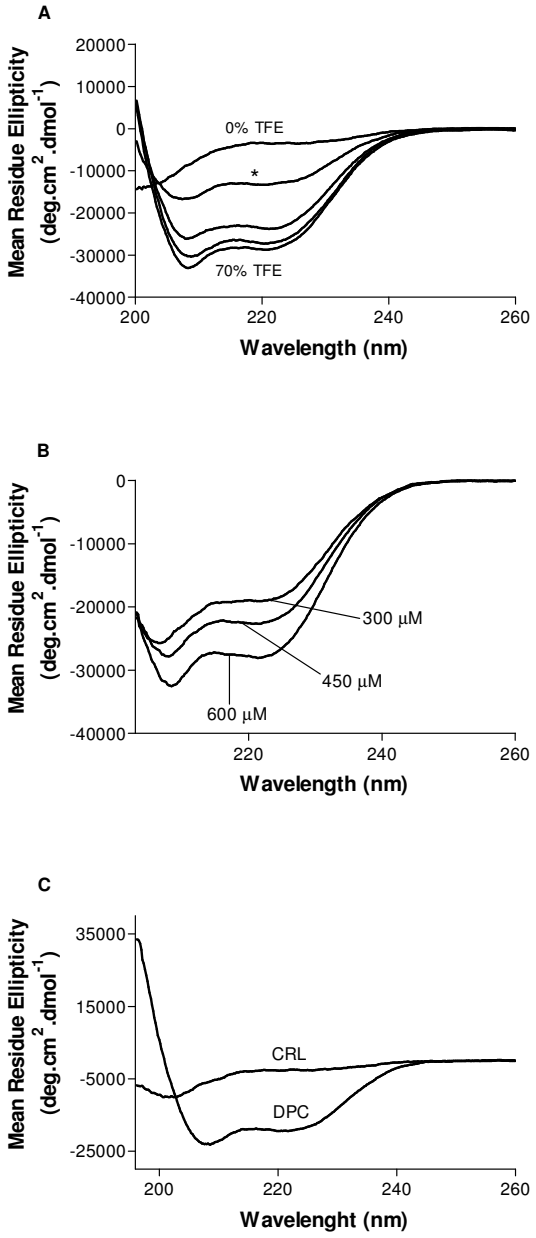

Figure 25 CD spectra of the synthetic peptide Datl-coil

A) CD spectra of Datl-coil at different TFE concentrations. Spectra were recorded in 50 mM phosphate buffer, pH 7, KCl 50mM in the presence of increasing concentrations of TFE. Peptide concentration was 60 uM. TFE concentrations used were 10 (*), 30, 50 and 70%.

B) CD spectra of Datl-coil as function of peptide concentration. Spectra were recorded in 50 mM phosphate buffer, pH 7, KCl 50mM and the peptide concentration used were 300 uM, 450 uM and 600 uM.

C) CD spectra of Datl-coil in a membrane mimetic environment. Spectra were recorded in 50 mM phosphate buffer, pH 7, KCl 50mM with or without 150 mM DPC. The peptide concentration used was 60 uM.

4.4 Datlastin region mediating self-interaction

To provide direct experimental evidence supporting the prediction that the 383-419 region, located immediately N-terminal to the bipartite transmembrane segment, mediates the physical interaction between Datlastin molecules, a series of deletion constructs were generated: $Datl^{1-303}$ encompassing the GTP binding domain, $Datl^{304-422}$ containing the putative coiled-coil, $Datl^{423-541}$ that includes the two transmembrane domains and the C-terminus, and $Datl^{304-541}$(3.1.2). The self-assembly capacity of these fragments was assessed by co-trasfecting HeLa cells with the two tagged forms (HA and Myc) of each fragment followed by co-immunoprecipitation on anti Myc beads. We found that only $Datl^{304-541}$ paralleled the behaviour of full length Datlastin and self-assembled in stable complexes, while $Datl^{1-303}$, $Datl^{304-422}$ and $Datl^{423-541}$ did not oligomerize (Figure 26). Though initially surprising, the finding that $Datl^{304-422}$ does not oligomerize is consistent with the CD observation that the coiled-coil region of Datlastin does not fold correctly when removed from its native context, and is thus unable to mediate homo-oligomerization. The retained self-assemble capacity of $Datl^{304-541}$ and the inability to oligomerize of $Datl^{423-541}$ suggest that the domain mediating Datlastin self-interaction resides in the region included between aminoacid residues 304 and 422, in agreement with *in silico* models that identified a coiled-coil region between methionine 383 and alanine 419.

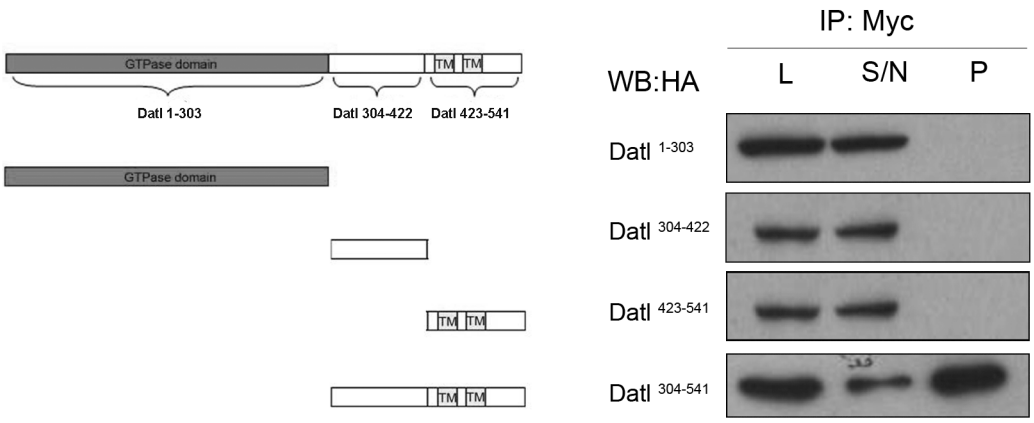

Figure 26 Datlastin region mediating self assembly

A series of Datlastin deletion constructs were generated and their self-assembly capacity was assessed by co-trasfecting HeLa cells with the two tagged forms (HA and Myc) of each fragment followed by co-immunoprecipitation on anti Myc beads. Only Datl$^{304-541}$ parallels the behaviour of full length Datlastin to self-assemble in stable complexes. L, lysate; S/N, supernatant; P, pellet.

4.5 Datlastin coiled-coil mutants are inactive and unable to self-assemble

Membrane tethering through the formation of stable *trans* complexes between proteins on adjacent membranes is a critical step for membrane fusion in general. Known fusogenic proteins such as SNAREs and mitofusins use coiled-coil mediated oligomerization to allow close membrane apposition, an essential step for further fusion. To test if the predicted coiled-coil region was also essential for Datlastin function in ER homotypic fusion, three aminoacid substitutions were designed to destabilize its structure and potentially prevent Datlastin oligomerization.

Leucine 396, Leucine 400 and Phenylalanine 404 were substituted with Proline in full length Datlastin. These three amino acids were chosen because previously identified by the molecular modelling approach as crucial for maintenance of the coiled-coil structure since they localize in the hydrophobic core (see 4.2). The effects of these substitutions on Datlastin function were studied in transfected HeLa cells (see 3.1.3). Because of Datlastin role in homotypic fusion of ER membranes, we analyzed the consequences of

the expression of Datlastin coiled-coil mutants on ER and Golgi morphologies and compared them with the phenotypes induced by the expression of wild type Datlastin.

As previously observed *in vivo* in *Drosophila* (see 1.4.3), overexpression of wild type Datlastin in HeLa cells caused excessive fusion of ER membranes, which resulted in the formation of enlarged ER cytosolic bodies and in the absence of normal perinuclear Golgi and redistribution of Golgi proteins to the ER (Figure 27 and Figure 28). Golgi disruption is a secondary effect due to secretory traffic blockage resulting from overfusion of the ER. The Golgi is not a conventional organelle, i.e. it is not an autonomous entity comprised of stable components, but it appears to function as a steady-state membrane structure that undergoes continuous outgrowth from and reconsumption by the ER through the formation of anterograde and retrograde transport intermediates.

Similarly to wild type Datlastin, coiled coil mutants Datlastin ^{L396P}, Datlastin ^{L400P} and Datlastin ^{F404P} were localized specifically to ER membranes, but they gave rise to a much milder phenotype: cells transfected with these single Datlastin coiled-coil mutants displayed normal Golgi morphology and perinuclear localization, and the ER showed a much reduced extent of fusion (Figure 27 and Figure 28). These results indicate that individually the L396P, the L400P and the F404P mutations diminished the function of Datlastin without completely inactivating the protein.

To establish if this functional impairment of Datlastin was due to the inability of coiled-coil mutants to self-assemble, we performed co-immunoprecipitation experiments. HeLa cells were co-transfected with the two tagged forms (HA and Myc) of each Datlastin coiled-coil mutant followed by co-immunoprecipitation on anti Myc beads. Co-immunoprecipitations showed that all of these individual substitutions Datlastin^{L396P}, Datlastin^{L400P} and Datlastin^{F404P} affected, but did not abolish, the capacity of Datlastin to self-assemble (Figure 29). These data confirm that the diminished activity of Datlastin coiled-coil mutants is associated with reduced self-assembly ability.

We therefore combined all three mutations in the same Datlastin molecule. In transfected HeLa cells Datlastin$^{L396P,\ L400P,\ F404P}$ displayed a normal reticular localization and didn't cause hyperfusion of ER membranes. The ER showed a normal morphology with the absence of hyperfused cytosolic ER bodies. Accordingly, Golgi apparatus morphology and perinuclear localization were not affected (Figure 27 and Figure 28).

To test if the simultaneous presence of L396P, L400P and F404P abolished Datlastin oligomerization ability, HeLa cells were co-transfected with HA or Myc tagged Datlastin^{L396P,L400P,F404P} constructs. Lysates prepared from these cells were immunoprecipitated using anti-Myc antibodies. The absence of HA tagged Datlastin^{L396P,L400P,F404P} in the immunoprecipitate indicated that the simultaneous presence of these three substitutions impaired the stability of the coiled-coil abolishing the ability of Datlastin to self-assemble (Figure 30). The previously described vesicle co-immunprecipitation assay was used to test if the inability of Datlastin$^{L396P, L400P, F404P}$ to self-assemble prevented the formation of trans-oligomeric complexes between Datlastin molecules on distinct ER membranes necessary to mediate tethering. Not surprisingly, Datlastin$^{L396P, L400P, F404P}$ was unable to link adjacent membranes (Figure 31), indicating that destabilization of the coiled-coil prevents membrane tethering. Thus, the coiled-coil region is critical for Datlastin-mediated homotypic fusion of ER membranes.

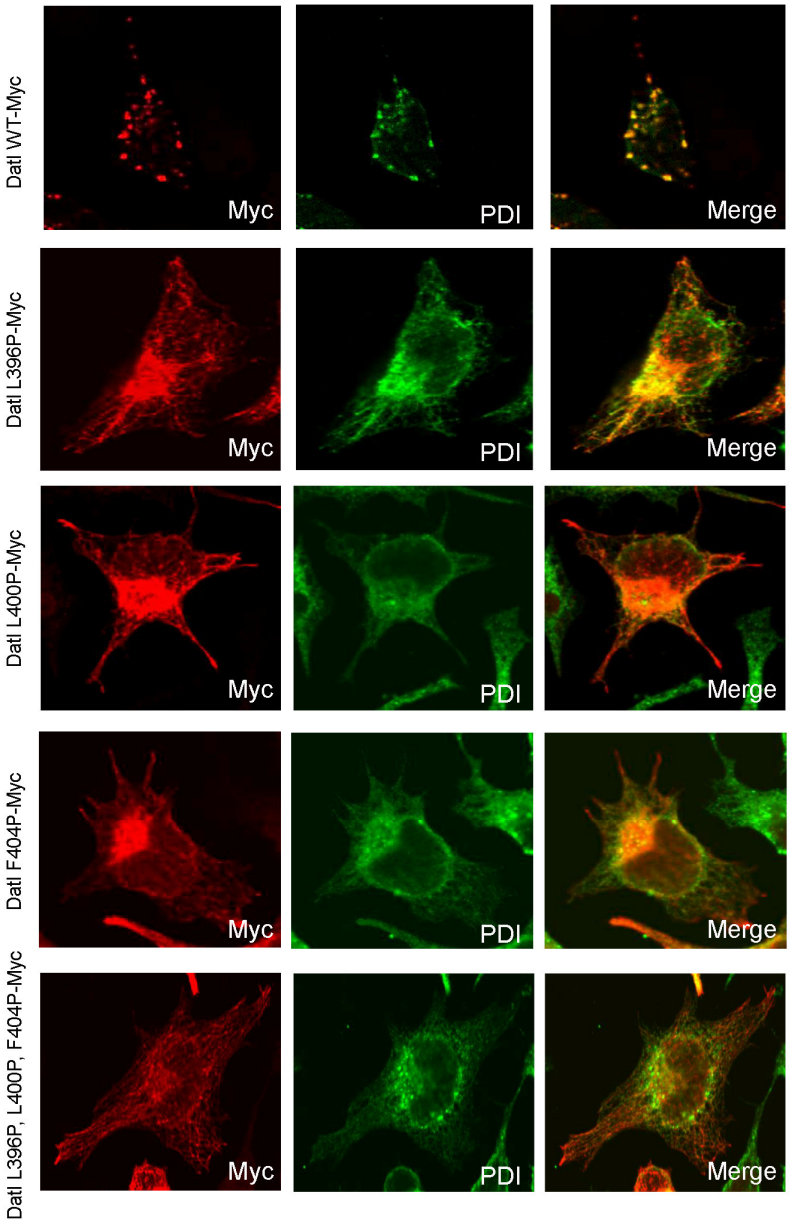

Figure 27 Datlastin coiled-coil mutants are inactive: effects of their expression on ER

Anti-PDI antibody was used to visualize ER morphology. Expression of wild type Datlastin-Myc in HeLa cells causes excessive fusion of ER membranes which results in the formation of enlarged ER cytosolic bodies. Expression of single coiled-coil mutants Datlastin^{L396P}, Datlastin^{L400P} and Datlastin^{F404P} gives rise to a milder phenotype with the ER showing a much reduced extent of fusion. The simultaneous presence of all three substitutions in Datlastin$^{L396P,\ L400P,\ F404P}$ mutant doesn't result in hyperfusion of ER membranes which show a normal reticular morphology.

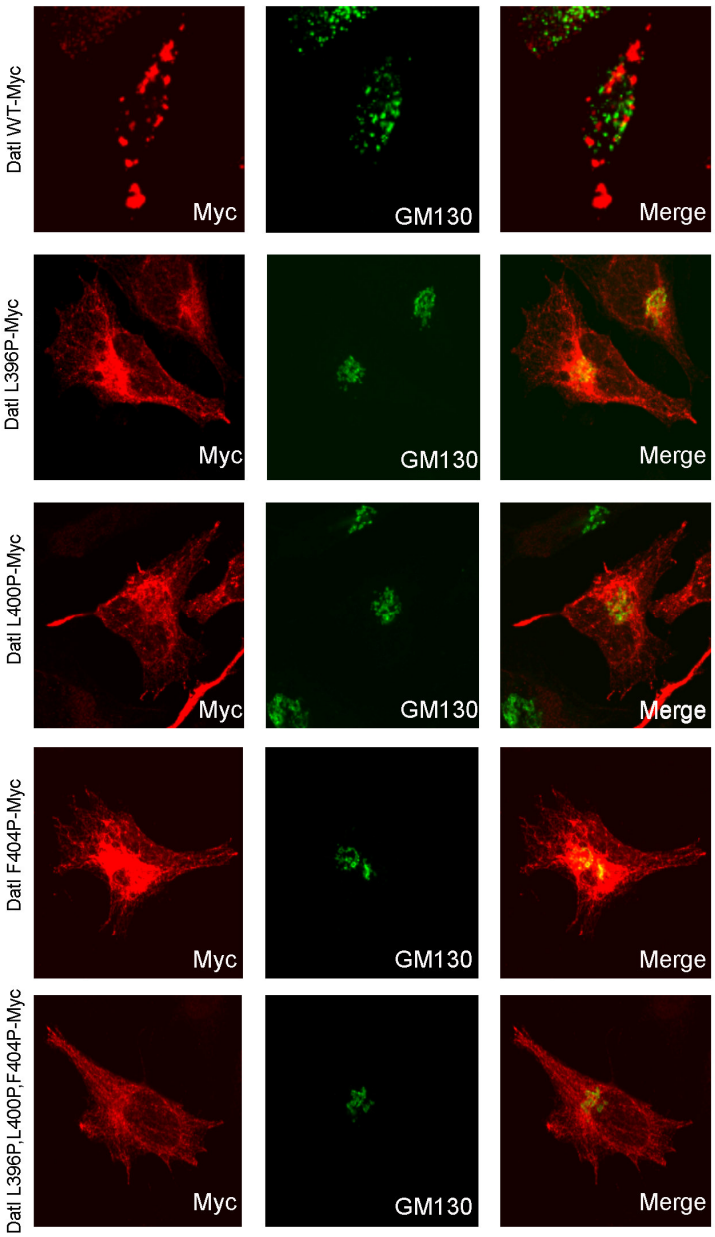

Figure 28 Datlastin coiled-coil mutants are inactive: effects of their expression on Golgi apparatus

Anti-GM130 antibody was used to visualize Golgi apparatus. After expression of wild type Datlastin-Myc in HeLa cells, the Golgi looses its integrity and its normal perinuclear localization and is reabsorbed to the ER. HeLa cells expressing Datlastin coiled coil mutants Datlastin^{L396P}, Datlastin^{L400P}, Datlastin^{F404P} and Datlastin$^{L396P, L400P, F404P}$ display a normal Golgi morphology with its typical perinuclear localization.

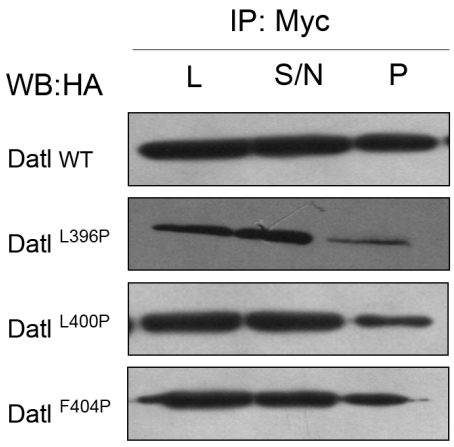

Figure 29 Single substitutions in Datlastin coiled-coil region affect, without abolishing, Datlastin self-assembly ability

HeLa cells were co-transfected with two differently tagged forms (HA and Myc) of each Datlastin coiled-coil mutants Datlastin^{L396P}, Datlastin^{L400P} and Datlastin ^{F404P}. Lysates prepared from these cells were immunoprecipitated using anti-Myc antibodies. Co-immunoprecipitations show that all of these individual substitutions L396P, L400P and F404P affect, but do not abolish, the capacity of Datlastin to self-assemble. L, lysate; S/N, supernatant; P, pellet.

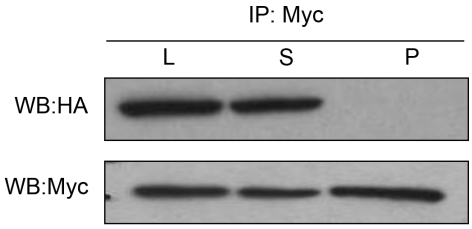

Figure 30 The simultaneous presence of L396P, L400P and F404P mutations abolishes Datlastin oligomerization ability

HeLa cells were co-transfected with HA and Myc tagged Datlastin$^{L396P,\ L400P,\ F404P}$ constructs. Lysates prepared from these cells were immunoprecipitated using anti-Myc antibodies. The absence of HA tagged Datlastin$^{L396P,\ L400P,\ F404P}$ in the immunoprecipitate indicates that the simultaneous presence of these three substitutions abolishes the ability of Datlastin to self-assemble. L, lysate; S, supernatant; P, pellet.

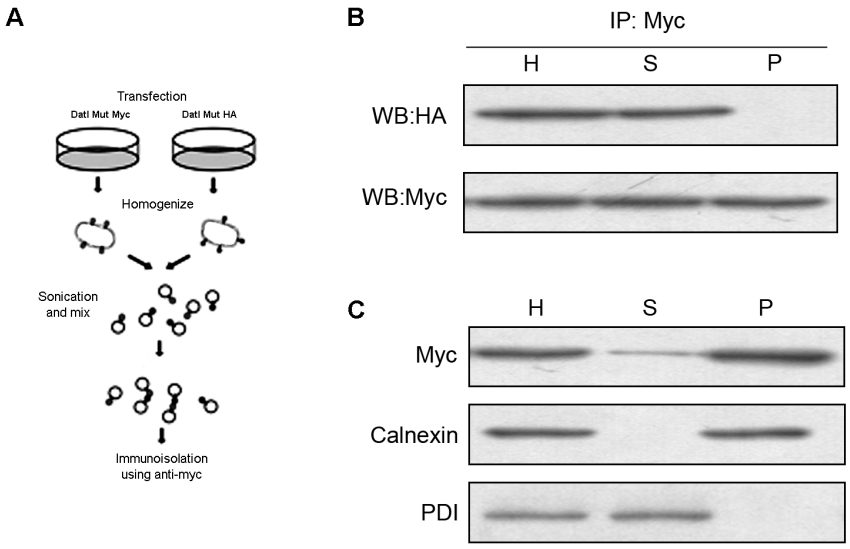

Figure 31 The simultaneous presence of L396P, L400P and F404P mutations abolishes Datlastin ability to mediate membrane tethering

(**A**) Schematic representation of the membrane vesicle immunoprecipitation assay (**B**) Cleared homogenates from HeLa cells expressing Datlastin$^{L396P,\ L400P,\ F404P}$-HA or Datlastin$^{L396P,\ L400P,\ F404P}$-Myc were sonicated, mixed and incubated. The reaction mixture was subjected to immunoprecipitation using anti-Myc antibody. The immunoprecipitate was analyzed by western blotting with anti-Myc and anti-HA antibodies. Datlastin$^{L396P,\ L400P,\ F404P}$ is unable to self-associate through the formation of a complex in *trans* between Datlastin molecules localized on adjacent ER membranes (**C**)Western blot analysis of the soluble and membrane fractions obtained by ultracentrifugation of cell homogenates demonstrates that Datlastin$^{L396P,\ L400P,\ F404P}$ fractionates exclusively with the membrane pellet together with the ER membrane protein calnexin, while the ER-lumenal protein PDI is found in the soluble cytosolic fraction. H, cell homogenate; S, supernatant; P, pellet.

4.6 GTPase-deficient Datlastin mutant is inactive

To test if Datlastin involvement in the homotypic fusion of ER membranes was dependent on its GTPase activity, *Drosophila* transgenic lines were generated for the expression of Datlastin^{K51A} mutant (UAS-Datlastin^{K51A}-Myc; see introduction 1.2 and methods 3.6). Datlastin^{K51A} carries a substitution in the P-loop of the GTPase domain that abolishes GTP binding thus preventing the GTP hydrolysis. The replacement of the

corresponding Lysine in other GTP binding domains is known to inactivate the protein function (Praefcke and McMahon 2004).

The K51A substitution was introduced in the Datlastin cDNA by site directed mutagenesis (3.1.3) and its presence was confirmed by sequence analysis. To generate *Drosophila* transgenic lines, the mutated cDNA was introduced in the pUAST vector, which is designed for successful transgene incorporation into the *Drosophila* genome (3.1.4), in frame at the 3' terminal with a Myc tag. The final Datlastin^{K51A}/pUAST construct was microinjected in *Drosophila* embryos and the obtained transgenic lines were then mapped to a specific chromosome and balanced (Table 5). All of these pUAST-Datlastin^{K51A}-Myc transgenic lines showed similar Datlastin^{K51A} expression level and line 7 was chosen for further experiments.

Transgenic line	Chromosome localization
1 Datlastin^{K51A}-Myc	III
2 Datlastin^{K51A}-Myc	III
3 Datlastin^{K51A}-Myc	II
5 Datlastin^{K51A}-Myc	II
7 Datlastin^{K51A}-Myc	II

Table 5 Datlastin^{K51A}-Myc transgenic lines

To study the effects of *in vivo* Datlastin^{K51A} overexpression, we took advantage of the UAS/GAL4 system. In the Datlastin^{K51A}/pUAST construct Datlastin^{K51A} is placed under the control of UAS, the yeast transcriptional activator GAL4 binding sequence. In the absence of GAL4, the transgene is inactive. When flies carrying UAS-Datlastin^{K51A} are crossed to flies that express GAL4 in a specific tissue or cell type, the transgenic protein is made only in these tissues or cells (see introduction 1.2).

While overexpression of wild type UAS-Datlastin Myc with a number of ubiquitous and tissue specific promoters led to lethality during early development, overexpression of UAS-Datlastin^{K51A}-Myc with the same drivers allowed survival of the flies (Table 6) These phenotypes indicated that the replacement of Lysine 51 with Alanine results in an inactive protein. Moreover while eye-specific overexpression of UAS-Datlastin Myc

using GMR-Gal4 driver line gave rise to a small and rough eye, overexpression of Datlastin^{K51A}-Myc had not phenotype (Figure 32).

Driver	UAS-Datlastin-Myc	UAS-Datlastin^{K51A}-Myc
GMR-Gal4	Small and rough eye	Normal eye
Tubulin-Gal4	Lethal	No phenotype
Elav-Gal4	Lethal	No phenotype
MEF2-Gal4	Lethal	No phenotype

Table 6 Phenotypes derived from overexpression of UAS-Datlastin-Myc and UAS-Datlastin^{K51A}-Myc with different drivers

GMR (Glass Multimer Response) is a eye-specific promoter; Tubulin is an ubiquitous promoter; Elav (Embryonic Lethal, Abnormal Vision) is a pan-neural promoter and MEF2 (Myocyte Enhancer Factor 2) is a muscle promoter.

Then *in vivo* effects of UAS-Datlastin^{K51A}-Myc expression on ER and Golgi morphologies were analyzed and compared with those caused by expression of wild type Datlastin-Myc. To test these effects, we used the motor neuron driver D42-Gal4 which allows individuals overexpressing wild type Datlastin to reach pupa stage thus allowing the comparison. Immunohistochemistry and electron microscopy analyses of larva preparations revealed that, in contrast to wild type Datlastin (see introduction 1.4.3), expression of Datlastin^{K51A}-Myc under the control of D42-Gal4 driver results in unaltered ER and Golgi morphologies (Figure 33). Similarly, expression in HeLa cells of Datlastin^{K51A}-Myc didn't cause fusion of ER membranes with the formation of the typical ER cytosolic bodies induced by the expression of wild type Datlastin-Myc (Figure 34). Unlike cells transfected with wild type Datlastin, cells transfected with Datlastin^{K51A}-Myc displayed a normal Golgi apparatus which retained its perinuclear localization (Figure 35). Taken together these results demonstrate that formation of an aberrant ER depends crucially on the GTPase activity of Datlastin.

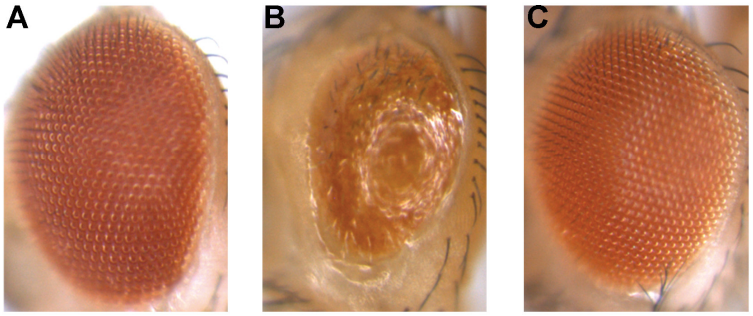

Figure 32 GTPase-deficient K51A Datlastin mutant eye expression

(**A**) Wild type adult *Drosophila* eye. (**B**) Overexpression of wild type Datlastin under the control of GMR-Gal4 causes a small eye phenotype. (**C**) GMR-Gal4 driven overexpression of Datlastin^{K51A} has no phenotypic consequences, suggesting that this mutant is functionally inactive.

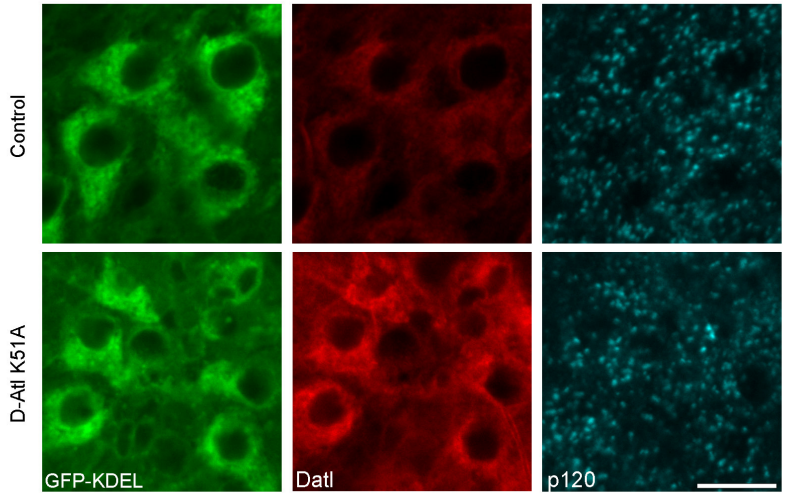

Figure 33 GTPase-deficient K51A Datlastin mutant is inactive: *in vivo* effects of its overexpression

Simultaneous visualization of ER marker GFP-KDEL (green), Golgi p120 (blu) and Datlastin^{K51A} (red) by confocal microscopy of tubulin-Gal4/+;UAS-Datlastin^{K51A}-Myc /+ ventral ganglion neurons, indicates that mutant Datlastin normally localizes to the endoplasmic reticulum and that upon its overexpression ER and Golgi morphologies are preserved (as indicated by the normal pattern of GFP-KDEL and p120 fluorescence).

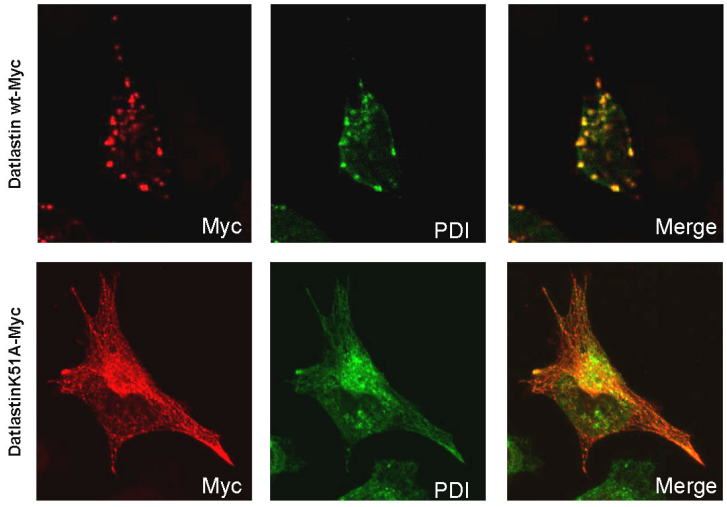

Figure 34 GTPase-deficient K51A Datlastin mutant is inactive: *in vitro* effects of its overexpression on ER

HeLa cells transfected with wild type Datlastin-Myc or Datlastin^{K51A}-Myc constructs were labelled with anti-PDI to visualize ER. Datlastin^{K51A}-Myc doesn't cause fusion of ER membranes with the formation of the typical ER cytosolic bodies induced by the expression of wild type Datlastin-Myc.

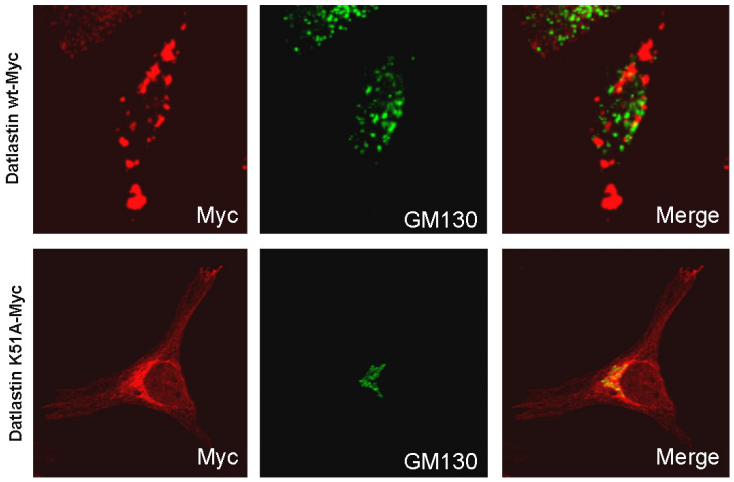

Figure 35 GTPase-deficient K51A Datlastin mutant is inactive: *in vitro* effects of its overexpression on Golgi apparatus

HeLa cells transfected with wild type Datlastin-Myc or Datlastin^{K51A}-Myc constructs were labelled with anti-GM130 to visualize Golgi. In Datlastin^{K51A}-Myc transfected cells Golgi apparatus is integral and

retains its perinuclear localization whereas overexpression of the functional wild type Datlastin-Myc causes Golgi reabsorption into ER.

4.7 GTPase defiecient Datlastin mutant is unable to mediate tethering of ER membranes

To understand the mechanism by which loss of GTPase activity resulted in loss of Datlastin function, we tested if the GTPase activity might regulate Datlastin self-assembly ability. HeLa cells were co-transfected for the expression of Datlastin^{K51A}-HA and Datlastin^{K51A}-Myc (3.1.3) and the lysate obtained from these cells was immunoprecipitated using anti-Myc antibodies. Because co-immunoprecipitation of HA tagged Datlastin ^{K51A} did not occur (Figure 36), this result demonstrates that GTPase activity is critical for self-association of Datlastin molecules.

We then performed the previously described vesicle co-immunprecipitation assay to establish whether the inability of GTPase deficient Datlastin mutant to self-assemble prevented the formation of *trans* oligomeric complexes between distinct ER membranes. Membrane vesicles were prepared from HeLa cells separately transfected with Datlastin^{K51A}-HA or Datlastin^{K51A}–Myc constructs. The absence of Datlastin^{K51A}-HA in the Datlastin^{K51A}-Myc immunoprecipitate shows that the two type of vesicle are unable to bind to each other (Figure 37). This result strongly suggests that the inabiltity of Datlastin^{K51A} to oligomerize prevents the formation of *trans*-oligomeric complexes between Datlastin^{K51A} molecules on distinct membranes. Thus, GTPase-deficient Datlastin^{K51A} lacks the competence to mediate membrane tethering. Centrifugal fractionation of cleared cell homogenates showed that Datlastin^{K51A}, like wild type Datlastin, was exclusively found in the membrane fraction (Figure 37).

Together, these data indicate that the Datlastin^{K51A} GTPase mutant is functionally inactive and that this inactivity is due to the inability to self-associate and to mediate membrane tethering.

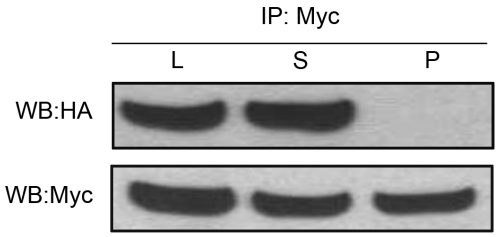

Figure 36 GTPase-deficient DatlastinK51A is unable to self-associate

Anti-Myc immunoprecipitates from HeLa cells co-transfected with Datlastin^{K51A}-HA and Datlastin^{K51A} -Myc were devoid of Datlastin^{K51A}-HA, indicating the inability of GTPase-deficient Datlastin^{K51A} to self-associate. L, lysate; S, supernatant; P, pellet.

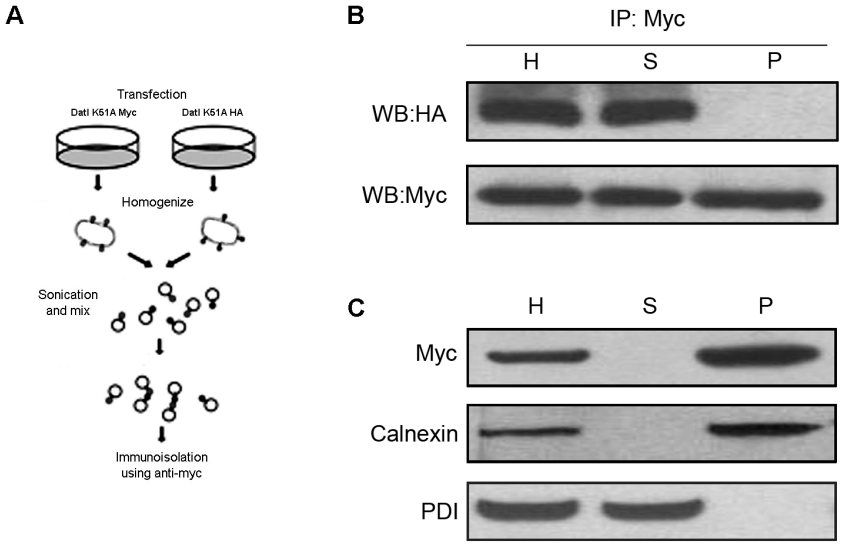

Figure 37 Membrane tethering by Datlastin is GTP-dependent

(**A**) Schematic representation of the membrane vesicle immunoprecipitation assay (**B**) Cleared homogenates from HeLa cells expressing Datlastin^{K51A}-HA or Datlastin^{K51A}-Myc were sonicated, mixed and incubated. The reaction mixture was subjected to immunoprecipitation using anti-Myc antibody. The immunoprecipitate was analyzed by western blotting with anti-Myc and anti-HA antibodies. Datlastin^{K51A} is unable to self-associate through the formation of a complex in *trans* between Datlastin molecules localized on adjacent ER membranes. (**C**) Western blot analysis of the soluble and membrane fractions obtained by ultracentrifugation of cell homogenates demonstrates that Datlastin^{K51A} fractionates exclusively with the membrane pellet together with the ER membrane protein calnexin, while the ER-lumenal protein PDI is found in the soluble cytosolic fraction. H, cell homogenate; S, supernatant; P, pellet

5 Discussion

Mutations of the SPG3a gene, which encodes for Atlastin-1, are responsible for a form of Hereditary Spastic Paraplegia (HSP), a clinically and genetically group of inherited disorders mainly characterized by progressive lower extremity spasticity and weakness.
Atlastin-1 belongs to the dynamin superfamily of large GTPases (Zhao, Alvarado et al. 2001): it contains a large GTPase domain and two transmembrane domains reportedly targeting the protein to either Golgi (Zhu, Patterson et al. 2003) or Endoplasmic reticulum membranes (Sanderson, Connell et al. 2006; Namekawa, Muriel et al. 2007). Atlastin-1 has been implicated in ER-Golgi vesicle trafficking and Golgi morphogenesis (Zhao, Alvarado et al. 2001; Zhu, Patterson et al. 2003; Namekawa, Muriel et al. 2007), however the identification of two additional atlastin proteins (Atlastin-2 and Atlastin-3) in the human genome (Zhu, Patterson et al. 2003) has complicated the analysis of its cellular role. Although mammalian Atlastin-2 and-3 were shown to reside in the ER and all atlastins were proposed to be involved both in Golgi and ER morphogenesis, their precise function remains unexplained.
In our laboratory, we used *Drosophila* as a model organism to study Atlastin function. The presence in the *Drosophila* genome of a single high conserved Atlastin ortholog (Datlastin) combined with the wide array of experimental tools available, makes *Drosophila* a valuable system to investigate the role of Atlastin.
Experiments carried out *in vivo* and *in vitro* have shown that Datlastin is implicated in the homotypic fusion of Endoplasmic reticulum membranes. The ER is a membrane-bound organelle composed by a network of interconnected tubules that pervades the cytoplasm of eukaryotic cells. The elaborate structure of the ER reflects its complex cellular role, and maintenance of this architecture is instrumental for proper execution of ER functions. The ER is continuously rearranged while maintaining its characteristic structure, and ER dynamics are the result of movement of tubules along the cytoskeleton (Waterman-Storer and Salmon 1998; Lane and Allan 1999) and GTP-dependent homotypic fusion events (Dreier and Rapoport 2000; Voeltz, Prinz et al. 2006; Anderson and Hetzer 2007). Datlastin has been identified as the GTPase directly responsible for ER homotypic fusion.

The studies I have conducted during my Ph.D. have focused on the mechanisms underlying Datlastin function.

Numerous membrane-fusion processes have been extensively studied and many molecules that are involved in fusion have been identified (Figure 9). From these studies it is clear that there are distinct and structurally unrelated membrane fusion molecules, but also that general principles operate in all fusion events (homotypic and heterotypic). Membrane fusion requires an initial tethering step which locks apposing membranes together, followed by the merger of the lipid bilayers.

By analogy with known systems (SNARE mediated fusion or viral fusion), also ER homotypic fusion requires an initial tethering step to take membranes into close apposition. Accordingly, *in vitro* experiments of ER network formation have shown that ER vesicles first form cluster-like structures in a reaction that requires GTP hydrolysis and that has been proposed to correspond to the tethering of membrane vesicles (Dreier and Rapoport 2000).

In my PH.D. work I have shown that Datlastin can mediate membrane tethering. Immunoprecipitation experiments demonstrate that Datlastin is capable of homo-oligomerization similarly to its human counterparts. Self-association can occur within the same membrane (Figure 20) as well as between opposing membranes as demonstrated by the vesicle co-immunoprecipitation assay (Figure 21). The self-assembling property leads to the formation of *trans* complexes between Datlastin molecules on distinct ER membranes that can connect adjacent ER vesicles via a homotypic interaction. This tethering leads eventually to full membrane fusion.

Importantly, we established the region of Datlastin involved in self-association.

Since primary sequence analysis didn't reveal the presence of obvious domains implicated in oligomerization, we used molecular modelling analysis to identify a coiled-coil domain between Methionine 383 and Alanine 419. CD experiments confirmed the coiled coil proprieties of the Datlastin Met 383-Ala 419 region (Figure 25). Datl-coil peptide (synthesized from this region) can fold into alpha helix and shows a concentration-dependent augmentation of its alpha helical content, a typical behaviour of alpha helical structures that are dependent on oligomerization.

Coiled-coil domains are protein-protein interaction motifs which mediate subunit oligomerization of a large number of proteins. They consist of two or more alpha

helices (up to seven) that twist around each other to form a supercoil. Coiled-coil domains play a central role in membrane fusion mediated by SNARE proteins, viral envelope glycoproteins and mitofusins (Eckert and Kim 2001; Bonifacino and Glick 2004; Koshiba, Detmer et al. 2004).

Mitofusins, another large GTPases of the dynamin superfamily, present characteristics similar to Datlastin: both are transmembrane GTPases and both are involved in homotypic fusion events; but while Datlastin is involved in ER membrane fusion, mitofusins are essential for eukaryotic mitochondrial fusion. It has been shown that mitofusins can, through homo-oligomerization, tether mitochondria to each other (Koshiba, Detmer et al. 2004). Mitofusins self assembly is mediated by a C-terminal heptad repeat coiled coil domain (HR2).

Also in SNARE mediated membrane fusion, the formation of a tethering complex is a critical step for membrane apposition leading to full fusion. SNAREs consist of a membrane-spanning region, although some SNAREs are attached to the membrane by posttranslational modifications (Kammerer 1997; Mason and Arndt 2004), but essentially they consist of SNARE motifs, alpha helical coiled-coil motifs responsible for the assembly of the four helix bundle which leads to fusion of juxtaposed lipid bilayers.

Mutations in Datlastin coiled-coil region designed in order to destroy its alpha helical structure gave rise to inactive Datlastin molecules. The integrity of the identified coiled-coil region is critical for Datlastin-mediated ER homotypic fusion and its destabilization results in the loss of Datlastin self-assembling and fusogenic abilities (Figure 27 and Figure 31).

CD experiments shown also that Datl-coil peptide folds into alpha helix in the presence of a membrane mimetic environment. Interestingly the coiled-coil region of Datlastin is positioned 3/4 aminoacid residues N-terminal to the bipartite transmembrane anchor, in very close proximity of the ER membrane in a manner strikingly reminiscent of SNAREs.

Because of the substantial sequence homology of Datlastin with the GCN4 leucine zipper domain (Figure 23), Datlastin may assemble into a parallel dimeric coiled-coil. Datlastin localized on opposing membranes would bring the membranes into very close proximity through the formation of parallel trans-oligomers between molecules.

Artificial lipid bilayers have been proposed to initiate fusion when they are separated by ~1 nm (Kozlovsky, Dreiangel et al. 1991), however it is believed that a ~3-4 nm gap between fusing membranes accommodates the SNARE complex in its fusogenic conformation (Martens and McMahon 2008). The 3/4 aminoacid juxtamembrane region of Datlastin accounts for an approximate length of 5-6 Å, while the width of short dimeric coiled-coils ranges between 20 and 30 Å (O'Shea, Klemm et al. 1991; Thepaut, Maiorano et al. 2004). Opposing membranes linked by Datlastin would thus be separated by a gap whose width is consistent with the close apposition necessary for the Datlastin complex to force membrane fusion. Hence, the distance between the alpha-helix and the transmembrane domains is probably the primary determinant of Datlastin ability to promote fusion directly.

The GTPase activity of mitofusin is essential for mitochondria fusion (Ishihara, Eura et al. 2004). GTPase deficient mitofusin molecules are unable to self-assemble. Similarly, Datlastin requires GTP binding and hydrolysis to exert its function. Overexpression of the GTPase-deficient Datlastin^{K51A} mutant, *in vivo* and in HeLa cells, results in a normal ER morphology: ER is depleted of the expanded ER cisternae of hyperfused membranes observed upon Datlastin wild type overexpression (Figure 33 and Figure 34). Co-immunoprecipitation experiments revealed that Datlastin^{51A} inactivity is due to its inability to homo-oligomerize and so to mediate membrane tethering (Figure 36 and Figure 37).

These findings allow use to propose a model for atlastin-mediated homotypic fusion of ER membranes. Upon GTP hydrolysis, Datlastin inserted within the ER membrane is likely to undergo a conformational change which exposes the alpha-helix making it available for interaction with a similarly primed atlastin molecule located on an adjacent membrane. Because of the close juxtaposition between the alpha-helix and the transmembrane segment, bundling of the alpha-helices into a coiled-coil structure brings the two membranes into very close proximity. The energy released following atlastin complex formation could be transduced through the membrane anchor to the lipid bilayers resulting in their destabilization. The combination of close proximity and membrane destabilization would then drive the fusion reaction.

The identification of the coiled-coil region and its position relative to the ER membrane provide new mechanistic insight into the fusogenic properties of Datlastin. Membrane

fusion in general requires molecules that tether membranes, molecules that bring them into close apposition and molecules that disturb the lipid bilayers locally to overcome the energy barriers preventing fusion. Unlike in SNARE-mediated endocellular fusion events where the different functions mentioned above are carried out by different sets of proteins, during ER homotypic fusion Datlastin appears to provide all these functions, including a GTP-dependent tethering step that in SNARE-dependent fusion requires the activity of Rab GTPases and tethering factors (Cai, Reinisch et al. 2007). Therefore, Datlastin is a novel fusogen protein which combines features of both endocellular and viral fusion activities. While GTP-dependent tethering and juxtamembrane coiled-coil formation suggest shared mechanistic aspects with SNARE-mediated fusion, the unique ability of Datlastin to autonomously carry out the distinct steps involved in membrane fusion is more reminiscent of viral fusion proteins (Martens and McMahon 2008).
The discovery of atlastin as a simplified but complete membrane fusion machinery may provide answers to several open questions, including those concerning the biophysical mechanisms underlying membrane fusion.

The largest number of known HSP genes encodes proteins implicated with varying degree of certainty into the general class of trafficking and transport proteins (Soderblom and Blackstone 2006). Analysis of the effects of a number of atlastin-1 pathological mutants has shown that their expression in cell lines affects ER morphology with consequences for the Golgi apparatus that suggest traffic defects (Namekawa, Muriel et al. 2007). Although these phenotypes depend on significant overexpression and thus their relevance to HSP pathogenesis is unclear, they demonstrate that the presence of disease-causing mutations does not abolish atlastin function. The *Drosophila* model indicates that manipulation of Datlastin function perturbs the structural organization of the ER and that these alterations can eventually lead to membrane traffic defects. It is therefore plausible that small disturbances of ER architecture brought about by pathogenic atlastin-1 expressed at endogenous levels in HSP patients may also impact traffic. Therefore, the pathological mechanism responsible for atlastin-1 linked HSP could be perturbation of ER homeostasis ultimately leading to secondary membrane traffic defects, to which the long corticospinal axons affected by HSP are particularly vulnerable.

6 References

Adamson, J. G., N. E. Zhou, et al. (1993). "Structure, function and application of the coiled-coil protein folding motif." Curr Opin Biotechnol **4**(4): 428-37.

Anderson, D. J. and M. W. Hetzer (2007). "Nuclear envelope formation by chromatin-mediated reorganization of the endoplasmic reticulum." Nat Cell Biol **9**(10): 1160-6.

Baumann, O. and B. Walz (2001). "Endoplasmic reticulum of animal cells and its organization into structural and functional domains." Int Rev Cytol **205**: 149-214.

Behan, W. M. and M. Maia (1974). "Strumpell's familial spastic paraplegia: genetics and neuropathology." J Neurol Neurosurg Psychiatry **37**(1): 8-20.

Berman, H. M., J. Westbrook, et al. (2000). "The Protein Data Bank." Nucleic Acids Res **28**(1): 235-42.

Bier, E. (2005). "Drosophila, the golden bug, emerges as a tool for human genetics." Nat Rev Genet **6**(1): 9-23.

Bierzynski, A., P. S. Kim, et al. (1982). "A salt bridge stabilizes the helix formed by isolated C-peptide of RNase A." Proc Natl Acad Sci U S A **79**(8): 2470-4.

Bonifacino, J. S. and B. S. Glick (2004). "The mechanisms of vesicle budding and fusion." Cell **116**(2): 153-66.

Brand, A. H. and N. Perrimon (1993). "Targeted gene expression as a means of altering cell fates and generating dominant phenotypes." Development **118**(2): 401-15.

Brown, J. E. and W. A. Klee (1971). "Helix-coil transition of the isolated amino terminus of ribonuclease." Biochemistry **10**(3): 470-6.

Cai, H., K. Reinisch, et al. (2007). "Coats, tethers, Rabs, and SNAREs work together to mediate the intracellular destination of a transport vesicle." Dev Cell **12**(5): 671-82.

Depienne, C., G. Stevanin, et al. (2007). "Hereditary spastic paraplegias: an update." Curr Opin Neurol **20**(6): 674-80.

Dreier, L. and T. A. Rapoport (2000). "In vitro formation of the endoplasmic reticulum occurs independently of microtubules by a controlled fusion reaction." J Cell Biol **148**(5): 883-98.

Dube, M. P., M. A. Mlodzienski, et al. (1997). "Hereditary spastic paraplegia: LOD-score considerations for confirmation of linkage in a heterogeneous trait." Am J Hum Genet **60**(3): 625-9.

Dyson, H. J., G. Merutka, et al. (1992). "Folding of peptide fragments comprising the complete sequence of proteins. Models for initiation of protein folding. I. Myohemerythrin." J Mol Biol **226**(3): 795-817.

Dyson, H. J., J. R. Sayre, et al. (1992). "Folding of peptide fragments comprising the complete sequence of proteins. Models for initiation of protein folding. II. Plastocyanin." J Mol Biol **226**(3): 819-35.

Eckert, D. M. and P. S. Kim (2001). "Mechanisms of viral membrane fusion and its inhibition." Annu Rev Biochem **70**: 777-810.

Errico, A., A. Ballabio, et al. (2002). "Spastin, the protein mutated in autosomal dominant hereditary spastic paraplegia, is involved in microtubule dynamics." Hum Mol Genet **11**(2): 153-63.

Evans, K., C. Keller, et al. (2006). "Interaction of two hereditary spastic paraplegia gene products, spastin and atlastin, suggests a common pathway for axonal maintenance." Proc Natl Acad Sci U S A **103**(28): 10666-71.
Fink, J. K. (2003). "Advances in the hereditary spastic paraplegias." Exp Neurol **184 Suppl 1**: S106-10.
Fortini, M. E., M. P. Skupski, et al. (2000). "A survey of human disease gene counterparts in the Drosophila genome." J Cell Biol **150**(2): F23-30.
Greenfield, N. and G. D. Fasman (1969). "Computed circular dichroism spectra for the evaluation of protein conformation." Biochemistry **8**(10): 4108-16.
Gruber, M., J. Soding, et al. (2006). "Comparative analysis of coiled-coil prediction methods." J Struct Biol **155**(2): 140-5.
Haller, O. and G. Kochs (2002). "Interferon-induced mx proteins: dynamin-like GTPases with antiviral activity." Traffic **3**(10): 710-7.
Hansen, J. J., A. Durr, et al. (2002). "Hereditary spastic paraplegia SPG13 is associated with a mutation in the gene encoding the mitochondrial chaperonin Hsp60." Am J Hum Genet **70**(5): 1328-32.
Harding, A. E. (1993). "Hereditary spastic paraplegias." Semin Neurol **13**(4): 333-6.
Hodges, R. S., N. E. Zhou, et al. (1990). "Synthetic model proteins: contribution of hydrophobic residues and disulfide bonds to protein stability." Pept Res **3**(3): 123-37.
Hu, C., M. Ahmed, et al. (2003). "Fusion of cells by flipped SNAREs." Science **300**(5626): 1745-9.
Ishihara, N., Y. Eura, et al. (2004). "Mitofusin 1 and 2 play distinct roles in mitochondrial fusion reactions via GTPase activity." J Cell Sci **117**(Pt 26): 6535-46.
Kammerer, R. A. (1997). "Alpha-helical coiled-coil oligomerization domains in extracellular proteins." Matrix Biol **15**(8-9): 555-65; discussion 567-8.
Kano, F., H. Kondo, et al. (2005). "NSF/SNAPs and p97/p47/VCIP135 are sequentially required for cell cycle-dependent reformation of the ER network." Genes Cells **10**(10): 989-99.
Kano, F., H. Kondo, et al. (2005). "The maintenance of the endoplasmic reticulum network is regulated by p47, a cofactor of p97, through phosphorylation by cdc2 kinase." Genes Cells **10**(4): 333-44.
Keller, W., P. Konig, et al. (1995). "Crystal structure of a bZIP/DNA complex at 2.2 A: determinants of DNA specific recognition." J Mol Biol **254**(4): 657-67.
Kenwrick, S., A. Watkins, et al. (2000). "Neural cell recognition molecule L1: relating biological complexity to human disease mutations." Hum Mol Genet **9**(6): 879-86.
Klein, D. E., A. Lee, et al. (1998). "The pleckstrin homology domains of dynamin isoforms require oligomerization for high affinity phosphoinositide binding." J Biol Chem **273**(42): 27725-33.
Koshiba, T., S. A. Detmer, et al. (2004). "Structural basis of mitochondrial tethering by mitofusin complexes." Science **305**(5685): 858-62.
Kozlovsky, A., A. Dreiangel, et al. (1991). "The "chewing wheel" device: plaque-removing efficiency and use in oral hygiene programs." Quintessence Int **22**(9): 727-30.

Krishnan, K. S., R. Rikhy, et al. (2001). "Nucleoside diphosphate kinase, a source of GTP, is required for dynamin-dependent synaptic vesicle recycling." Neuron **30**(1): 197-210.
Lane, J. D. and V. J. Allan (1999). "Microtubule-based endoplasmic reticulum motility in Xenopus laevis: activation of membrane-associated kinesin during development." Mol Biol Cell **10**(6): 1909-22.
Lau, S. Y., A. K. Taneja, et al. (1984). "Synthesis of a model protein of defined secondary and quaternary structure. Effect of chain length on the stabilization and formation of two-stranded alpha-helical coiled-coils." J Biol Chem **259**(21): 13253-61.
Lee, Y., D. Paik, et al. (2006). "Loss of spastic paraplegia gene atlastin induces age-dependent death of dopaminergic neurons in Drosophila." Neurobiol Aging.
Lemmon, M. A. and K. M. Ferguson (2000). "Signal-dependent membrane targeting by pleckstrin homology (PH) domains." Biochem J **350 Pt 1**: 1-18.
Lupas, A. (1996). "Coiled coils: new structures and new functions." Trends Biochem Sci **21**(10): 375-82.
Malsam, J., S. Kreye, et al. (2008). "Membrane fusion: SNAREs and regulation." Cell Mol Life Sci **65**(18): 2814-32.
Marsh, J. L. and L. M. Thompson (2004). "Can flies help humans treat neurodegenerative diseases?" Bioessays **26**(5): 485-96.
Martens, S. and H. T. McMahon (2008). "Mechanisms of membrane fusion: disparate players and common principles." Nat Rev Mol Cell Biol **9**(7): 543-56.
Mason, J. M. and K. M. Arndt (2004). "Coiled coil domains: stability, specificity, and biological implications." Chembiochem **5**(2): 170-6.
McDermott, C., K. White, et al. (2000). "Hereditary spastic paraparesis: a review of new developments." J Neurol Neurosurg Psychiatry **69**(2): 150-60.
Miller, D. F., S. L. Holtzman, et al. (2002). "Customized microinjection glass capillary needles for P-element transformations in Drosophila melanogaster." Biotechniques **33**(2): 366-7, 369-70, 372 passim.
Munoz, V. and L. Serrano (1997). "Development of the multiple sequence approximation within the AGADIR model of alpha-helix formation: comparison with Zimm-Bragg and Lifson-Roig formalisms." Biopolymers **41**(5): 495-509.
Muqit, M. M. and M. B. Feany (2002). "Modelling neurodegenerative diseases in Drosophila: a fruitful approach?" Nat Rev Neurosci **3**(3): 237-43.
Nakajima, K., H. Hirose, et al. (2004). "Involvement of BNIP1 in apoptosis and endoplasmic reticulum membrane fusion." Embo J **23**(16): 3216-26.
Namekawa, M., M. P. Muriel, et al. (2007). "Mutations in the SPG3A gene encoding the GTPase atlastin interfere with vesicle trafficking in the ER/Golgi interface and Golgi morphogenesis." Mol Cell Neurosci **35**(1): 1-13.
Namekawa, M., P. Ribai, et al. (2006). "SPG3A is the most frequent cause of hereditary spastic paraplegia with onset before age 10 years." Neurology **66**(1): 112-4.
Nelson, J. W. and N. R. Kallenbach (1986). "Stabilization of the ribonuclease S-peptide alpha-helix by trifluoroethanol." Proteins **1**(3): 211-7.
Niemann, H. H., M. L. Knetsch, et al. (2001). "Crystal structure of a dynamin GTPase domain in both nucleotide-free and GDP-bound forms." Embo J **20**(21): 5813-21.
O'Shea, E. K., J. D. Klemm, et al. (1991). "X-ray structure of the GCN4 leucine zipper, a two-stranded, parallel coiled coil." Science **254**(5031): 539-44.

Praefcke, G. J. and H. T. McMahon (2004). "The dynamin superfamily: universal membrane tubulation and fission molecules?" Nat Rev Mol Cell Biol **5**(2): 133-47.
Prakash, B., G. J. Praefcke, et al. (2000). "Structure of human guanylate-binding protein 1 representing a unique class of GTP-binding proteins." Nature **403**(6769): 567-71.
Prinz, W. A., L. Grzyb, et al. (2000). "Mutants affecting the structure of the cortical endoplasmic reticulum in Saccharomyces cerevisiae." J Cell Biol **150**(3): 461-74.
Reid, E. (1997). "Pure hereditary spastic paraplegia." J Med Genet **34**(6): 499-503.
Reid, E., M. Kloos, et al. (2002). "A kinesin heavy chain (KIF5A) mutation in hereditary spastic paraplegia (SPG10)." Am J Hum Genet **71**(5): 1189-94.
Reiter, L. T., L. Potocki, et al. (2001). "A systematic analysis of human disease-associated gene sequences in Drosophila melanogaster." Genome Res **11**(6): 1114-25.
Rismanchi, N., C. Soderblom, et al. (2008). "Atlastin GTPases are required for Golgi apparatus and ER morphogenesis." Hum Mol Genet **17**(11): 1591-604.
Sanderson, C. M., J. W. Connell, et al. (2006). "Spastin and atlastin, two proteins mutated in autosomal-dominant hereditary spastic paraplegia, are binding partners." Hum Mol Genet **15**(2): 307-18.
Schwarz, G. A. and C. N. Liu (1956). "Hereditary (familial) spastic paraplegia; further clinical and pathologic observations." AMA Arch Neurol Psychiatry **75**(2): 144-62.
Shin, H. W., H. Takatsu, et al. (1999). "Intermolecular and interdomain interactions of a dynamin-related GTP-binding protein, Dnm1p/Vps1p-like protein." J Biol Chem **274**(5): 2780-5.
Soderblom, C. and C. Blackstone (2006). "Traffic accidents: molecular genetic insights into the pathogenesis of the hereditary spastic paraplegias." Pharmacol Ther **109**(1-2): 42-56.
Terasaki, M., L. B. Chen, et al. (1986). "Microtubules and the endoplasmic reticulum are highly interdependent structures." J Cell Biol **103**(4): 1557-68.
Thepaut, M., D. Maiorano, et al. (2004). "Crystal structure of the coiled-coil dimerization motif of geminin: structural and functional insights on DNA replication regulation." J Mol Biol **342**(1): 275-87.
Uchiyama, K., E. Jokitalo, et al. (2002). "VCIP135, a novel essential factor for p97/p47-mediated membrane fusion, is required for Golgi and ER assembly in vivo." J Cell Biol **159**(5): 855-66.
Vedrenne, C. and H. P. Hauri (2006). "Morphogenesis of the endoplasmic reticulum: beyond active membrane expansion." Traffic **7**(6): 639-46.
Vinogradov, A. A., F. Mari, et al. (1996). "1H NMR studies of prototypical helical designer peptides. A comparative study of the amide chemical shift dependency on temperature and polypeptide sequence." Int J Pept Protein Res **47**(6): 467-76.
Voeltz, G. K., W. A. Prinz, et al. (2006). "A class of membrane proteins shaping the tubular endoplasmic reticulum." Cell **124**(3): 573-86.
Voeltz, G. K., M. M. Rolls, et al. (2002). "Structural organization of the endoplasmic reticulum." EMBO Rep **3**(10): 944-50.
Waterman-Storer, C. M. and E. D. Salmon (1998). "Endoplasmic reticulum membrane tubules are distributed by microtubules in living cells using three distinct mechanisms." Curr Biol **8**(14): 798-806.

Weber, T., B. V. Zemelman, et al. (1998). "SNAREpins: minimal machinery for membrane fusion." Cell **92**(6): 759-72.
Zhang, P. and J. E. Hinshaw (2001). "Three-dimensional reconstruction of dynamin in the constricted state." Nat Cell Biol **3**(10): 922-6.
Zhao, X., D. Alvarado, et al. (2001). "Mutations in a newly identified GTPase gene cause autosomal dominant hereditary spastic paraplegia." Nat Genet **29**(3): 326-31.
Zhu, P. P., A. Patterson, et al. (2003). "Cellular localization, oligomerization, and membrane association of the hereditary spastic paraplegia 3A (SPG3A) protein atlastin." J Biol Chem **278**(49): 49063-71.
Zhu, P. P., C. Soderblom, et al. (2006). "SPG3A protein atlastin-1 is enriched in growth cones and promotes axon elongation during neuronal development." Hum Mol Genet **15**(8): 1343-53.

Thanks to Diana Pendin and Genny Orso who have worked with in me on this project.

Thanks to Stefano Moro and Giorgio Cozza for performing Molecular modelling.

Thanks to Stefano Mammi and Massimo Bellanda for invaluable help with Circular Dichroism experiments.

Thanks to Roman S. Polishchuk and Massimo Micaroni for EM experiments.